ISAS - INTERNATIONAL SCHOOL FOR ADVANCED STUDIES

Variational Approach to Strongly Correlated Systems

Thesis submitted for the degree of

"Doctor Philosophiæ"

CANDIDATE
Franjo Franjić

SUPERVISOR
Dr. Sandro Sorella

October 1996

SISSA - SCUOLA INTERNAZIONALE SUPERIORE STUDI AVANZATI
TRIESTE
Strada Costiera 11

TRIESTE

SISSA ISAS
SCUOLA INTERNAZIONALE SUPERIORE DI STUDI AVANZATI
INTERNATIONAL SCHOOL FOR ADVANCED STUDIES

Variational Approach to Strongly Correlated Systems

Thesis submitted for the degree of
"Doctor Philosophiæ"

CANDIDATE
Franjo Franjić

SUPERVISOR
Dr. Sandro Sorella

October 1996

Table of Contents

List of Figures

List of Tables

Acknowledgments

This is a special point of my life and I have big debt to express my gratitude to all people who helped me to arrive here. First of all I'm very grateful to my supervisor Sandro Sorella. I hardly can express all my appreciations for time he devoted to illuminate the wonderful world of strongly correlated systems and patience he answered all my questions. He unveiled me a lot of secretes of the computational physics which have lead to this thesis. I'm also very grateful to Prof. Erio Tosatti. His teaching and conveying physics brought another cornerstone of the thesis. The stimulating strongly correlated group, Richard Hlubina, Alberto Parola, Giuseppe Santoro and Michele Fabrizio helped me to enter into this exciting zoo of spinons, holons, anyons, ..., and I'd like to thank them all again.

SISSA is a wonderful place, not only because of my friends, Paolo, Gabriele, Guido, Sandro, Francesca, Michele, Lucian, Zhong. A very pleasant and worm atmosphere created by other SISSA student and staff is something I'll missed a lot.

I na kraju hvala mojim najdražima: Lovorki na svemu što dijelimo, Nenadu, Biserki i Branku na podršci i ohrabrenjima i mojim roditeljima na razumijevanju i strpljenju.

1 Introduction

1.1 Strongly correlated systems

The physics of strongly correlated electrons is at the moment one of the most active field of the condensed matter physics due to the recent discovery of high-temperature superconducting (HTSC) materials. The motivations for studying HTSC are coming not only from expectations to find technologically useful materials but also because the HTSC problem comprise almost all complexities of strongly correlated systems on the lattice.

The initial motivation to study strongly correlated system derived from the problem of ferromagnetism in transition metals. These studies have born out the Hubbard model [2] where electron-electron repulsion is described by a local on-site term. The Hubbard Hamiltonian became a paradigmatic model for strongly correlated systems. Later more phenomena demanding an explanation in the framework of strongly correlated electrons were observed. The discovery of heavy fermion compounds, where electron spectrum is strongly renormalized by electron-electron interactions, rose a substantial interest for better theoretical understanding of the subject. But Bednorz and Müller ten years ago [3] initialized an explosion of excitement and interest for strongly correlated systems discovering that some copper-oxide compounds like $La_{2-x}Ba_xCuO_4$ are superconductors at a relatively high temperature of 35 K. Since then, superconductivity was found in many other similar materials with transition temperature rising over 130 K. Besides their exceptionally high superconducting transition temperatures, collected experimental data reveal that copper-oxide based HTSC materials also have exceptional normal state properties. They have a very rich phase diagram: the superconducting transition occurs near an antiferromagnetic as well as a structural instability, and the metal-insulator transition add new complications to this already complex phase diversity.

The parent, undoped compounds of the copper-oxide based HTSC materials are antiferromagnetic Mott insulators. Namely according to the standard band structure theory they should be metallic but instead they are insulators, indicating that the Coulomb repulsion between electrons dominates their kinetic energy. These properties present HTSC materials as the most interesting examples of strongly correlated systems. Another important clue for understanding the problem

of HTSC is the layered structure of these compounds. The copper-oxide HTSC compounds have one or more CuO_2 planes in the unit cell separated by the layers of other ions. As a result, a high anisotropy of the electronic and in particular superconducting properties is specific for these materials. It is probably this quasi-two-dimensional character of HTSC materials involved with strong interaction which prevents proposed theoretical models to converge to the accepted physical picture for HTSC. In spite of large number of studies devoted to two-dimensional correlated electron systems there is still no model able to cope with all main aspects of this problem.

The importance of the low dimensionality in HTSC was not so surprising for the solid state theoreticians. Though interactions in an electronic system in three or higher dimensions can be renormalized, leading to the Landau fermi liquid theory, in one dimension the perturbation theory is not renormalizable. The properties of one-dimensional systems are instead described by the Luttinger liquid theory. Two-dimensional systems are somehow in between these two concepts. It is not clear which one of them should be adopted as appropriate framework for describing the elementary excitations from the ground state. Inclining to one of these theories leads to physical consequences which cannot be easily harmonized with all observed properties and experimental data. For example, the Luttinger liquid scheme predicts that the spin and charge degrees of freedom have different dynamics and Anderson [4] argued that this is in fact the mechanism driving the unusual behavior of HTSC materials. Therefore a lot of efforts are devoted to understand if it is possible to realize a Luttinger liquid also in the two-dimensional electron system.

Probably the only achieved consensus was that magnetism has an important role for understanding the normal state of HTSC materials and that it could have a part in the interactions leading to the superconducting state. In the mentioned Anderson hypothesis the superconductivity appears from the unconventional ground state for the antiferromagnetically coupled spins in the CuO_2 planes. Instead of the classical (Néel) ground state he proposed a disordered state in the form of resonating valence bonds. Anderson suggested that the appropriate model for HTSC is the two-dimensional one band Hubbard model in the limit of extremely strong repulsion. The considerations of more general models which takes into account the more detailed orbital structure of the CuO_2 planes [5] yield essentially the same Hamiltonian, the so-called t-J model, as the relevant physical picture of the low-energy excitations in the CuO_2 planes. The model essentially describes the antiferromagnetically coupled electrons with the constraint of no doubly occupied sites:

$$\mathcal{H}_{tJ} = -t \sum_{<i,j>,\sigma} (c^{\dagger}_{i\sigma} c_{j\sigma} + c^{\dagger}_{j\sigma} c_{i\sigma}) + J \sum_{<i,j>} (\vec{S}_i \cdot \vec{S}_j - \frac{1}{4} n_i n_j) \ , \tag{1.1}$$

where $c^{\dagger}_{i\sigma}$ is the creation operator of an electron of spin $\sigma = \uparrow, \downarrow$, $\vec{S}_i$ and n_i are the electron spin and the electron density operator, respectively. At half-filling the t-J model reduces to the quantum spin system described by the Heisenberg Hamiltonian which describes well the spin dynamics of the undoped copper-oxide materials. The Heisenberg Hamiltonian is a rather old model but HTSC recently renewed interests for it when it was realized that the understanding of two-dimensional spin systems, especially when frustrated, is not complete and demands more studies.

1.2 Quantum antiferromagnets

The physical picture of the spin interactions comes from considering two electrons localized on energically close orbitals. They are interacting repulsively, but the spin coupling can be ferromagnetic or antiferromagnetic. If the orbitals are orthogonal but occupy the same region in space then by the parallel (ferromagnetic) alignment of spins the interaction energy of the system is reduced. On the other hand, electrons in the spatially separated non-orthogonal orbitals will be antiparallel (antiferromagnetically) aligned in order to reduce their kinetic energy. Based on this simple picture, the notion of quantum magnets as a rather elementary model of strongly correlated systems was conceived. Particularly, quantum antiferromagnets used to be considered a rather well-understood strongly correlated system. This considerably changed when the HTSC problem appeared and a proper understanding of the two-dimensional spin system was questioned.

In one dimension the Bethe-ansatz provide an exact solution for the spin 1/2 case and after that it was shown that the correlation functions in this case follow a power-law decay. However, for chains of spins $S > 1/2$ there is no exact solution. Haldane conjectured [6] that the excitation spectrum of spin chains has an interesting property. He proposed that the excitations of the half-integer spin chains are gapless with power-law behavior of the spin correlation functions, whereas in the spectrum of the integer spin chains a finite gap appears, leading to an exponential decay of correlation functions.

In dimensions higher than one, the exact solution for the infinite lattice problem is not known, but there are some rigorous proofs regarding the nature of the ground state. Three-dimensional Heisenberg antiferromagnets have long-range antiferromagnetic order for all spins $S > 1/2$ whereas for the two-dimensional case the existence of a broken symmetry state have been proved only for $S > 1$. Since the antiferromagnetic coupling in the copper-oxide planes is described by spin-1/2 Heisenberg model, the applicability of the standard spin-wave theory was under suspicions due to the missing the proof of long-range order. However, many numerical calculations support the hypothesis that even for $S = 1/2$ true long-range order exists in the ground state of two-dimensional Heisenberg model.

When low-dimensional spin systems are frustrated, the already present strong quantum fluctuations are even enhanced leading to new phases. In frustrated spin systems the energy of each bond cannot be minimized simultaneously and the ground state is often degenerate. The quantum and thermal fluctuations can then select new ordered phases. The frustration usually can also modify the nature of the underlying order parameter. From the HTSC problem point of view, the transition to the quantum disordered phase of two-dimensional quantum antiferromagnets and the study of its ground state properties is of a particular interest. The motivation is coming from the mentioned Anderson's suggestion that such new disordered phases may be the key to explain the phenomenon of superconductivity in these materials. Namely, the cuprates undergo a transition to a quantum disordered ground state upon doping with a small concentration of mobile holes. At

lower doping the holes are localized and a description within the Heisenberg Hamiltonian is adequate, but at higher doping the holes become mobile, requiring the study of quantum-disordered antiferromagnets in the presence of propagating holes. The new quantum phase rises few important questions:1) What is the symmetry of the quantum disordered state ?; 2) What is the nature of the excitations (spinons) above the ground state ?; and 3) Do spinon carry fractional spin quantum numbers or they are always confined in pairs leading to integer spin excitations? In this respect, the study of quantum two-dimensional antiferromagnets is of great interest in its own right.

The study of strongly correlated electron models is a difficult problem. There are no well-developed analytical techniques to treat the models, e. g. the standard many-body perturbation theory cannot be applied since no small parameters are present, neither in Hubbard Hamiltonian nor Heisenberg one. Theories that start with the same Hamiltonian may arrive to completely different descriptions of their properties. With regards to expansion of computer resources. numerical methods start providing important tool to judge the models and to close the gap between different approaches and mean-field solutions. The numerical calculations can also indicate directions in which new approaches should be developed. A review of computational studies of models of correlated electronic system can be found in Ref. [7].

1.3 Variational calculation

Variational theory is one of the most powerful methods for understanding strongly correlated electron system. The properly chosen variational wavefunction gives an insight into the dominant physical processes. Variational approach fills the gap between the analytical and numerical calculation providing a test for qualitatively developed physical pictures and giving quantitative values to be compared with other models and experimental results. Thus, the variational method links the simplified view of the system to other numerical methods which consider the model without approximations as the exact diagonalization and Quantum Monte Carlo techniques.

Although results obtained by exact diagonalization techniques are unbiased, they are limited to study small systems. Dimension of Hilbert space is growing exponentially with system size, and the upper limits of computer memory and of reasonable time needed for computations, are reached by relatively small systems. The Quantum Monte Carlo methods, see e. g. [8], on the other hand, can treat systems of bigger size, but the algorithm for the case of interacting electrons on the lattice mainly suffers from the negative sign problem. The average of some physical quantity obtained by any quantum Monte Carlo distribution should be normalized by average sign of configuration weights. The average sign could be very small quantity significantly affecting the final results. With an accurate trial wavefunction obtained from variational calculation one can be quite close to the exact ground state so that convergence can be reached before the sign becomes a problem. In order to use some variational wavefunction as the trial state, one requires that it includes all important interactions in a simplified way which is easy to compute. The variational wavefunction formulated

in this thesis was developed also with this motivation.

The variational Monte Carlo method is a combination of the variational theory with the Monte Carlo technique for evaluating expectation values. In the variational theory the energy expectation value is estimated with a given trial state $|\psi_\gamma>$ as a function of a set of variational parameters γ. Once the optimal γ, for which the estimated energy has the minimum is found, the other physical quantities can be calculated.

The variational Monte Carlo method use the random walk in the system configuration space to construct the probability distribution by which the average physical quantities will be computed. The random walk is generated by Metropolis algorithm for importance sampling where the probability of accepting a step from configuration C to configuration C' is given by

$$P(C - C') = \min\left[1, \left|\frac{\psi_\gamma(C')}{\psi_\gamma(C)}\right|^2\right] , \tag{1.2}$$

where $\psi_\gamma(C) =< \psi_\gamma|C >$ is the trial state and $|C >$ is the state of the system with a certain configuration C, say electrons localized at some fixed positions. The variational expectation value of an operator O is defined as:

$$\langle O\rangle_\gamma = \frac{< \psi_\gamma|O|\psi_\gamma >}{< \psi_\gamma|\psi_\gamma >}. \tag{1.3}$$

Inserting the complete set of states $\sum_C |C >< C| = 1$ in the nominator and the denominator. the expectation value can be written as:

$$\langle O\rangle_\gamma = \frac{\sum_C |\psi_\gamma(C)|^2 \left[\frac{<C|O|\psi_\gamma>}{\psi_\gamma(C)}\right]}{\sum_C |\psi_\gamma(C)|^2} . \tag{1.4}$$

By the Metropolis algorithm the probability distribution given by the probability density (1.2) is generated:

$$P_\gamma(C) = \frac{|\psi_\gamma(C)|^2}{\sum_{C'} |\psi(C')|^2} . \tag{1.5}$$

The expectation value can be now written as:

$$\langle O\rangle_\gamma = \sum_C P_\gamma(C)\frac{< C|O|\psi_\gamma >}{\psi_\gamma(C)} . \tag{1.6}$$

The sum over configurations in Monte Carlo method is then replaced by the sum over configurations sampled by the Metropolis algorithm:

$$\langle O\rangle_\gamma \simeq \frac{1}{M}\sum_{m=1}^{M} \frac{< C_m|O|\psi_\gamma >}{\psi_\gamma(C_m)} . \tag{1.7}$$

where C_m is the m-th configuration created by the random walk and M is the total number of configurations. Since the probability is positive definite there is no sign problem. The statistical errors can be significantly reduced by taking a sufficiently large number M, which guarantees statistical independence among samples.

Variational Monte Carlo has a very important zero variance property: as the trial function approaches an exact eigenstate of the Hamiltonian $\mathcal{H}$, the variance

$$\sigma_E^2 = < (\mathcal{H} - E_\gamma)^2 >_\gamma \tag{1.8}$$

vanishes, where $E_\gamma = < \mathcal{H} >_\gamma$. This means that an exact eigenstate has no statistical fluctuations and E_γ becomes the eigenenergy of the Hamiltonian for any configuration $|C>$. On the other hand, a too bad trial wavefunction results in an appreciable variance. Thus in the actual variational Monte Carlo computations, it is convenient to improve the trial wavefunction by minimizing the variance instead of the energy. We should moreover notice that the minimum of σ_E does not mean the minimum of the variational energy.

1.4 Structure of the thesis

The thesis has two parts: the first one concerns the variational approach to strongly correlated systems using a variational wavefunction defined for all considered models by the linear spin-wave expansion; in the second part the method of integration over boundary conditions is applied to calculate the conductivity of the electrons for the Hubbard model in the honeycomb lattice. In the first part the variational Monte Carlo was used, whereas the second one contains the results from exact diagonalization by the Lanczos method.

The spin-wave variational wavefunction was applied to several different problems, from one-dimensional chains to hard-core bosons and t-J model. The results show that this wavefunction can be very successfully applied to the study of strongly correlated systems. It is practically the exact numerical solution for the hard-core bosons, by this state the J_1-J_2 model can be described even in the strong frustration regime where the spin-wave theory fails and in the t-J model it is competitive with the Luttinger liquid state, at least when hole doping is not too small.

In this thesis the integration over boundary condition technique was applied for the first time in the calculation of an important quantity such as the conductivity. The results are relevant to explain the recently observed surface charge density waves, showing that the observed conductivity in the low-temperature phase can be interpreted as a consequence of strong electron-electron interactions.

The thesis is organized as follows: in Chapter 2 the variational wavefunction is introduced. The formalism is developed considering the spin-wave expansion for the generalized XXZ model. The variational state is of the Jastrow type where the long-range behavior of the Jastrow potential is determined by the linear spin-wave analysis. The formalism can be rather easily applied to other spin systems and the resulting wavefunction is simple and computationally undemanding.

In Chapter 3 the physics described by this variational state is studied for one-dimensional systems. The proposed state correctly describes the spin-1/2 Heisenberg model in spite of the fact that one-dimensional chains do not have true long-range order and the spin-wave expansion for such system

is not properly defined. The state is tested on the exactly solvable Haldane-Shastry model showing that it represents the exact ground state. The variational state is also applied to the spin-1 case showing a phase transition by changing the strength of the Jastrow potential.

Chapter 4 is devoted to the variational study of the J_1-J_2 model, the frustrated Heisenberg model on the square lattice. The variational calculation was done by using the state directly obtained from the spin-wave expansion and by the procedure which use the constraints coming from the sum rules for the structure factor. The order parameter is determined applying the finite-size scaling analysis indicating that long-range order is destroyed for frustrations over $J_2/J_1 = 0.41$.

A very successful application of the spin-wave variational wavefunction to the hard-core bosons is presented in Chapter 5. The system has long-range order and spin-wave expansion is appropriate for this system. However, it is surprising how accurate is the spin-wave state: it has an overlap square with the exact ground-state wavefunction bigger than 99.8%. The hard-core boson structure factor and momentum distribution function is compared with the spin-less fermions.

Variational calculations for the t-J model is presented in Chapter 6. The ground state energy obtained by the spin-wave variational state is compared to the Luttinger liquid variational estimate. The variational state, constructed as a product of fermionic state and hard-core boson wavefunction, describes a Fermi liquid state. The computation is done for doping $\delta \approx 0.3$ and doping $\delta \approx 0.1$. For larger doping we show that the Fermi state is more stable than the Luttinger liquid one, whereas for small doping the two variational energies are no longer substantially different.

Chapter 7 is dedicated to verify a scenario for the behavior of the conductivity on the honeycomb lattice. The simple Hubbard model is used to demonstrate that the effects of strong correlations actually can produce the peak of conductivity which is consistent with the metallic behavior of the system. This calculation is an extension of the integration over boundary condition technique to the calculation of the electron conductivity.

2 Derivation of the "spin-wave" variational wavefunction

2.1 Introduction

The low-lying energy states of spin systems coupled by exchange interactions are wavelike modes. The waves are called spin waves and the unit of energy of a spin wave is called magnon. Spin waves have been studied for all types of ordered spin arrays, including ferromagnetic, antiferromagnetic, ferrimagnetic, and less common spiral arrays. We will focus our study to the antiferromagnetic systems, first presenting a general method for derivation of the variational wavefunction based on the spin-wave expansion.

The simplest model describing the dynamics of the spin systems is the isotropic Heisenberg Hamiltonian:

$$\mathcal{H} = J \sum_{<i,j>} \vec{S}_i \cdot \vec{S}_j \ . \tag{2.1}$$

The sum is running over the pairs of nearest-neighbor sites $< i, j >$ of the d-dimensional lattice. For antiferromagnetic interactions $J > 0$ and a negative $J < 0$ describes the ferromagnetic interactions. The spins $\vec{S}_i$ are quantum spin operators obeying the commutation relations:

$$[S_l^\alpha, S_{l'}^\beta] = i S_l^\gamma \delta_{ll'} \ , \tag{2.2}$$

where the superscripts α, β and γ stand for x, y and z components or any cyclic permutation of them. We will consider the finite lattices of L sites in $d = 1$ and $d = 2$, but an extension of the method to higher dimensions is straightforward. In our units, the lattice spacing a and Planck constant $\hbar$ are taken to be $a = \hbar = 1$.

The system of classical spins, i. e. fixed-length classical vectors, has the minimal energy in the state where all spins are parallel for $J < 0$, or neighboring spins antiparallel for $J > 0$. The ground state of classical spins for the antiferromagnetic coupling is known as the Néel state and for the ferromagnetic one as the Nagaoka state. If we introduce the spin rising S^+ and spin lowering S^- operators

$$S_l^+ \ = \ S_l^x + i S_l^y \ , \tag{2.3}$$

$$S_l^- = S_l^x - iS_l^y \ , \tag{2.4}$$

the Hamiltonian (2.1) can be written in a very instructive form of two terms, the spin-flip term and the Ising term:

$$\mathcal{H} = J \sum_{<i,j>} \left[\frac{1}{2}(S_i^+ S_j^- + S_i^- S_j^+) + S_i^z S_j^z \right] \ . \tag{2.5}$$

Since the spin-flip term exchange the spins on the neighboring sites, the Néel state is not an eigenstate of the quantum Hamiltonian, whereas the Nagaoka state is indeed the quantum ground state for $J < 0$. A natural question to ask is when we can consider the Néel state as a satisfactory approximation for the ground state of the quantum antiferromagnets and whether or not long-range antiferromagnetic order of spins exists.

In the limit $S \to \infty$ the spin commutator is much smaller than the square of the spin variables and the quantum spins become classical. In fact, Anderson [9] and Kubo [10] have shown that already the first order in the $1/S$ perturbation expansion from the Néel state describes very accurately the ground state of the quantum antiferromagnets in $d = 3$. The physical picture is that for large S we expect S^z to make at each of lattice sites only small deviation from the classical values $\pm S$ which can be treated in the harmonic approximation, similarly to the lattice vibration. But the zero-point motion of the quantum spins considerably reduce the sublattice magnetization in lower dimensions. In two dimensions any finite temperature excites enough spin waves to destroy long-range order of spins, whereas in one dimension the quantum fluctuations suppress the magnetization even at zero temperature.

A convenient way to develop the $1/S$ spin-wave expansion is to represent the spin operators in terms of bosons using the Holstein-Primakoff transformation [11]. For a ferromagnet one use the expressions

$$S_l^z = S - a_l^\dagger a_l \ , \tag{2.6}$$

$$S_l^+ = \sqrt{2S} \left(1 - \frac{a_l^\dagger a_l}{2S} \right)^{1/2} a_l \ , \tag{2.7}$$

$$S_l^- = \sqrt{2S} a_l^\dagger \left(1 - \frac{a_l^\dagger a_l}{2S} \right)^{1/2} \ , \tag{2.8}$$

whereas for an antiferromagnet on a bi-partite lattice this has to be defined slightly different. In addition to above expressions valid for sublattice A, for sublattice B one defines:

$$S_l^z = -S + b_l^\dagger b_l \ , \tag{2.9}$$

$$S_l^+ = \sqrt{2S} b_l^\dagger \left(1 - \frac{b_l^\dagger b_l}{2S} \right)^{1/2} \ , \tag{2.10}$$

$$S_l^- = \sqrt{2S} \left(1 - \frac{b_l^\dagger b_l}{2S} \right)^{1/2} b_l \ . \tag{2.11}$$

Here the a_l and b_l are boson destruction operator which satisfy the usual commutation relations

$$[a_{l'}, a_l^\dagger] = [b_{l'}, b_l^\dagger] = \delta_{ll'} \ . \tag{2.12}$$

Substituting in above expressions the expansion of $f(n_l) = \sqrt{1 - n_l/(2S)}$, where $n_l = a_l^\dagger a_l = b_l^\dagger b_l$, in powers of $1/S$:

$$f(n_l) = 1 - \frac{n}{4S} - \frac{n^2}{32S^2} - \cdots \ , \tag{2.13}$$

the Hamiltonian in the spin-wave representation can be obtained. In the linear spin-wave approximation one retains only the first term in Eq. (2.13) approximating $f(n_l) \sim 1$.

For the sake of generality, instead of the Hamiltonian (2.1) we consider the XXZ Hamiltonian with general couplings between spins:

$$\mathcal{H} = \sum_{i,j} [- J_{i,j}^{xy}(S_i^x S_j^x + S_i^y S_j^y) + J_{i,j}^z S_i^z S_j^z] \ . \tag{2.14}$$

Within the XXZ-model notation, the isotropic Heisenberg Hamiltonian is obtained taking $J_{i,j}^{xy} = -J_{i,j}^z$ for the ferromagnetic case, whereas for the antiferromagnet case $J_{i,j}^{xy} = J_{i,j}^z$, after changing the sign of the spin-rising operator on the one of sublattices by means of the usual transformation $S_l^+ = (-1)^l S_l^+$. The isotropic condition is obtained by the continuity for $|J^z| \to J$.

As a basis of the Hilbert space of general spin Hamiltonians we can take the product of the eigenstates $|S_l^z>$ of the operator of the z-component of the spin S_l^z:

$$|\{S_l^z\}> \equiv \prod_l |S_l^z> \ . \tag{2.15}$$

Since the operator of z-component of the total spin $S_{tot}^z = \sum_l S_l^z$ commute with the Hamiltonian (2.14) and its eigenvalues are constants of the motion, we can choose to work in the subspace of given value of the z-component of the total spin. For antiferromagnets Marshall [12] has proved the ground-state wavefunction is nodeless on the bipartite lattice and characterized by $S_{tot}^z = 0$.

2.2 Linear spin-wave theory

Assuming that the couplings $J_{i,j}^{xy}$ and $J_{i,j}^z$ allow a stabile ferromagnetic solution on the xy-plane, we can apply the linear spin-wave theory to the Hamiltonian (2.14). For convenience the ferromagnetic order parameter is set along the x-axis:

$$S_l^x = S - a_l^\dagger a_l \ , \tag{2.16}$$

$$S_l^y = \sqrt{\frac{S}{2}}(a_l^\dagger + a_l) \ , \tag{2.17}$$

$$S_l^z = i\sqrt{\frac{S}{2}}(a_l^\dagger - a_l) \ . \tag{2.18}$$

The spin commutation relations (2.2) in above linear spin-wave representation are obeyed up to the order $1/S$. Note a little bit uncommon choice of the direction of the order parameter, but the advantage of the present orientation will be realized soon after the variational wavefunction is introduced.

In the bosonic representation the Hamiltonian reads:

$$\mathcal{H} = -S^2 \sum_{i,j} J_{i,j}^{xy} + S \sum_{i,j} [2a_i^\dagger a_i J_{i,j}^{xy} + a_i^\dagger a_j (-J_{i,j}^{xy} + J_{i,j}^z) - \frac{1}{2}(a_i^\dagger a_j^\dagger + a_i a_j)(J_{i,j}^{xy} + J_{i,j}^z)] \ . \tag{2.19}$$

Introducing the Fourier transformation of the bosonic operators:

$$a_q^\dagger = \frac{1}{\sqrt{L}} \sum_l e^{-iqR_l} a_l^\dagger \ , \tag{2.20}$$

$$a_q = \frac{1}{\sqrt{L}} \sum_l e^{iqR_l} a_l \ ; \tag{2.21}$$

and couplings

$$J^{xy}(q) = \frac{1}{L} \sum_{i,j} e^{iq(R_i - R_j)} J_{i,j}^{xy} \ , \tag{2.22}$$

$$J^z(q) = \frac{1}{L} \sum_{i,j} e^{iq(R_i - R_j)} J_{i,j}^z \ , \tag{2.23}$$

Hamiltonian (2.19) can be written in a compact form:

$$\mathcal{H} = S \sum_q [D_q a_q^\dagger a_q + \frac{\eta_q}{2}(a_q^\dagger a_{-q}^\dagger + a_q a_{-q})] \ , \tag{2.24}$$

where

$$D_q = 2J^{xy}(0) - J^{xy}(q) + J^z(q) \ , \tag{2.25}$$

$$\eta_q = -(J^{xy}(q) + J^z(q)) \ . \tag{2.26}$$

The quadratic form of the bosonic operators in Eq. (2.24) is usually obtained in the linear spin-wave theory and it can be easily diagonalized by the Bogoliubov transformation

$$a_q^\dagger = u_q \beta_q^\dagger + v_q \beta_{-q} \ . \tag{2.27}$$

The transformation functions are given by

$$u_q = \sqrt{\frac{D_q + \epsilon_q}{2\epsilon_q}} \ , \tag{2.28}$$

$$v_q = -\mathrm{sign}(\eta_q) \sqrt{\frac{D_q - \epsilon_q}{2\epsilon_q}} \ , \tag{2.29}$$

$$\epsilon_q = \sqrt{D_q^2 - \eta_q^2} \ . \tag{2.30}$$

The diagonalized Hamiltonian now reads:

$$\mathcal{H} = S\sum_q [\epsilon_q \beta_q^\dagger \beta_q + \frac{1}{2}(\epsilon_q - D_q)] \ , \tag{2.31}$$

where ϵ_q is the normal-mode excitation energy and $\frac{1}{2}(\epsilon_q - D_q)$ is their zero-point energy.

For $q = 0$, the linear spin-wave Hamiltonian factors D_q and η_q become equal up to a sign, and the spin-wave excitation energy ϵ_q vanishes. The Bogoliubov transformation is then not well defined and for this reason this mode will be called "singular mode". On an infinite lattice this problem is not important because $q = 0$ is just a point in a continuous spectrum, but for a finite lattice we should pay a special attention to this singular mode contribution and handle this wavevector carefully. In Ref. [13] Sorella and Zhong have shown by a careful analysis that this singular $q = 0$ mode can be written as the projector of the spin-wave ground state onto the subspace where the z-component of the total spin vanishes. This projection will be denoted as $P_{S^z_{tot}=0}$.

2.3 "Spin-wave" variational wavefunction

The ground state $|\psi_{GS}>$ of the spin-wave Hamiltonian (2.31) is defined as the vacuum of the spin-wave magnons β_q:

$$\beta_q|\psi_{GS}>= 0 \ . \ \text{for all } q \tag{2.32}$$

Using the inverse transformation

$$\beta_q = u_q a_q - v_q a_{-q}^\dagger \ , \tag{2.33}$$

it can be easily proven that $|\psi_{GS}>$ has a Gaussian form:

$$|\psi_{GS}>= P_{S^z_{tot}=0} \prod_{q\neq 0} \frac{1}{u_q} e^{\frac{v_q}{2u_q} a_q^\dagger a_{-q}^\dagger} |F> \ , \tag{2.34}$$

which represents the ground state of the quantum harmonic oscillator Hamiltonian (2.31). Here $|F>$ is the x-axis ferromagnetic state $|F>= \prod_l |S_l^x = S>$. Because of the linear spin-wave approximation, the Hamiltonian (2.24) connects the physical states satisfying the constraint $a_l^\dagger a_l \leq 2S$ with states having the number of bosons at a given lattice site bigger than it is allowed in the spin operators' original Hilbert space, namely $a_l^\dagger a_l > 2S$. The constraint $a_l^\dagger a_l \leq 2S$ is obviously violated in the wavefunction (2.34) and we need an improved state.

Instead of the harmonic oscillator wavefunction, which is the ground state of the linear spin-wave Hamiltonian of the original model, we can introduce a variational state $|\psi_V>$ which is defined in the correct Hilbert space and only in the spin-wave limit when $S \to \infty$ it reduces to the harmonic oscillator form (2.34):

$$|\psi_V>= P_{S^z_{tot}=0} e^{\frac{1}{2}\sum_q \frac{2}{S} g_q S_q^z S_{-q}^z} |F> \ , \tag{2.35}$$

where S_q^z is the z-component Fourier transform of the spin operator

$$S_q^z = \frac{1}{\sqrt{L}} \sum_l e^{-iqR_l} S_l^z \ . \tag{2.36}$$

The unknown function g_q can be determined by requiring that the Schrödinger eigenvalue equation

$$H|\psi_V> = E|\psi_V> \tag{2.37}$$

is satisfied in the large spin limit.

The exponent in the expression (2.35) can be seen as a classical Jastrow factor with the two-body potential

$$v(R) = \frac{2}{SL} \sum_{q \neq 0} e^{-iqR} g_q \ , \tag{2.38}$$

acting on the classical configurations

$$|C_i> = |S_1^z S_2^z \ \ldots \ S_L^z> \ , \quad -S \leq S_l^z \leq S \ . \tag{2.39}$$

Namely, in the ferromagnetic state $|F>$ each site has the maximum eigenvalue of the spin x-component:

$$|F> = \prod_l |S_l^x = S> \ . \tag{2.40}$$

In the basis of the spin z-component this state can be written as (see *e. g.* [14])

$$|S_l^x = S> = \frac{1}{2^S} \sum_{S_l^z=-S}^{S_l^z=S} \sqrt{\binom{2S}{S - S_l^z}} |S_l^z> \ . \tag{2.41}$$

After projection, the ground state is given as a sum over the classical configurations (2.39)

$$P_{S_{tot}^z=0}|F> = \sum_i c_i |C_i> \ . \tag{2.42}$$

The sum runs over the whole Hilbert space. For the nonfrustrated case, the coefficients c_i are all positive, and configurations due to the projection satisfy $\sum_l S_l^z = 0$. Since $c_i > 0$ for all i, the Perron-Frobenius theorem ensures that the $|\psi_V>$ is not orthogonal to the true ground state for any finite S and therefore it will necessarily collapse to it as $S \to \infty$, provided that Schrödinger equation is (2.37) is verified. For frustrated case, we expect that the "spin-wave" variational wavefunction remains a good approximation of the ground state.

We expect that our variational wavefunction is not only valid when there is true long-range order, but also in the one dimensional cases. For example, the one-dimensional spin $S = 1/2$ isotropic antiferromagnetic Heisenberg model, as there is no long-range order represents a very bad case for the application of the linear spin-wave approximation. Nevertheless, the ground state energy agrees within 2% with the exact value obtained by the Bethe ansatz, as already noticed by Anderson in the seminal paper of the spin wave theory [9].

Once the physics of the ground state is correctly described by this wavefunction obtained from the self-consistency criteria in the eigenvalue equation, we can expect that also the long-distance spin-spin correlations are correctly determined. For the mentioned example of the one-dimensional $S = 1/2$ Heisenberg antiferromagnet, we will see in Chapter 3 that the long-range order present in the wavefunction $P_{S^z_{tot}=0}|F>$ is readily destroyed by the long-range Jastrow potential $v(R) \sim \log R$, consistently determined in the large-S limit of the eigenvalue equation (2.37).

In order to determine the unknown function g_q, or equivalently to solve (2.37) in the limit $S \to \infty$, we have to perform large-S limit of Eq. (2.35) and using (2.18) after a simple Gaussian integration, see Appendix A, we obtain the following form of the variational wavefunction:

$$|\psi_V> \propto P_{S^z_{tot}=0} e^{\frac{1}{2}\sum_{q\neq 0} -\frac{g_q}{1-g_q} a^\dagger_q a^\dagger_{-q}} |F> \ . \tag{2.43}$$

The function g_q is given by matching the two expressions for the ground-state wavefunction (2.34) and (2.43):

$$g_q = \frac{v_q}{v_q - u_q} = \frac{1}{2}\left[1 - \sqrt{\frac{D_q - \eta_q}{D_q + \eta_q}}\right] \ . \tag{2.44}$$

The Jastrow g_q is singular only for $q \to 0$ and in this limit it behaves as $-g_0/|q|$ where g_0 is a constant, e. g. $g_0 = \sqrt{d}$ in the case of the nearest-neighbor model. The small wavevector limit determines the long-range behavior of the Jastrow potential (2.38), for example in one dimension we obtain the logarithmic potential between spins, recovering the wavefunction used by Hellberg and Mele [15] to study the Luttinger liquid.

In order to study the physics of the spin systems described by this variational wavefunction, it will be applied to one (for the cases spin $S = 1/2$ and $S = 1$) and to two dimensions ($S = 1/2$). As was already stressed, in one dimension the linear spin-wave theory is a rather bad approximation, the investigated cases are used to compare the variational state with the exactly known results and to establish the reliability of the wavefunction. The application in the two-dimensional cases brings more interesting physics, especially for the hard-core bosons and the $J_1 - J_2$ Heisenberg model.

2.4 Summary and discussion

We have presented a quite general method for deriving the variational wavefunction for the antiferromagnets based on the spin-wave expansion. The wavefunction has a Jastrow form where the long range behavior of the potential is determined by the soft magnon modes. The wavefunction has no variational parameters at all, but it is reasonable to introduce at least one to compensate error made by linear spin-wave approximation. A natural choice is to treat the Jastrow potential at nearest-neighbor sites as the parameter because the energy is very sensible to short-range correlations. The more sophisticated variational calculation could be performed considering the structure factor at the $q \to 0$ limit and forcing the long range behavior of the wavefunction to be consistent

with the sum rules in the one-magnon approximation. An example of such calculation is done in Chapter 4.

The particular form (2.35) of the variational wavefunction has been first applied by Suzuki and Miyashita [16]. However it can be considered a generalization to discrete models of Jastrow wavefunction used some time ago for the helium. The same form of the variational wavefunction was used by Huse and Elser for a variational study of the two-dimensional spin $S = 1/2$ Heisenberg model [17] with the long-range Jastrow potential described by a set of variational parameters. Using a rather involved method based on the paired-magnon analysis Manousakis [18] derived the correct long-range behavior of the Jastrow potential for this model on the square lattice. His wavefunction, of course, coincides with the one introduced here because the long-distance behavior of the Jastrow potential are derived in both methods from the magnon zero-point motion. However, the method described here can be very easily applied for a large class of spin systems, whereas the Manousakis paired-magnon analysis is difficult to extend to general spin models, other than the square lattice spin $S = 1/2$ Heisenberg. Thus, the present method is enough simple to be used in a complicated model and robust to grasp the important physics of quantum antiferromagnets.

3 One-dimensional applications

3.1 Introduction

The variational state introduced in Chapter 2 is based on the assumption of spontaneously broken symmetry in the spin system and appearance of long-range order. It is generally expected that when the temperature in a spin system is lower than the typical spin-coupling energy, the thermal excitation of higher energy levels which reduce the spin correlations, becomes sufficiently week to allow that the system has a non-vanishing magnetization even when it is not in an external magnetic field. At this critical temperature continuous $SO(3)$ symmetry in the spin space is broken down to $SO(2)$ symmetry and the long-range order between spins appears. This spontaneous symmetry breaking is accompanied with the appearance of massless excitations – magnons well described by the spin-wave theory. But if the space dimension is low, that is $d = 1$ or $d = 2$, the quantum fluctuations coming from the zero-point motion can considerably contribute in the reduction of the magnetization. As Mermin-Wagner theorem shows [19], for a large class of one and two dimensional spin systems with short-range interactions the spontaneous ordering is possible only at zero temperature. However, in one dimension the quantum fluctuations could be strong enough to prevent the ordering even at $T = 0$. The spin-wave calculation for the isotropic Heisenberg model shows that the reduction of the sublattice magnetization by quantum fluctuations diverges indicating that the Néel state is unstable in one dimension.

The spin-wave theory demonstrates that quantum fluctuations destroy long-range order in one-dimensional quantum antiferromagnet independently of the value of the spin S. Actually, the $S = 1/2$ one-dimensional Heisenberg model can be exactly solved by the Bethe-ansazt and the low-energy excitations are gapless. However, Haldane suggested [6, 20] that for integer-spin chains there is a finite gap and correlation functions decay exponentially whereas for half-integer spin chains gapless excitations can exist with power-law decaying spin correlations. This conjecture relied on the different topological structure of the corresponding continuum limit theory. In the last few years there is a considerable number of numerical and experimental confirmations of the Haldane surmise (for a review see [21]).

The lack of the quantum ordered state prevents the spin-wave theory to be applicable for one-

dimensional systems. Nevertheless it is an interesting question how the variational wavefunction introduced in Chapter 2 describes the ground state of antiferromagnetic chains. Here we will study the spin $S = 1/2$ and the spin $S = 1$ Heisenberg chains. We have found that the variational state correctly describes the power-law fall-off of the spin-spin correlations of the $S = 1/2$ chain. The $S = 1$ chain exhibits very interesting phase transition, but it was impossible to conclude the presence of the Haldane gap phase.

3.2 Spin $S = 1/2$ chains

The linear spin-wave Hamiltonian functions (2.25) and (2.26) for the isotropic Heisenberg chain have form $D_q = 1$ and $\eta_q = -\cos q$. The corresponding Jastrow wavefunction is

$$g_q = \frac{1}{2}(1 - |\cot\frac{2}{q}|) = -\frac{1}{|q|} + \cdots , \tag{3.1}$$

with long-range behavior

$$\lim_{R\gg} v(R) = \frac{2}{SL}\sum_q(-\frac{1}{|q|}) = -\frac{2}{SL}\frac{4\pi}{L}\mathrm{Re}\sum_{n>0}\frac{1}{n}e^{i\frac{2n\pi}{L}R} \approx \frac{4}{\pi}\log\left(\frac{2\pi}{L}R\right) . \tag{3.2}$$

The variational state (2.35) can be represented by a classical system of charged particles on the lattice interacting by the Jastrow potential and infinite on-site repulsion. For $S = 1/2$ each site contains one positive or negative charge and the projection onto the subspace with vanishing z-component of the total spin corresponds to zero total charge. A similar variational state with logarithmic interaction between classical hard-core gas was investigated by Hellberg and Mele [15]. As was shown in this paper and related comments [22], the long-range Jastrow with a logarithmic interaction describes the Luttinger liquid state, or the power-law large-distance behavior of correlation functions.

A Luttinger-liquid type of analysis can be applied to the system described by these long-range variational wavefunctions. The spin-spin correlation function $c(R)$ behaves like:

$$< S_0^z S_R^z > \quad \propto \quad \frac{1}{R^{\mu_z}} , \tag{3.3}$$

$$< S_0^x S_R^x > \quad \propto \quad \frac{1}{R^{\mu_x}} . \tag{3.4}$$

The exponents μ_z and μ_x are given by the coefficient in the logarithmic Jastrow potential:

$$\mu_z = \frac{1}{\mu_x} = \frac{\pi}{2g_0} . \tag{3.5}$$

In order to change the strength of the interaction we can introduce a factor γ to the Jastrow potential of the variational wavefunction: $g_q \to \gamma g_q$. This factor appears in front of the logarithmic Jastrow (3.2) and changes the exponents of correlation functions to $\mu_z = 1/\mu_x = \pi/(2\gamma g_0)$. To

γ	$< S_0^z S_{L/2}^z >$		$< S_0^+ S_{L/2}^- >$	
	μ_z	$\frac{\pi}{2\gamma}$	μ_x	$\frac{2\gamma}{\pi}$
1.0	1.59 ± 0.03	1.5708	0.64 ± 0.09	0.6366
1.1	1.43 ± 0.01	1.4280	0.6 ± 0.1	0.7003

Table 3.1: The power-low exponents for the spin $S = 1/2$ chains. The Luttinger liquid analysis gives $\mu_z = 1/\mu_x = \pi/2\gamma$.

verify the behavior (3.4) and (3.3) of the spin-spin correlation functions $c(R)$ we have performed variational Monte Carlo calculation on the chains of size up to $L = 68$. For the small chains we have compared the variational estimates for $< S_0^z S_R^z >$ correlation function with the value obtained by the exact sampling of all configurations in the Hilbert space. The results are the same within the error bars of the variational estimate.

The very precise results for small chains enable to use the finite size correction term in the data fit [23]

$$\log c(\frac{L}{2}) = \mu \log L + a + \frac{b}{L} , \tag{3.6}$$

where μ is the power-law exponents, a and b are finite-size fit parameters. The fit is shown in Fig. 3.1. We used two values for γ and the obtained results are in very good agreement with the Luttinger liquid prediction $\mu_z = 1/\mu_x$ as can be seen in Table 3.1. The in-plane and out-of-plane correlations clearly demonstrate that the variational state has power-law decay and that the order present in the classical state is completely destroyed. The agreement of the predicted exponents confirms that our method determines a very reasonable wavefunction and extends the validity of the spin-wave analysis to the one dimensional spin systems.

A good check of the method is an application to an exactly solvable model where we can transparently see the behavior of both the wavefunctions, the ground state of the Hamiltonian and the present variational wavefunction.

Let us consider the exactly solvable Haldane-Shastry model [24, 25] defined by the Hamiltonian:

$$\mathcal{H} = \sum_{n,n'} J(n-n')(S_n^x S_{n'}^x + S_n^y S_{n'}^y + \Delta S_n^z S_{n'}^z) , \tag{3.7}$$

where the spin coupling $J(n-n')$ decays with the inverse square of distance $d(n-n')$ between sites n and n'

$$J(n-n') = \frac{1}{d^2(n-n')} . \tag{3.8}$$

With periodic boundary condition we can take for d the chord distance

$$d(n-n') = \frac{L}{\pi} |\sin \frac{\pi}{L}(n-n')| . \tag{3.9}$$

The wavefunction (2.35) is the exact solution of the Haldane-Shastry model for the particular

Jastrow potential

$$v(R) = \log \sin^2(\frac{\pi R}{L}) \ . \tag{3.10}$$

In order to determine this potential in spin-wave approximation we must determine the Fourier transform of the couplings (2.22) and (2.23):

$$J^{xy}(q) = -\frac{1}{2}(\pi - q)^2 \mathrm{mod}(0, \pi) \ , \tag{3.11}$$

$$J^{z}(q) = \frac{1}{2} q^2 \mathrm{mod}(0, \pi) \ . \tag{3.12}$$

By applying Eqs. (2.25), (2.26), and (2.44) the Fourier transform of the Jastrow potential can be easily obtained:

$$v_q = \frac{2}{S} g_q = -2 \left(\frac{\pi - q}{q} - 1 \right) \mathrm{mod}(0, \pi) \ , \tag{3.13}$$

i. e. its inverse Fourier transform asymptotically converges to the exact solution (3.10) in the thermodynamical limit. Thus, for this example of an exactly solvable spin model, the variational state is asymptotically exact. This is very encouraging to investigate the spin $S = 1$ model where a gap phase should appear in the isotropic case.

3.3 Spin $S = 1$ chain

As for the previous $S = 1/2$ case we consider the isotropic Heisenberg chain with $S = 1$ spins. Apart from the prefactor, the function g_q is insensitive to the actual value of the spin. But the variational state changes drastically compared to the $S = 1/2$ case. The states in the $S = 1$ Hilbert space are represented not only by two opposite charged particles, as is in the $S = 1/2$ case, but the holes corresponding to $S_l^z = 0$ should also appear. The holes are completely decoupled from the system of charges because of zero charge.

Therefore it is not difficult to realize that the $S = 1$ model corresponds to the one dimensional lattice gas model with charges $S_l^z = \pm 1$ and empty space corresponding to the holes. The Coulomb gas model with logarithmic interaction has been encountered several times in the literature and its, probably complete, phase diagram has been established [26]. However, the mapping of the present variational wavefunction model to the Kane and Fisher one is not direct. The Coulomb gas model is defined on a continuum and in the low charge-density limit, whereas our model is on a lattice and we are interested in the large density of charges. Thus, the conclusion from the Kane-Fisher study can not be safely transfered to our model. Therefore we have studied the properties of the variational state numerically by the variational Monte Carlo calculation of the spin correlation functions.

Introducing the variational parameter γ as a prefactor in the Jastrow potential we can change the strength of the interaction between the charges and study the possible phases. The phase diagram is characterized by the out-of-plane spin correlation function, shown in Fig. 3.2. For large γ there

is a dielectric phase that reminds the Haldane phase with an hidden order parameter. Here the order is not hidden and the variational wavefunction is quantitatively meaningless. When the γ is lowered the system goes to the new phase where the charges are confined and spin correlation follow a power-law decay. This suggests that for small γ the spin $S = 1$ chain remains gapless, as is in the spin $S = 1/2$ case, and the ground state is characterized by quasi-long-range order.

The disordered phase corresponds to the power-law behavior in the phase diagram of the spin $S = 1$ chains obtained by Nijs and Rommelse [27]. They have found that antiferromagnetically coupled Heisenberg spin chains have a phase similar to the one of the present model. for small enough J^z coupling. In the Coulomb gas model correlation functions in both phases – the ordered dielectric phase and the disordered plasma one – have a power-law decay. From the variational Monte Carlo calculation is very hard to obtain estimate with small enough error in the ordered phase because of the very low acceptance ratio in the sampling of the variational wavefunction distribution. Therefore, our numerical data does not obviously show that the ordered phase is gapless or there is a finite correlation length as expected from the existence of the Haldane gap, see Fig. 3.3. After the phase transition, for large γ, the new phase ground state cannot be probably classically described by the antiferromagnetic state and the spin-wave expansion used in the derivation of the variational state is no longer valid. This means that the "spin-wave" variational wavefunction is not a proper choice for this state.

3.4 Summary and discussion

The introduced scheme for derivation of the spin-wave variational wavefunction was applied to one-dimensional systems. The strong quantum fluctuations in one-dimensional spin chains destroy long-range order and prevent the spin-wave theory, depending on the existence of the broken-symmetry ground state, to be applicable. Nevertheless, for such one-dimensional systems, the method leads to a state which reasonably describes the spin $S = 1/2$ Heisenberg model. The obtained power-law exponents for the correlation functions are consistent with previous findings that the isotropic Heisenberg model in the long-wavelength limit has a Luttinger liquid character. The exactly solvable model introduced by Haldane and Shastry of $S = 1/2$ spins coupled with interaction which decays as the inverse square distance has the ground state given exactly by the proposed variational wavefunction in the thermodynamical limit. The spin $S = 1$ Heisenberg chain exhibits phase transition from the clearly power-law phase to the ordered phase for which we are not able to conclude between gapless and gap-full state.

These one-dimensional examples encourage us to apply the method to two-dimensional systems. Two-dimensional quantum antiferromagnets have still quite strong quantum fluctuations to reveal interesting phases, such as disordered spin-liquid phases. We will show that our approach, even though is based on spin-wave theory is at least valid to study the instability of the classical Nèel state. The method will be rather successfully used in the next chapters for the frustrated Heisenberg

model on the square lattice and for the hard-core bosons. In the latter case the variational state is almost the exact ground state.

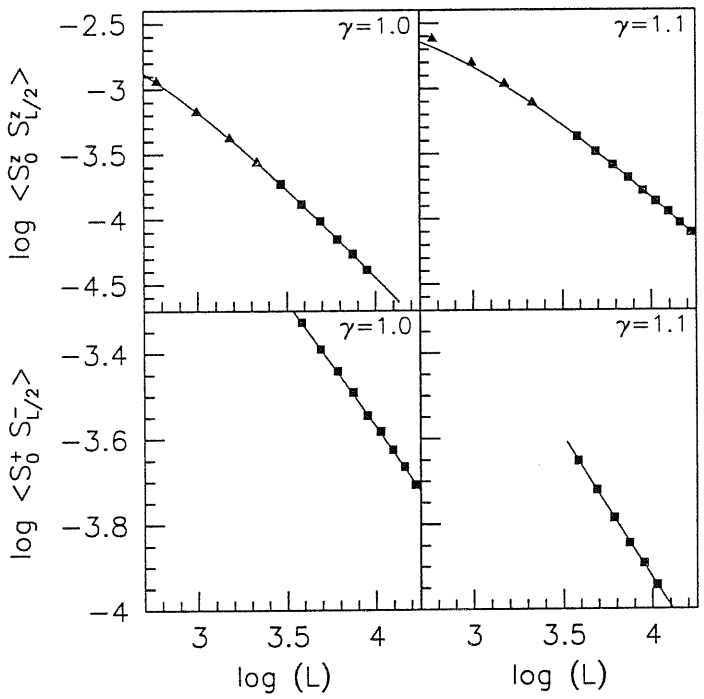

Figure 3.1: The in-plane spin correlation function (lower figures) and out-of-plane (upper figures) for two values of the interaction strength parameter γ. Data obtained by variational Monte Carlo calculation are represented by squares and triangles represent the ones from exact sampling of all configurations of the wavefunction. Lines represent the fit by the finite-size formula.

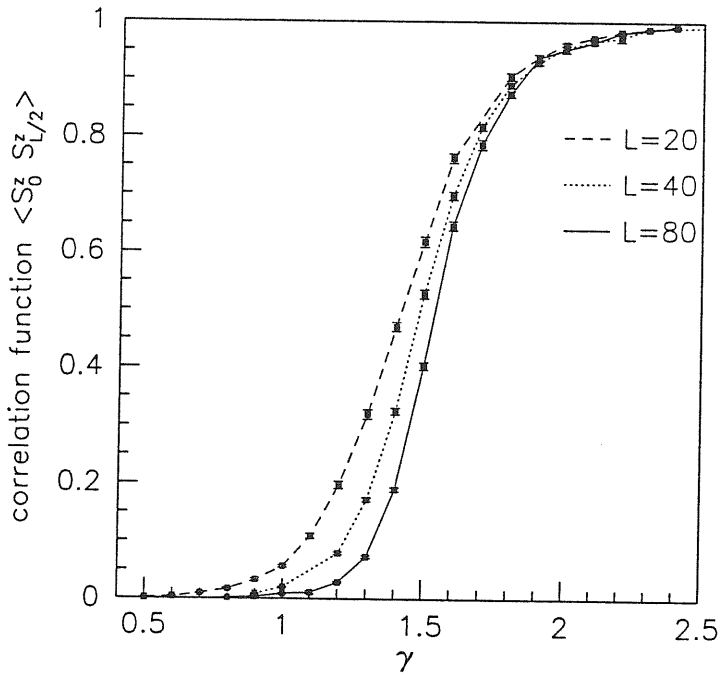

Figure 3.2: Spin $S = 1$ out-of-plane correlation function as a function of the interaction strength parameter γ for chains with $L = 20$ (dashed line), $L = 40$ (doted line), and $L = 80$ (full line). Lines are guide to the eye.

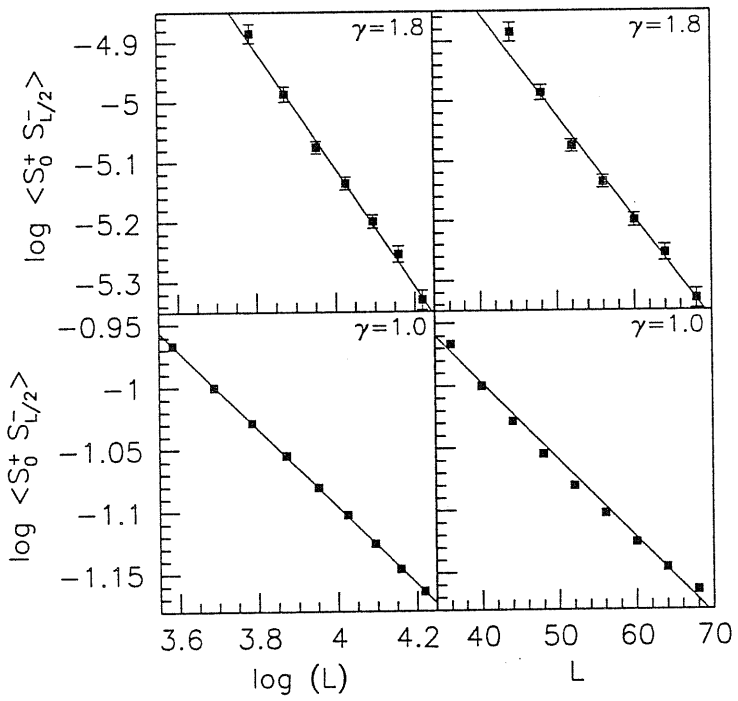

Figure 3.3: The in-plane correlation function in the disordered (lower figures) and in the ordered phase (upper figures). In the left figures power-law fit is used, whereas on the left figures an exponential fit behavior is used.

4 J_1-J_2 Model

4.1 Introduction

A very interesting case where the developed spin-wave variational wavefunction can be applied is the two-dimensional frustrated spin S=1/2 Heisenberg model on the square lattice. The model is defined by the Hamiltonian

$$\mathcal{H} = J_1 \sum_{<i,j>} \vec{S}_i \cdot \vec{S}_j + J_2 \sum_{[i,j]} \vec{S}_i \cdot \vec{S}_j \ , \tag{4.1}$$

where the symbols $< i, j >$ and $[i, j]$ mean that the summations run over the nearest-neighbor and next-nearest-neighbor sites, respectively. Each bond should be counted only once. In what follows we put $J_1 = 1$ and $\alpha = J_2/J_1$.

The attention to this particular model has been recently renewed to understand the nature of the high-temperature superconductor ground state. The ground state of most of undoped copper-oxide superconductors is well described by the spin-1/2 antiferromagnetic nearest-neighbors Heisenberg model on the square lattice. A good understanding of this model is now achieved [28]; it is well-established that the model has the conventional antiferromagnetic order in the ground state though a rigorous proof is still missing (for the last obtained limits see e. g. [29]). On the other hand, multi-band Hubbard model calculations show [30, 31] that, even in the undoped case, small but finite frustration J_2 is present in the CuO_2 planes and by doping can be increased [32]. Apart from interests for the frustrated Heisenberg Hamiltonian as a simplified model for doped high-temperature superconductors, understanding of the frustration in the spin systems is of a rather more general relevance. The strong correlation effects in quantum antiferromagnets may lead to new phases and reveal inherent characteristic of many-body systems. In the J_1-J_2 model the quantum fluctuations destroying the classical order are enhanced by the frustration and the low dimensionality giving an example for studying a transition between the magnetically ordered and the quantum disordered phase. A complete understanding of this model, ground state phases and transitions, would provide a better insight to the behavior of systems where the critical regime is driven by quantum fluctuations.

For the J_1-J_2 model there was a considerable number of analytical and numerical studies, but

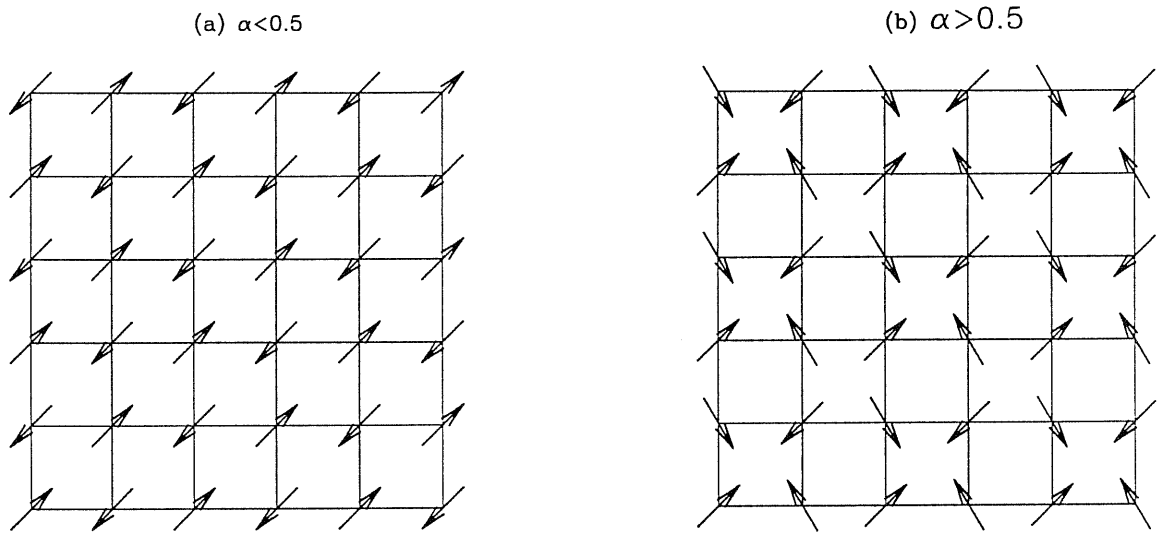

Figure 4.1: The classical ground states for $\alpha < 0.5$ (a) and $\alpha > 0.5$ (b), where $\alpha = J_2/J_1$. The arrow represent the orientation of the classical spins in the lattice site. The classical state for $\alpha > 0.5$ has a continuous degeneracy due to the independence of the relative orientation of the local magnetization in the two sublattices. The one shown is not special.

a satisfactory understanding of its ground-state properties is still not reached [21]. The classical ground state has the transition point at $\alpha = 0.5$; the phase for $\alpha < 0.5$ is represented by a standard two-sublattice Néel state whereas if $\alpha > 0.5$ the two sublattices become decoupled and a four-sublattice antiferromagnetic state is stable, where the order parameters in sublattices can have an arbitrary orientation with respect to one another. These states are represented in Fig. 4.1. Inclusion of the quantum fluctuations, which are in the spin-1/2 case very strong, offers the possibility to destroy long-range order and to open a window in the phase diagram of a spin-liquid phase without conventional antiferromagnetic order for a parameter region around $\alpha \sim 0.5$. A simple linear spin-wave analysis already reveals such tendency, however the next-order in the large-S expansion shows divergences [13] leaving an open question how to sum up all the terms of the spin-wave expansion. The proposed variational wavefunction maybe a good starting wavefunction to understand the model.

There are at least two important issues concerning the ground-state phase diagram of the model. The first is the location of the phase-transition boundary. Some theoretical [33, 34] and numerical [35, 36, 37] estimates give the critical value close to $\alpha_c = 0.4$ whereas the last exact diagonalization data [1] indicate the transition at $\alpha_c = 0.34$. However, in the Schwinger-boson mean-field calculations [38] a smaller value $\alpha_c = 0.15$ was found, whereas larger values around $\alpha_c = 0.6$ are also

obtained by self-consistent theories [39, 40, 41] and quantum Monte Carlo calculation [42]. The second issue is related to the question of existence and nature of the magnetically disordered phase in the strongly frustrated region. The main candidates are the magnetically disordered spin-Peierls dimer state and the chiral state. The first state is preferred by numerical studies [35, 36, 37], some analytical approaches like series expansion [43], and the 1/N expansion technique [44]. The other one was motivated by spontaneous time-reversal symmetry braking in high-temperature superconductors [45, 46, 47].

From our starting point we cannot say much about the nature of the ground state after the antiferromagnetic order is lost and phase transition is turned over, but we can determine the critical point α_c and the behavior of model parameters with increasing frustration as the ground state energy, the spin-wave velocity and the spin stiffness constant. Namely, starting from the antiferromagnetically ordered state we construct the variational wavefunction using the linear spin-wave theory and by monitoring the order parameter, the staggered magnetization, we can arrive at the phase transition point where the initial physical picture of the ground state is no longer valid. In order to reach other side of the critical point and to describe the new state which is set down, a different approach, such as Green function Monte Carlo, would be more appropriate and we should restrict our goal to the first question of the quantum phase transition in this model.

4.2 Spin-wave theory

Using the method developed in Chapter 2 we can construct the variational wavefunction for the J_1-J_2 model. The first step is to apply the linear spin-wave theory to the Hamiltonian (4.1). This Hamiltonian is a particular case of the more general Hamiltonian studied in Chapter 2 and the derived formulae yield the following expressions:

$$D_q = 1 - \alpha(1 - \cos q_x \cos q_y) , \tag{4.2}$$

$$\eta_q = -(\cos q_x + \cos q_y)/2 , \tag{4.3}$$

which via Eqs. (2.35) and (2.44) define the Jastrow potential and the variational wavefunction for the frustrated Heisenberg model:

$$v(R) = = \frac{2}{L}\sum_q e^{iqR}\left[1 - \sqrt{\frac{1 - \alpha(1 - \cos q_x \cos q_y) + (\cos q_x + \cos q_y)/2}{1 - \alpha(1 - \cos q_x \cos q_y) - (\cos q_x + \cos q_y)/2}}\right] , \tag{4.4}$$

$$|\psi_V> = P_{S^z_{tot}=0} e^{\frac{1}{2}\sum_{R,R'} v(R-R')S^z_R S^z_{R'}} |F> . \tag{4.5}$$

By means of this wavefunction our aim is to measure variational approximations of the ground-state energy and the order parameter on finite lattices. The variational calculation is performed by the standard Monte Carlo method.

The order parameter is given by the staggered magnetization

$$M_L^2 = \frac{1}{L(L+2)} \sum_{i,j} < \vec{S}_i \cdot \vec{S}_j > \zeta_{ij} \ , \tag{4.6}$$

where ζ_{ij} is the phase factor between two sublattices:

$$\zeta_{i,j} = \begin{cases} 1, & \text{if } i \text{ and } j \text{ are on the same sublattices;} \\ -1, & \text{if } i \text{ and } j \text{ are on the different sublattices.} \end{cases} \tag{4.7}$$

The unusual form of the normalization prefactor $1/[L(L+2)]$ is used in order to get an entirely size-independent quantity in the case of a perfect Néel state [48]. In the thermodynamic limit this choice is obviously equivalent to the usual prefactor $1/L^2$ but it has an advantage to suppress overestimated contributions from the terms $i = j$ in the sum (4.6) present in the small cluster. This plausible argument has been already used in the recent exact diagonalization study [1] and to compare results with the presented ones, it is more convenient to use the same notation.

Supposing that, for small enough frustration, the system has long-range antiferromagnetic order in the ground state, the large-distance, long-time behavior of the model is described by the quantum nonlinear sigma model [49] in the (2+1)-Euclidean dimensions, with the effective action depending on gradients of the order parameter in both space and time:

$$\mathcal{S} = \frac{\rho_s}{2} \int_0^\beta \mathrm{d}\tau \int \mathrm{d}^2 R \left[(\nabla \cdot \vec{n})^2 + \frac{1}{c^2} (\frac{\partial \vec{n}}{\partial \tau})^2 \right] \ . \tag{4.8}$$

The three-component vector field $\vec{n} \equiv \vec{n}(R, \tau)$, with constraint $\vec{n}^2 = 1$, describes the orientation of the staggered magnetization around the position R. The integration over the imaginary time variable τ should be extended to $\beta \to \infty$ because we are interested in the ground state properties of the system. The space integrals are carried out up to the maximum wavevector Λ. The spin stiffness ρ_s and spin-wave velocity c are effective parameters which should be extracted from the microscopic dynamics described by the Hamiltonian of the model. These two parameters, together with the expectation value of the order parameter, completely describe the low-energy, small-momentum physics of the system [50]. The renormalization group flow [49], characterized by a dimensionless coupling constant $g = c/(\Lambda \rho_s)$, shows that at zero temperature there is a quantum phase transition point at $g_c = 4\pi$ (one-loop value). The Néel order persists up to g_c and for $g > g_c$ there is a quantum disordered phase with a finite gap in the excitation spectrum.

Quantities characterizing the system in the thermodynamical limit can be estimated by the finite-size scaling analysis of the results obtained for a set of finite clusters. Within the assumption that the leading size dependence of observables is controlled by small-momenta magnons, the correction formulae for the ground state energy and the staggered magnetization of the finite-size antiferromagnetic systems can be derived [51, 52, 50]. The ground state energy E_{GS} of the L-site cluster is given by

$$E_{GS}/L = e_0 + \bar{\beta} \frac{c}{\sqrt{L^3}} + \cdots \ , \tag{4.9}$$

and the staggered magnetization by:

$$M_L^2 = m_0^2[1 + \bar{\alpha}\frac{c}{\rho_s\sqrt{L}} + \cdots] \; . \tag{4.10}$$

Here e_0 and m_0 are the ground state energy and order parameter in the thermodynamic limit, respectively. In the chosen normalization the perfect Néel state has $m_0 = 0.5$. The prefactors $\bar{\alpha}$ and $\bar{\beta}$ are functions of the shape of the cluster, specifically they depends on the form of the cluster and the boundary conditions, numerically they are of the order 1.

A careful finite-size spin-wave analysis of the model by Sorella and Zhong [13] has shown that fluctuations have an important rule for the strongly frustrated regime. The break-down of the $1/S$ expansion appears well before the classical critical point $\alpha = 0.5$. For completeness and easy reference we will report here some of their results. The ground state energy is given by

$$E_0 = S^2 E_{cl} + S E_{SW} + E_{int} \; , \tag{4.11}$$

where E_{cl} and E_{SW} are the classical and the spin-wave energy, respectively:

$$E_{cl} = -2L(1-\alpha) \; , \tag{4.12}$$

$$E_{SW} = -2\sum_q (\epsilon_q - D_q) \; , \tag{4.13}$$

where $\epsilon_q = \sqrt{D_q^2 - \eta_q^2}$. The spin-wave interaction energy is given by:

$$E_{int} = -\frac{L}{2}(C_1^2 - \alpha C_2^2) + 2C_1 \; , \tag{4.14}$$

$$C_1 = \frac{2}{L}{\sum_q}'(v_q^2 + \eta_q u_q v_q) \; , \tag{4.15}$$

$$C_2 = \frac{2}{L}{\sum_q}'(1 - \cos q_x \cos q_y) v_q^2 \; , \tag{4.16}$$

where v_q and u_q are defined by Eqs. (2.29) and (2.28). Primes on sums denote exclusion of the singular modes. The expression for the magnetization reads:

$$M_L^2 = \sqrt{\frac{L}{L+2}}\left[(S - C_3)^2 + \alpha(C_1 - C_2)C_4 + C_5\right] \; , \tag{4.17}$$

$$C_3 = \frac{1}{L}{\sum_q}'\left[\frac{1 - \alpha(1 - \cos q_x \cos q_y)}{\epsilon_q} - 1\right] - \frac{2}{L} \; , \tag{4.18}$$

$$C_4 = \frac{1}{L}{\sum_q}'\frac{(1 - \cos q_x \cos q_y)\eta_q}{\epsilon_q^3} \; , \tag{4.19}$$

$$C_5 = \frac{1}{2L^2}{\sum_q}'\frac{\eta_q^2}{\epsilon_q^2} \; . \tag{4.20}$$

The normalization in Eq. (4.17) is changed with respect to the one of Ref. [13] in order to be consistent with Eq. (4.6).

In the following expressions for the spin-wave velocity and spin stiffness the infinite-size limit of C_1 and C_2 should be used:

$$c = 2S\left[\sqrt{2(1-2\alpha)} - \frac{1}{2S}\left((1-\alpha)C_1^{(\infty)} - \alpha C_2^{(\infty)}\right)\right] , \tag{4.21}$$

$$\rho_s = \frac{m_0^2 c}{\kappa^2} . \tag{4.22}$$

$$\kappa^2 = \frac{1}{\sqrt{2(1-2\alpha)}}\left[(2S - m_0) + \alpha\frac{C_1^{(\infty)} - C_2^{(\infty)}}{4(1-2\alpha)}\right] . \tag{4.23}$$

The infinite size staggered magnetization m_0 is obtained taking the limit $L \to \infty$ in Eq. (4.17).

4.3 Sum-rule consistent variational calculation

The form of the variational wavefunction (4.5) follows from the requirement to properly include the zero-point motion of the spin-waves into the variational state. The long-wavelength spin waves then determine the long-range behavior of the Jastrow potential, which is in two dimensions:

$$\lim_{R\to\infty} v(R) = -\frac{g_0}{\pi R} , \tag{4.24}$$

where g_0 is the constant in the expansion of the function g_q:

$$g_q = \frac{g_0}{q} + \cdots . \tag{4.25}$$

The system described by the variational state (2.35) can be equivalently represented as the system of hard-core bosons on the lattice having the same Jastrow potential Eq. (2.38) where S_R^z operator corresponds to the boson density operator ρ_R. The spin-wave excitations of the spin system have a correspondence with the density fluctuations of the boson system. In the analogous way as in the spin system, the zero-point motion of phonons produces the long-range tail of the bosonic Jastrow wavefunction, as have been shown by Reatto and Chester [53, 54]:

$$\lim_{R\to\infty} v(R) = -\frac{mc}{4\pi\rho R} , \tag{4.26}$$

where c is the sound velocity, m mass, and ρ density of bosons. Bosons on the lattice have "mass" $m = 2$ and $S_{tot}^z = 0$ state of spin system corresponds to $\rho = 1/2$. The influence of the long-range behavior on the spin-wave velocity can be used to improve the variational wavefunction using the sum rules.

Following Liu and Manousakis [55] we can define the dynamical structure factor:

$$S(q,\omega) = \sum_n | < n|S_q^z|0 > |^2 \delta(\omega - (E_n - E_0)) , \tag{4.27}$$

where $|n>$ represents the complete set of the eigenstates of the Hamiltonian (4.1) with energies E_n, and $|0>$ being the ground state. The integrals of $S(q,\omega)$ give three useful sum rules which

can be easily proved using standard methods [56]:

$$S(q) = \int_0^\infty S(q,\omega)\mathrm{d}\omega = < 0|S_q^z S_{-q}^z|0 > , \tag{4.28}$$

$$\int_0^\infty \omega S(q,\omega)\mathrm{d}\omega = \frac{1}{2} < 0|[S_{-q}^z,[\mathcal{H},S_q^z]]|0 > \tag{4.29}$$

$$= f_1[4-2(\cos q_x + \cos q_y)] + f_2[4 - 4\cos q_x \cos q_y] ,$$

$$\frac{1}{2e''} = \lim_{q\to 0}\int_0^\infty \frac{S(q,\omega)}{\omega}\mathrm{d}\omega = \lim_{q\to 0}\sum_{n\neq 0}\frac{|< n|S_q^z|0 >|^2}{E_n - E_0} , \tag{4.30}$$

where $S(q)$ is the structure factor, and f_1, f_2 being the spin equivalent of the kinetic energy average:

$$f_l = -\frac{1}{4} < 0|S_i^+ S_j^- + S_i^- S_j^+|0 > , \tag{4.31}$$

$$l = \begin{cases} 1, & i \text{ and } j \text{ are nearest neighbors;} \\ 2, & i \text{ and } j \text{ are next-nearest neighbors.} \end{cases} \tag{4.32}$$

In the third sum rule e'' is the second derivative of the ground state energy per site with respect to the total magnetization of the system $M = 1/L < 0|\sum_i S_i^z|0 >$. The argument of Ref. [55] for the isotropic Heisenberg model can be extended to the frustrated case and it follows that the spin-wave velocity and spin stiffness are given by

$$c = \sqrt{2(f_1+f_2)e''} , \tag{4.33}$$

$$\rho_s = 2(f_1+f_2) . \tag{4.34}$$

Namely, in the long-wavelength limit the right-hand side of the second sum rule gives $(f_1+f_2)q^2$ whereas the left-hand side, assuming that the sum rule is exhausted by a single magnon, can be estimated by $\omega_q S(q)$. By the same assumption, the third sum rule gives $S(q) \approx \omega_q/2e''$ and using $\omega_q = cq$, the expression (4.33) for the spin-wave velocity follows. Noticing that the susceptibility per site χ for a field perpendicular to the staggered magnetization is defined by $\chi = 1/e''$, it follows the relation for the spin stiffness (4.34). The susceptibility can be obtained by considering the ground-state energy as a function of the total magnetization M.

In the derivation of the variational wavefunction there have not been introduced any variational parameter at all. In order to improve the variational state we can modify the Jastrow potential to give a lower ground state energy and to obey the sum rules. The minimal change which can fulfill both requirements and would not spoil the important long-range behavior of the potential is to take the values of the Jastrow at the nearest-neighbors and the coefficient g_0 as variational parameters. Accommodating the Jastrow potential at the short distance to obtain the lower ground state energy the long-range tail is not changed and the sum rule can be satisfied. In fact, if for a given value g_0 we determine the curvature of the ground-state energy with the total magnetization M and the averages f_1 and f_2, then from Eq. (4.33) follows the spin-wave velocity c. Such obtained spin-wave velocity should be consistent with the Chester and Reatto relation (4.24) and (4.26). This defines a self-consistent procedure to obtain the variational parameter g_0.

The iteration process converges very fast and the stable value is obtained after few steps, rendering the iteration calculation feasible in a reasonable time. The bare small-q limiting value is renormalized between 10% and 20%. The self-consistency should be obtained for a series of values for α in order to describe the full phase diagram for the antiferromagnetic state. To obtain the complete result for one value of the frustration parameter α, including the self-consistency iteration and the variational calculation of the energy and the order parameter we needed up to 10 hours of the CPU time on the `IBM RS6000/590` computer.

The model parameters can be now calculated by two independent methods: using the finite-size scaling analysis and by the sum-rule consistent procedure. Both methods are essentially based on the one-magnon approximation and the results for the model parameters should not be too different. After the phase transition the used approximation are no longer valid and a big discrepancy between the two methods could appear. Our numerical results corroborate the consistency of the two methods showing well agreement of the spin-wave velocity and spin stiffness data calculated by the two independent ways, as could be seen from the next section.

4.4 Results of the variational calculation

The Jastrow potential in the momentum space g_q (2.44) is singular for $\alpha = 0.5$ not only at the center of the Brillouin zone $q = (0,0)$, but also at the lines where $q_x = 0$ or $q_y = 0$. For $\alpha < 0.5$ g_q is finite at these lines but it still remains much bigger than in the remaining points of the Brillouin zone. In order to avoid a bias in the results from the inappropriate influence of the modes with $q_x = 0$ or $q_y = 0$ on the variational wavefunction, it is better to perform the variational calculation on lattice with boundary conditions where the number of such modes is minimal. We have chosen the set of tilted lattices of the Oitmaa-Betts type [57] of size $L = (2n+1)^2+1$, $n = 2, 3, \ldots, 10$ with periodic boundary conditions. For these clusters $q = (0,0)$ appears to be the only singular point, therefore they are a proper choice for the variational calculation with the spin-wave wavefunction. An example of the lattice of the size $L = 50$ is shown in Fig. 4.2 and the corresponding Brillouin zone is shown in Fig. 4.3.

Comparison of the variational ground-state energy and staggered magnetization with the spin-wave results is shown in Fig. 4.4 and Fig. 4.5. For small frustration, the second order of the finite-size spin-wave expansion gives almost the same results as the variational calculation. When the frustration increases the variational results show an improvement with respect to the spin-wave. The frustration strongly destabilize the $1/S$ spin-wave expansion, e. g. the second order contribution for the magnetization becomes meaningless soon after $\alpha = 0.3$ whereas the variational calculation gives reasonable results up to $\alpha = 0.45$.

Besides the spin-wave theory treatment, it is possible to compare the variational results with the recent exact diagonalization studies by Schulz, Ziman, and Poilblanc [1, 37]. The clusters in their

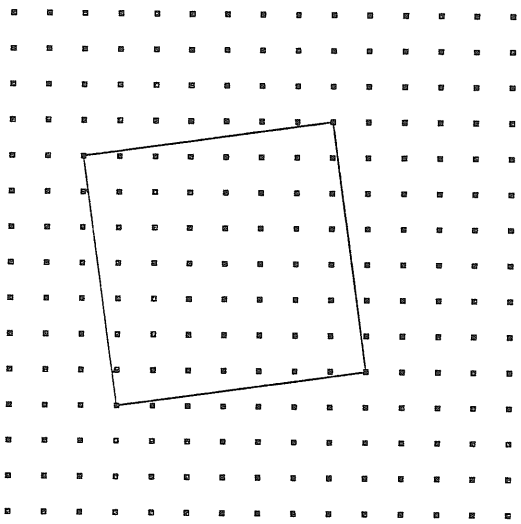

Figure 4.2: An example of the clusters used in the variational calculation corresponding to $L = 50$ sites. The whole plane could be covered by suitable translations of the denoted cell.

study ($L = 16, 20, 32, 36$) are not a well suitable choice for our variational wavefunction which is especially revealed for the $L = 16$ cluster where almost half of the q-points become anomalous in the Jastrow potential. The $L = 20$ cluster has a special symmetry and we have not considered this case. The comparison of the variational and the exact ground-state energy is shown in Fig. 4.6 and the one for the finite-size order parameter in Fig. 4.7.

The variational calculation, even with the plain wavefunction without adjustment of the nearest-neighbor coupling yields the ground-state energy very close to the exact one. The difference between exact and variational ground-state energy is not specially pronounced for the spin-wave very anomalous $L = 16$ cluster because the energy is not very much affected by the long-range shape of the wavefunction. The order parameter instead is more sensitive to the long-range Jastrow tail. There is a big discrepancy between exact and variational data for $L = 16$ cluster whereas for the $L = 36$ case having relatively small portion of singular point the staggered magnetization differs less than 1% for the plain wavefunction, and less than 0.1% for data from the self-consistent calculation. After the transition point, which is from the variational data a little over $\alpha = 0.4$, the accordance of data is lost and the new phase in not well described by the spin-wave variational state.

The finite-size staggered magnetization results indicate the phase transition for frustration over $\alpha = 0.4$. In Fig. 4.8 least square fit of our variational data with the finite-size scaling formula (4.10) is shown. Data follow the scaling line very well up to the frustration $\alpha < 0.41$. After $\alpha = 0.41$ the scaling-law becomes poor and the infinite-size order parameter seems to vanish, indicating

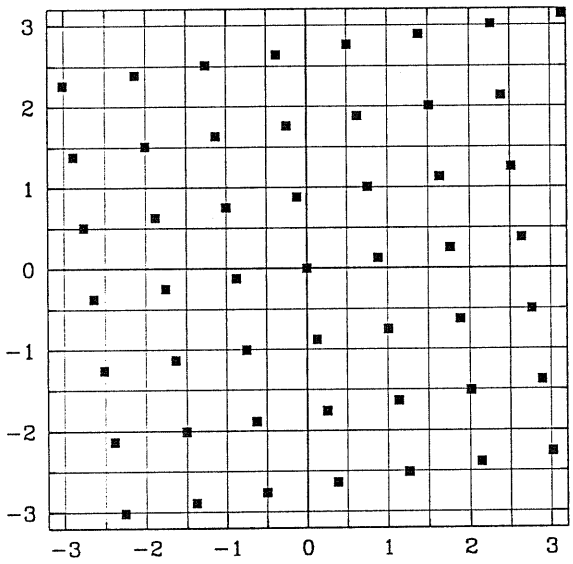

Figure 4.3: The first Brillouin zone for the lattice with $L = 50$ sites and periodic boundary conditions. In this particular lattice symmetry the most of the points being singular for the Jastrow potential at $J_2/J_1 = 0.5$ are avoided.

a phase transition. The resulting phase diagram is displayed in Fig. 4.9, the data represented by triangles correspond to the plain variational wavefunction without any adjusting parameter, whereas by squares we represented data from the wavefunction which is consistent with the sum rules. The extrapolated value in the isotropic limit $\alpha = 0$ is $m_0 = 0.3354(3)$ which is close to the exact diagonalization estimate [1] $m_0 = 0.3245$ and not very far from the best current estimates from Quantum Monte Carlo calculations [58] $m_0 = 0.307$ and the spin-wave estimate $m_0 = 0.3034$.

The self-consistent modification of the long-range prefactor in the Jastrow potential moves the critical point from $\alpha_c \approx 0.46$ to $\alpha_c \approx 0.41$. The exact diagonalization data [1] give the critical value α_c being in the interval $0.31 - 0.48$ depending on the combination of the clusters used in the finite-size analysis, with a slightly better fit for $\alpha_c = 0.34$ which represents the suggested value for the transition point. However, since in the smaller cluster the variational data and exact diagonalization ones are in very good agreement, we are more confident of the infinite-size extrapolation obtained at the variational level with size up to 442.

In the direct calculation of the spin stiffness by exact diagonalization Einarsson and Schulz [59] obtained the critical point to be grater than 0.4 which is in agreement with our estimate of the transition point.

Fits of the ground-state energy per site and extrapolated infinite-size value are shown in Fig. 4.10 and Fig. 4.11, respectively. The scaling law is satisfied better for the energy than the one for the

staggered magnetization, because of the smaller finite-size correction terms for the energy. After the transition the fit is considerably worse, as the assumption of the long-range order is probably not applicable to the new phase. The isotropic-limit value $e_0 = -0.6625(7)$ is very close to the best Green function Monte Carlo estimate $e_0 = -0.66934$ taken from Ref. [58]. The improvement by varying the nearest-neighbor value in the Jastrow is very small, less than 0.5%. The difference with respect to the spin-wave theory predications is much smaller for the energy than for the order parameter. The same observation was found for the exact diagonalization observation.

The nonlinear sigma model parameters are obtained from the finite-size scaling analysis using the formulae (4.9) and (4.10) where for the shape factors we have used the values [51] $\bar{\alpha} = 0.6208$, and $\bar{\beta} = 1.4372$. For $\alpha = 0$ the fit gives the spin-wave velocity $c = 1.367(25)$ and the spin stiffness $\rho_s = 0.170(5)$. The reliable results from Ref. [1] are $c = 1.28$ $\rho_s = 0.125$ and the spin-wave theory results is $c = 1.65$, and $\rho_s = 0.18$. The present results are very close to the spin-wave predictions. The agreement is even better for the values obtained from the sum rules consistency calculations, where we obtained $c = 1.552(5)$ and $\rho_s = 0.175(4)$. From the direct calculation of the spin stiffness [59] follows $\rho_s = 0.183(3)$ and $c = 1.67$ which is very close to the spin-wave theory values and to our estimates. The two methods of extracting the model parameters give consistent results. The agreement is better for the spin stiffness than for the spin-wave velocity, as can be seen from Fig. 4.12 and Fig. 4.13. The spin stiffness data for frustrated case are very similar to the ones from the direct calculation of Ref. [59], whereas for the spin-wave velocity there is bigger difference. The estimates beyond the critical point become worse which is consistent with the existence of a qualitatively different ground state.

4.5 Summary and discussion

In this chapter we have used the spin-wave variational wavefunction for the frustrated antiferromagnetic spin-1/2 Heisenberg model on the square lattice. The calculation was performed on tilted lattices with size $L = (2n+1)^2 + 1$ for $n = 2, \ldots, 10$. The variational state was improved using the constraint coming from the sum rules for the structure factor $S(q)$ and the known long-range behavior of the Jastrow potential coming from the zero-point motion of single-quasiparticle excitations. Using the nonlinear sigma model formulae for finite size corrections to the ground-state energy and staggered magnetization in the quantum antiferromagnet we estimated the parameters describing the system in the ordered state and the phase transition position. The spin-wave velocity and spin stiffness were determined independently by means of the scaling law and by the one-magnon approximation of sum rules.

Probably the most important result is that the antiferromagnetic order is destroyed well before the classical transition point. We found the critical frustration to be $J_2/J_1 = 0.41 \pm 0.01$. A very similar phase diagram was obtained by the finite size scaling analysis of exact diagonalization data [1] and by the direct calculation of the spin stiffness on the finite lattices [59], with critical cou-

plings $J_2/J_1 = 0.34 \pm 0.04$ and $J_2/J_1 = 0.4$, respectively. The linear spin-wave theory gives a very similar result, whereas in the higher orders in $1/S$ expansion the $J_2/J_1 \rightarrow 0.5$ singularity seems to be too strong and prevents reasonable extrapolations. For $J_2 = 0$, in the unfrustrated case, the ground-state energy and the order parameter are in good agreement with the best converged results by series expansion [60] and quantum Monte Carlo calculations [58]. Use of the variational wavefunction substantially improves the spin-wave expansion results for the strong frustration regime. Comparison with the exact diagonalization data [1] up to the transition point gives a very good agreement with some exception ($L = 16$), determined by the special symmetry of the cluster. The model parameters obtained from the sum-rule consistent method are in agreement with the ones obtained by an independent extrapolation of the finite size data. The present discrepancy is not too big and can be accepted.

The spin-wave variational wavefunction have been proved to be very useful in the study of the $J_1 - J_2$ model extending the linear spin-wave theory and overwhelming the difficulties coming from the $\alpha \rightarrow 0.5$ singularity present in higher order. Its estimates of the order-disorder phase transition point and the nonlinear sigma model parameters are consistent with the best exact diagonalization data. The wavefunction can be improved using only two variational parameters for the nearest-neighbor coupling and the long-range tail prefactor in the Jastrow potential. These features of the wavefunction can be very successfully used in quantum Monte Carlo methods that need a good starting guess of the ground state.

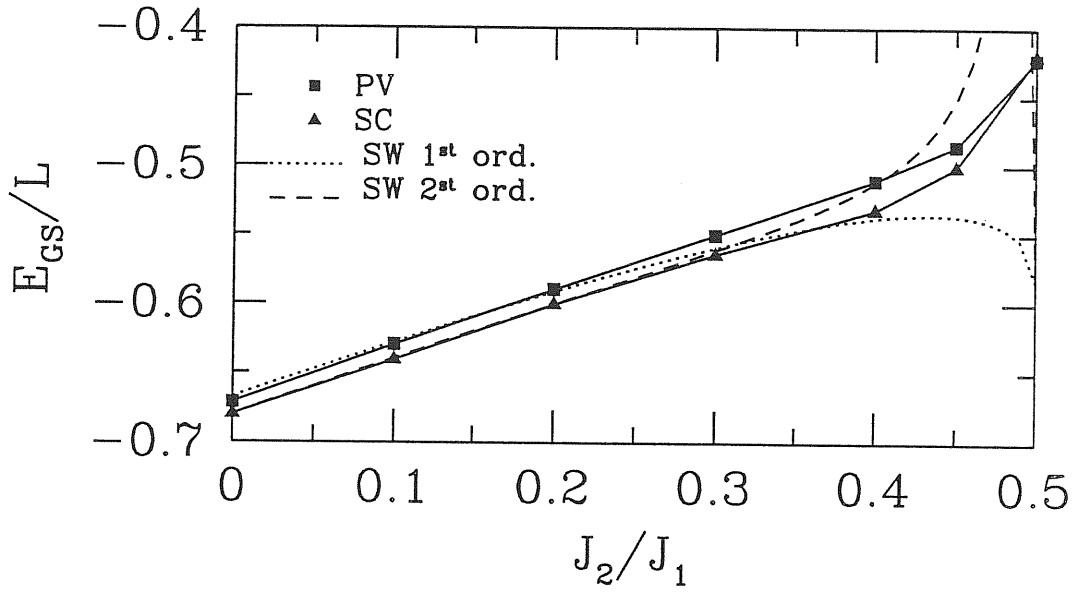

Figure 4.4: Comparison of the ground-state energy per site obtained by the plain variational wavefunction (squares) and by the sum-rule consistent method (triangles) with the spin-wave $1/S$ expansion results for lattices of size $L = 36$. The full lines are guides to the eye. The error bars are smaller than the size of the symbols.

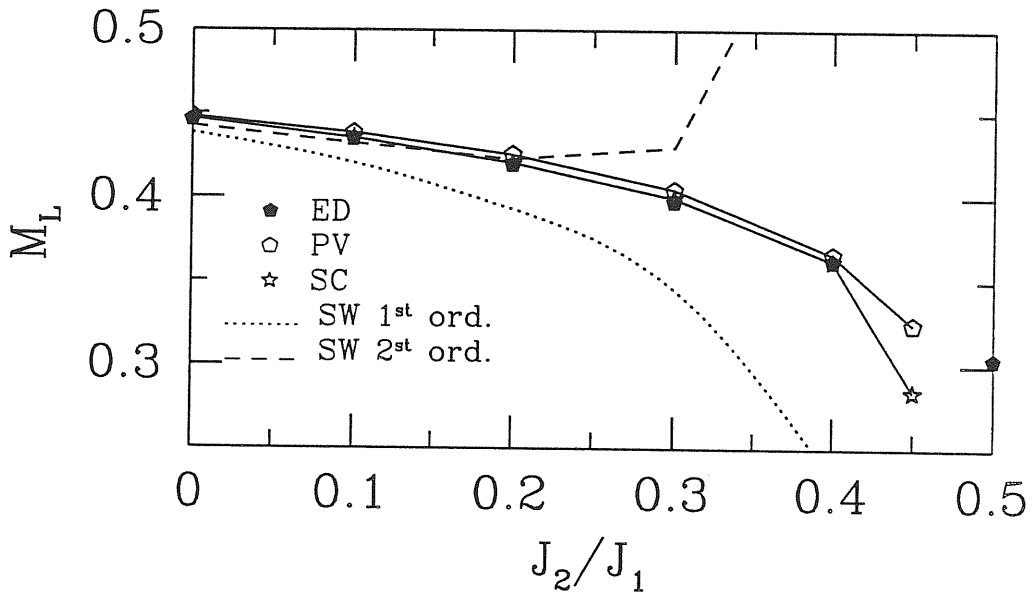

Figure 4.5: Comparison of the staggered magnetization obtained by the plain variational wavefunction Eq. (4.5) (PV) and by the sum-rule consistent method Eqs. (4.33) and (4.34) (SC) with the spin-wave $1/S$ expansion results (SW) for lattices of size $L = 36$. Symbols for the exact diagonalization data (ED) mainly cover the ones for the sum-rule consistent data. The full lines are guides to the eye. The error bars are smaller than the size of the symbols.

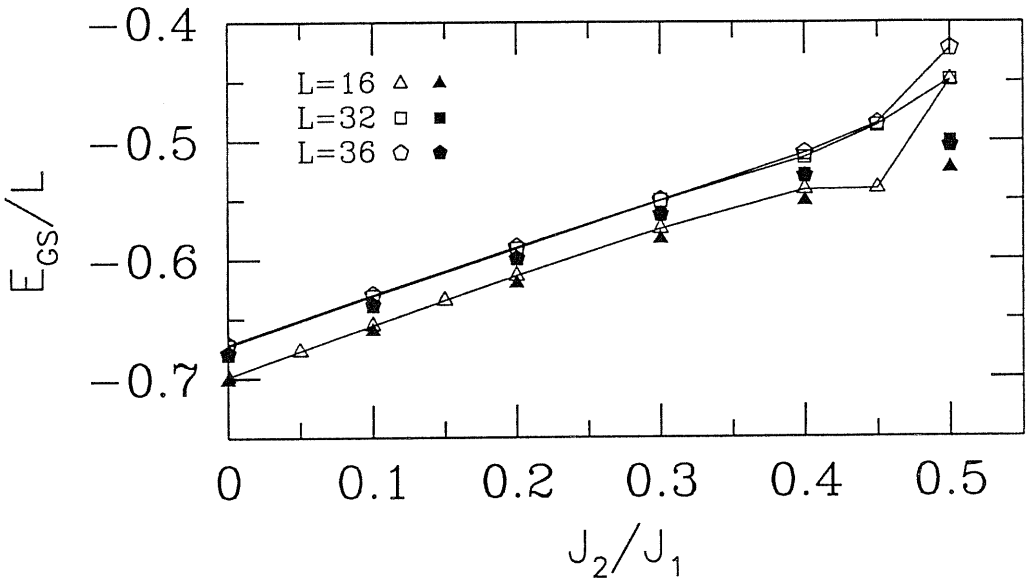

Figure 4.6: The ground-state energy per site obtained by the exact diagonalization [1] (full symbols) and by the sum-rule consistent variational calculation Eqs. (4.33) and (4.34) (empty symbols) for lattices of size $L = 16, 32, 36$. The error bars are smaller than the size of the symbols. The lines are guides to the eye.

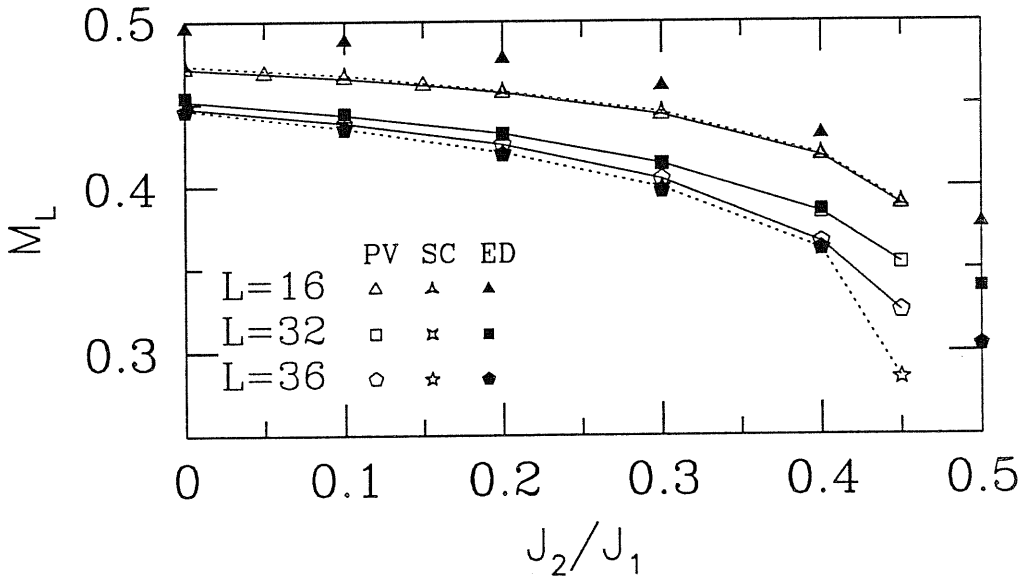

Figure 4.7: The staggered magnetization obtained by the exact diagonalization [1] (full symbols) and by the variational calculation with the plain wavefunction Eq. (4.5) and by the sum-rule consistent method Eqs. (4.33) and (4.34) (empty symbols) for lattice-sizes $L = 16, 32, 36$. The lines are guides to the eye: full lines connect data for the plain variational wavefunction and dotted line data for the sum-rule consistent one. The error bars are smaller than the size of the symbols.

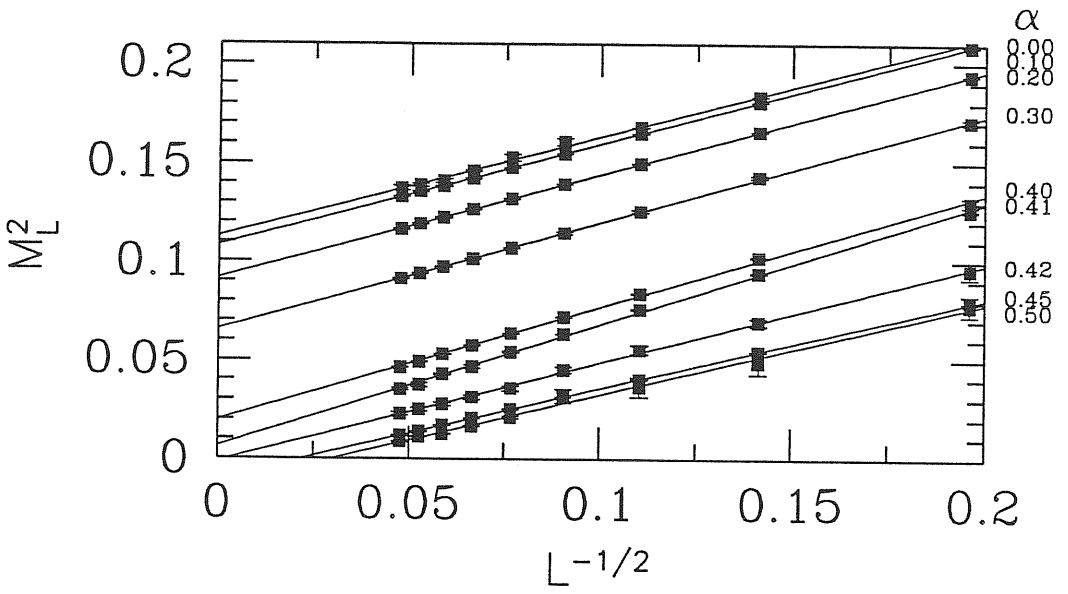

Figure 4.8: The finite-size scaling results for the variational estimate of the staggered magnetization M_L^2 obtained by the sum-rule consistent variational calculation Eqs. (4.33) and (4.34) for different frustrations $\alpha = J_2/J_1$. The straight lines are least square fit of the data to the scaling law.

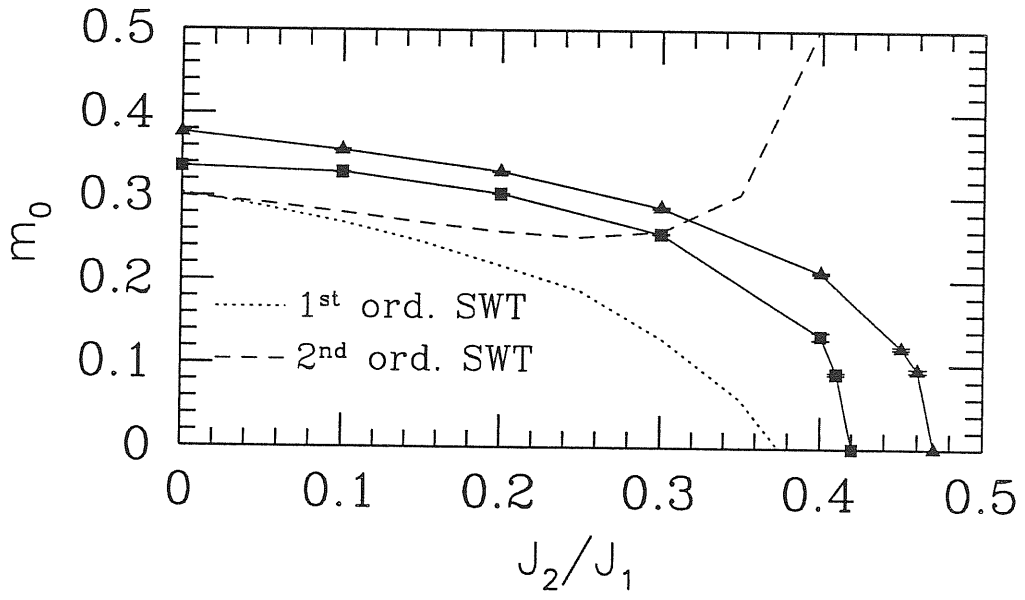

Figure 4.9: The infinite-size staggered magnetization m_0 for the plain variational state Eq. (4.5) (triangles) and for the sum-rule consistent one obtained from Eqs. (4.33) and (4.34)(squares). The full lines are guides to the eye. The dotted and the dashed lines are the first and the second order spin-wave expansion results, respectively.

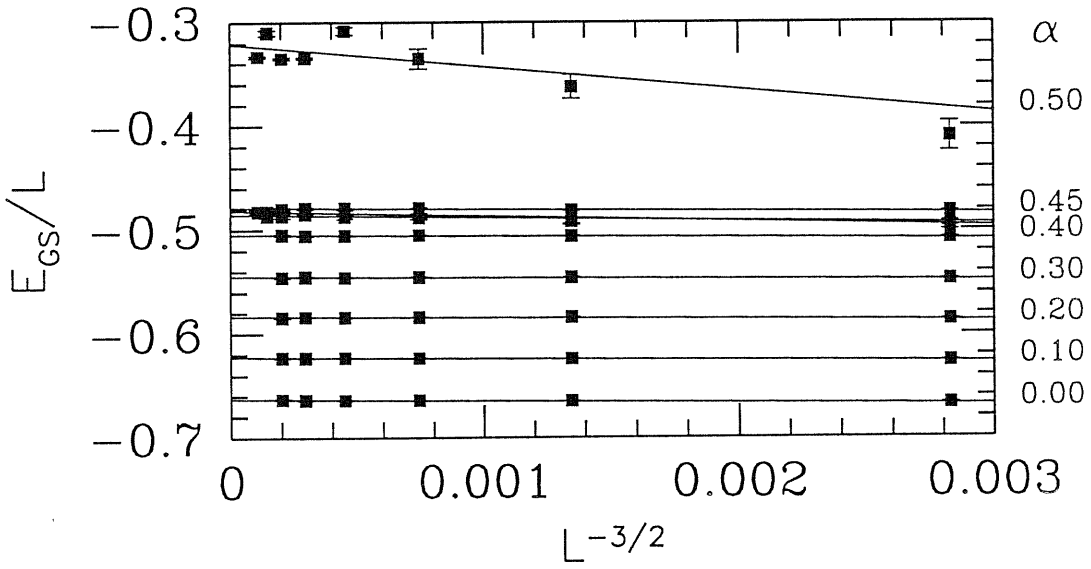

Figure 4.10: The finite-size scaling results for the ground state energy E_{GS} obtained by the sum-rule consistent method Eqs. (4.33) and (4.34) (empty symbols) for different frustrations $\alpha = J_2/J_1$. The straight lines are least square fit of the data to the scaling law.

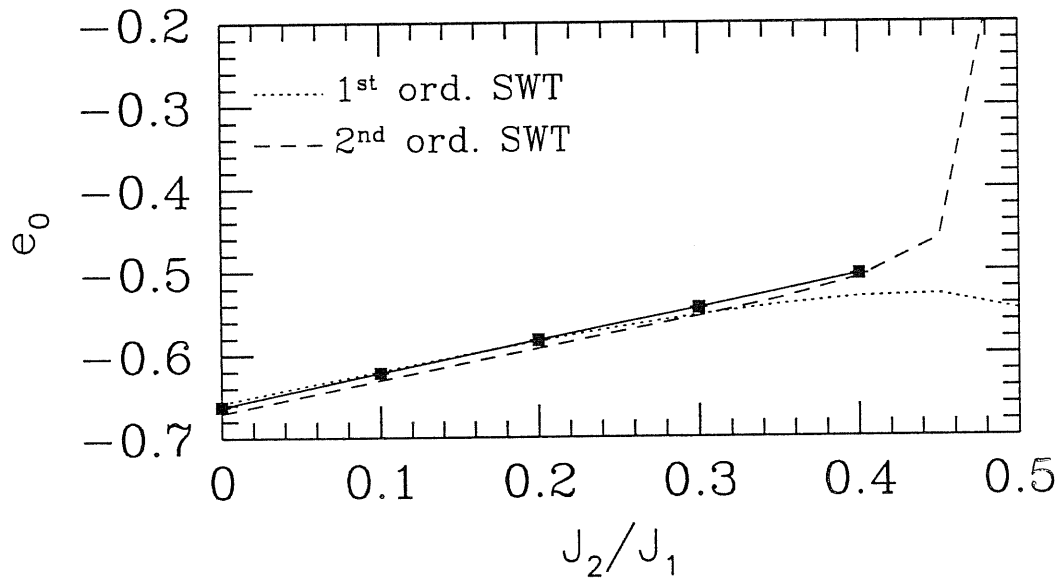

Figure 4.11: The infinite-size ground-state energy e_0 for the sum-rule consistent variational state (squares). The plain variational state results cannot be distinguished from the improved ones on this scale. The full line is a guide to the eye. The dotted and the dashed lines are the first and the second order spin-wave expansion results, respectively.

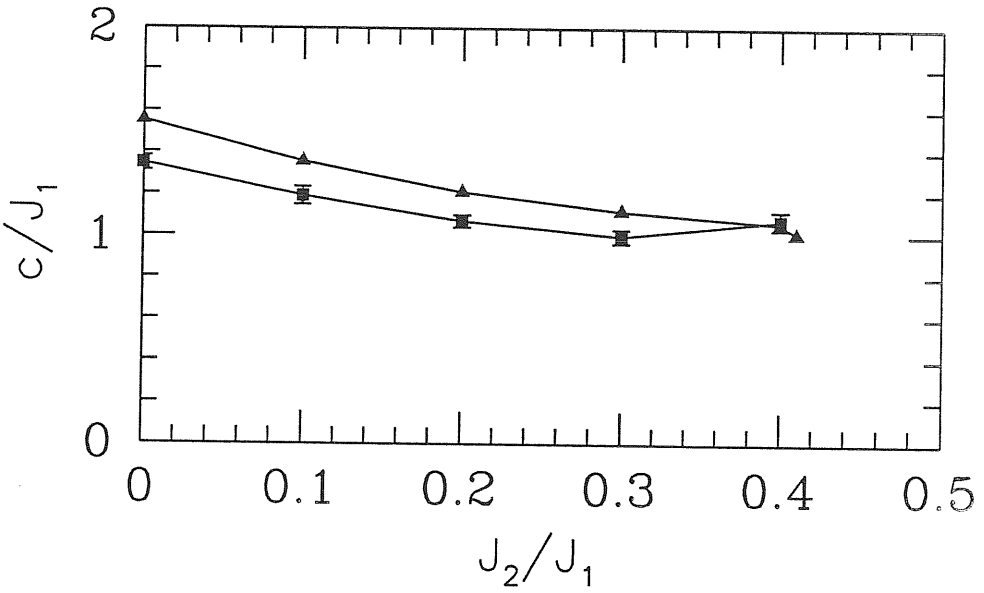

Figure 4.12: The spin-wave velocity c from the finite size scaling (squares) and the sum rule calculation (triangles). The full lines are guides to the eye.

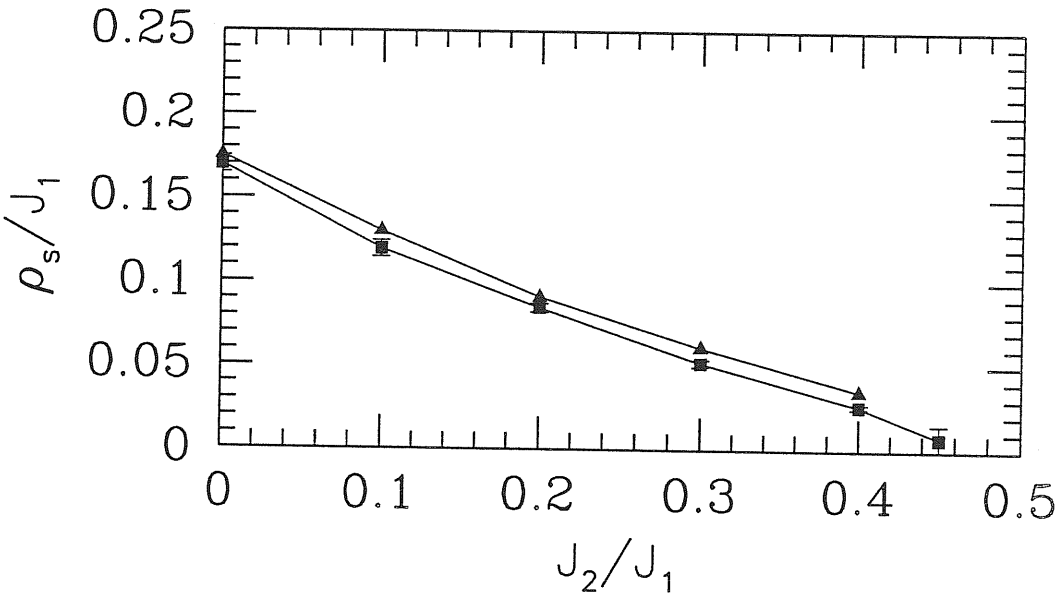

Figure 4.13: The spin stiffness from the finite size scaling (squares) and the sum rule calculation (triangles). The full lines are guides to the eye.

5 Hard-core bosons

5.1 Introduction

Probably one of the most successful application of our spin-wave variational wavefunction (2.35) is the case of the hard-core boson system in two dimensions. We consider the problem of N bosons on the square lattice with L sites with the Hamiltonian:

$$\mathcal{H} = -t \sum_{<i,j>} (b_i^\dagger b_j + b_j^\dagger b_i) - \mu \sum_i b_i^\dagger b_i \ , \tag{5.1}$$

where $b_i^\dagger$, b_i are bosonic operators:

$$[b_i, b_j^\dagger] = 1 \ , \tag{5.2}$$

which obey the hard-core constraint:

$$b_i^\dagger b_i \leq 1 \ . \tag{5.3}$$

The chemical potential μ is defined by the average density $\rho = N/L$. The constraint of no double occupancy represents the strong correlations between the bosons and it is difficult to treat by conventional many-body techniques. If the usual Bogoliubov theory of interacting boson gas is applied [61], the infinite on-site potential required by the hard-core nature of bosons gives a misleading result as the sound velocity becomes infinite.

The constraint of no double occupancy for spinless fermions is obviously satisfied by the Pauli principle and in this respect there should be a close relation between fermionic systems and hard-core bosons. In one dimension the mapping of the fermionic system to a bosonic system is an essential tool for the study of strongly correlated systems. One of the most famous example is the Lieb-Schulz-Mattis solution [62] of the one-dimensional spin $S = 1/2$ XY model by means of the Jordan-Wigner transformation. In this approach the spin system is mapped onto a free spinless fermion system using the soliton-like operator

$$K_l = e^{i\pi \sum_{j=1}^{l-1} S_j^+ S_j^-} = e^{i\pi \sum_{j=1}^{l-1} (S_j^z + \frac{1}{2})} \ . \tag{5.4}$$

The naive extension of this approach to higher dimensions leads to highly nonlocal interactions which are very hard to treat by standard methods. The new options for the two-dimensional systems arrive from the works on the fractional statistics and the Chern-Simons term in the corresponding field theory (see e. g. [63]).

Fradkin [64] have shown that the two-dimensional hard-core bosons can be mapped onto a system of fermions with an attached local flux determined by the local density of particles. This solution shows how to construct the mapping between fermionic and bosonic system but the resulting Hamiltonians are still hard to deal exactly. Here a different approach will be applied. Let us consider the two-dimensional spin $S = 1/2$ XXZ model in the presence of an external magnetic field h_z:

$$\mathcal{H} = \sum_{<i,j>} [-J(S_i^x S_j^x + S_j^x S_i^y) + J_z S_i^z S_j^z] - Sh \sum_i S_i^z \tag{5.5}$$

$$= \sum_{<i,j>} [-\frac{J}{2}(S_i^+ S_j^- + S_j^+ S_i^-) + J_z S_i^z S_j^z] - Sh \sum_i S_i^z \ , \tag{5.6}$$

where $S_l^+ = S_l^x + iS_l^y$ and $S_l^- = S_l^x - iS_l^y$ are spin-flip operators. They act on the ferromagnetic state $|F>$ as the creation and the destruction operators of a spin flip. On the different sites they commute $[S_l^+, S_{l'}^-] = 0$, but on the same site anticommute $\{S_l^+, S_l^-\} = 1$, because we can not flip spins twice on the same site. A natural representation of the spin-flip operators is by the bosonic ones with the hard-core constraint:

$$S_l^+ = b_l^\dagger \ , \tag{5.7}$$

$$S_l^- = b_l \ , \tag{5.8}$$

$$S_l^z = S - b_l^\dagger b_l \ . \tag{5.9}$$

Thus, the model equivalent to the one described by the Hamiltonian (5.5) in terms of the hard-core boson operators reads:

$$\mathcal{H}_b = -\frac{J}{2} \sum_{<i,j>} [b_i^\dagger b_j + b_j^\dagger b_i] + J_z \sum_{<i,j>} b_i^\dagger b_i b_j^\dagger b_j - (Sh + ZJ) \sum_i b_i^\dagger b_i + S^2 ZJL \ , \tag{5.10}$$

with constraint (5.3). Z is the lattice coordination number. If we take the limit $J_z = 0$ the resulting model is identical to the problem we are interested in, Eq. (5.1). This way of reasoning was used more than forty years ago by Matsubara and Matsuda [65].

The $J_z = 0$, $h_z = 0$ limit of the XXZ model is usually referred as the XY model. The $h = 0$ limit corresponds to the half-filled $N = L/2$ bosonic system. For this model Kennedy, Lieb and Shastry [66] proved that long-range order exists for the ground state in all dimensions grater than one and all spins $S \geq 1/2$. In the bosonic language this result implies the existence of the Bose condensate. Due to the proved long-range order, the variational wavefunction (2.35) should be appropriate to describe the ground state of the Hamiltonian. It is however amazing how accurately the spin-wave wavefunction works for the hard-core bosons. The variational estimation for the

ground-state energy is extremely close to the exact one (the relative error is less than $2 \cdot 10^{-4}$, but more important is that the ground state has an overlap square grater than 99.8% with the exact ground state. Thus, the spin-wave wavefunction yields practically an exact numerical solution of this model.

It is interesting to compare the hard-core boson density correlation function with analogous calculations for the two-dimensional $t-J$ model. This model was studied in an enormous number of articles because of its close relation to the high-temperature superconductivity, particularly as a main candidate to find the Luttinger liquid behavior in two dimensions. In one dimension a Luttinger liquid systems has the spin and charge degrees of freedom separated: at low energies they have independent elementary excitations with different velocities and characteristic wavevectors. The high temperature expansion results for the t-J density correlation functions by Putikka *et al* are very close to the one obtained here for the hard-core bosons. This means that the low-energy charge degrees of freedom in the $t-J$ model maybe represented by hard-core bosons only, implying that the spin degrees of freedom could be possibly decoupled.

5.2 Derivation of the "spin-wave" variational wavefunction

In Chapter 2 we have derived the form of the variational wavefunction for a quite general spin Hamiltonian, but the case with the coupling to the external magnetic field was not included. This additional term do not change conceptually the derivation scheme. However, the derivation of the wavefunction has some subtle point and it maybe useful to outline the main steps. At the classical level, the magnetic field orders the spins in the direction which points out from the XY plain where magnetization lays for zero field. This introduces a little more involved expressions.

In units $J = 2t = 1$, the XY Hamiltonian is:

$$\mathcal{H}_{\mathrm{XY}} = -\sum_{<i,j>} (S_i^x S_j^x + S_j^y S_i^y) - hS \sum_i S_i^z \ . \tag{5.11}$$

Assuming that the system has a stable long-range order, the linear spin-wave theory can be applied safely. For $h = 0$ the classical ground state is in the easy plane (x, y) and can be assumed that the order parameter is along the x-axis. When $h \neq 0$, in order to have the classical $S \to \infty$ solution parallel to the x-axis, the spin reference frame is rotated by an angle θ around the x-axis:

$$S_l^y = \bar{S}_l^y \ , \tag{5.12}$$

$$S_l^x = \cos\theta \bar{S}_l^x - \sin\theta \bar{S}_l^z \ , \tag{5.13}$$

$$S_l^z = \sin\theta \bar{S}_l^x + \cos\theta \bar{S}_l^z \ , \tag{5.14}$$

where $\bar{S}_i^\alpha$, $\alpha = x, y, z$ are spin operators in the rotated frame. In the rotated frame we can use the Holstein-Primakoff transformation:

$$\bar{S}_l^x = S - a_l^\dagger a_l \ , \tag{5.15}$$

$$\bar{S}_l^y = \sqrt{\frac{S}{2}}(a_l^\dagger + a_l) , \tag{5.16}$$

$$\bar{S}_l^z = i\sqrt{\frac{S}{2}}(a_l^\dagger - a_l) , \tag{5.17}$$

where $a_l^\dagger$ is the spin-wave creation operator. For the linear spin-wave Hamiltonian we obtain the usual quadratic form (2.24), where

$$D_q = = 4 - 2(1 + \sin^2\theta)\gamma_q , \tag{5.18}$$

$$\eta_q = -2\cos^2\theta\gamma_q . \tag{5.19}$$

The stability of the spin-wave Hamiltonian at the classical level requires that the order parameter is canted by the angle θ from the easy plane:

$$\sin\theta = \frac{h}{4} . \tag{5.20}$$

The magnetic field corresponds to the chemical potential of the bosonic system and should be obtained from the relation $\rho = 1/2 - m$ between the density of boson ρ and the uniform magnetization $m =< S_i^z >$. In the spin-wave theory the magnetization ranges in the interval $-S \leq m \leq S$ whereas the boson density is a given constant in the interval $0 \leq \rho \leq 1$. In order to satisfy the proper correspondence the magnetization has to be scaled by a factor $2S$; $m = 2S(1/2 - \rho)$.

Applying the Helmann-Feynman relation, the magnetic field is determined from the relation:

$$< S_i^z >= 2S(\frac{1}{2} - \rho) = -\frac{1}{LS}\frac{\partial}{\partial h} < \mathcal{H}_{\rm XY} > , \tag{5.21}$$

with the angular brackets denoting the ground-state expectation value. The angle θ in the linear spin-wave approximation is given by the equation:

$$\sin\theta = \sin\theta_0 + \frac{1}{S}\sin\theta_1 , \tag{5.22}$$

$$\sin\theta_0 = 1 - 2\rho , \tag{5.23}$$

$$\sin\theta_1 = -\frac{\sin\theta_0}{2L}\sum_q \gamma_q\sqrt{\frac{1-\gamma_q}{1-\sin^2\theta_0\gamma_q}} , \tag{5.24}$$

$$\gamma_q = \frac{1}{2}(\cos q_x + \cos q_y) , \tag{5.25}$$

and is shown in Fig. 5.1. The leading order ground-state energy in spin-wave expansion is given by

$$E_{SW} = -2L\left[S^2(1 - \sin^2\theta_0) + S(1 - \beta)\right] , \tag{5.26}$$

where $\beta = 1/L\sum_q \sqrt{(1-\gamma_q)(1-\sin^2\theta_0\gamma_q)}$.

The Jastrow potential $v(R)$ is determined as the Fourier transform of

$$v_q = \frac{2}{S}g_q = \frac{2}{\cos^2\theta}\left[1 - \sqrt{\frac{1-\sin^2\theta\gamma_q}{1-\gamma_q}}\right] . \tag{5.27}$$

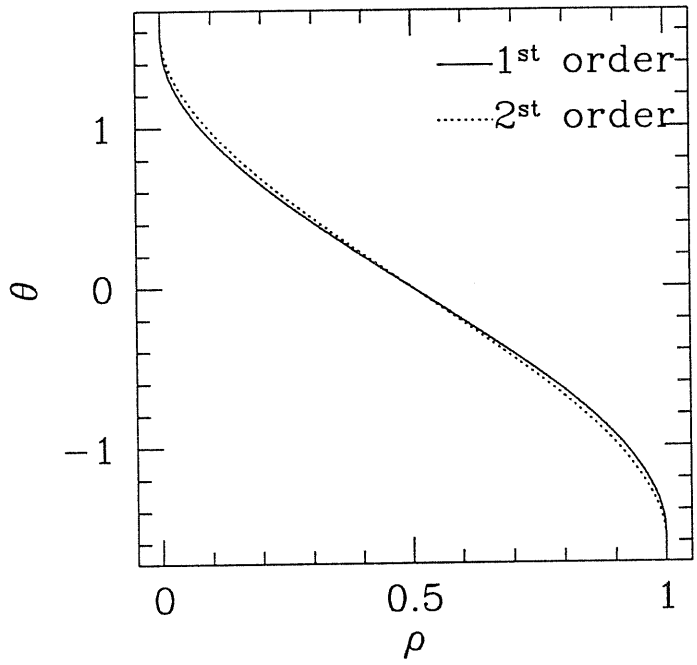

Figure 5.1: Dependence of the canting angle θ on the density of bosons ρ in the first (5.23) and second order (5.24).

In the limit of small wavevectors $g_q \propto 1/|q|$ yielding the long-distance behavior in the real space

$$v(R) \propto \frac{1}{|R|} \,. \tag{5.28}$$

In the variational wavefunction (2.35) the projection into the subspace of zero magnetization have to be changed to the finite magnetization determined by the density of bosons:

$$|\psi_V> = P_{<S^z_{tot}>} e^{\frac{1}{2}\sum_{i,j} v(R_i - R_j) S^z_i S^z_j} |F> \,, \tag{5.29}$$

where $|F>$ is the classical ferromagnetically ordered state in the original non rotated spin frame

$$|F> = \prod_i \left[\frac{1}{\sqrt{2}} (\cos\frac{\theta}{2} + \sin\frac{\theta}{2}) c^\dagger_{i\uparrow} + \frac{1}{\sqrt{2}} (\cos\frac{\theta}{2} - \sin\frac{\theta}{2}) c^\dagger_{i\downarrow} \right] |\text{vac}> \,. \tag{5.30}$$

$c^\dagger_{i\sigma}$ creates a fermion of the spin $|\sigma>$ in the site i, and $|\text{vac}>$ is the vacuum state $c_{i\sigma}|\text{vac}> = 0$. The variational calculation is now easily performed because all spin configuration selected by the

	4×4				6×6			
N	E_{SW}	E_V	E_{exact}	ζ	E_{SW}	E_V	E_{exact}	ζ
2	-3.78905	-3.78472	-3.78478	0.99998	-3.94798	-3.92025	-3.92027	0.99995
3	-5.31400	-5.33198	-5.33234	0.99990	-5.78373	-5.75355	-5.75369	0.99994
4	-6.57696	-6.62458	-6.62584	0.99963	-7.51823	-7.49372	-7.49406	0.99987
5	-7.56916	-7.64784	-7.65020	0.99937	-9.14706	-9.13506	-9.13577	0.99973
6	-8.28344	-8.38991	-8.39407	0.99889	-10.66674	-10.67273	-10.67399	0.99954
7	-8.71434	-8.84053	-8.84695	0.99820	-12.07438	-12.10253	-12.10451	0.99932
8	-8.85838	-8.99186	-8.99978	0.99762	-13.36753	-13.42080	-13.42368	0.99906
9					-14.54403	-14.62426	-14.62822	0.99876
10					-15.60195	-15.70995	-15.71519	0.99840
11					-16.53959	-16.67515	-16.68189	0.99798
12					-17.35543	-17.51740	-17.52582	0.99750

Table 5.1: Spin-wave energy E_{SW}, variational energy E_V, exact one E_{exact} in units of J, and overlap square $\zeta = |<\psi_V|\psi_{GS}>|^2$ of the corresponding wavefunctions for various clusters and number N of bosons.

projector have the same constant $2^{-L}\left(\cos\frac{\theta}{2}+\sin\frac{\theta}{2}\right)^{2(L-N)}\left(\cos\frac{\theta}{2}-\sin\frac{\theta}{2}\right)^{2N}$ which is irrelevant in the Monte Carlo calculation.

5.3 Variational estimate of the ground-state properties

In order to determine how accurate is the variational wavefunction, the expectation value for the ground-state energy was calculated by variational Monte Carlo and compared with the exact energy obtained by Lanczos diagonalization of the XY Hamiltonian. The exact calculation was feasible up to 12 bosons on $L = 36$ lattice. The variational estimate is extremely close to the exact ground-state energy as can be seen in Table 5.1. Not only the energy is well described by the variational wavefunction, but also all relevant parameters should be correctly estimated because the exact ground state wavefunction and the variational one have very big overlap. The variational state is obtained from the linear spin-wave theory. There was no need to adjust the parameters so that this variational state is relatively simple to implement and it is very convenient to use in the Green function Monte Carlo calculations.

In the small density limit ($\theta \to \pi/2$) the Jastrow potential is more singular in the small $|q|$ limit as it diverges like $1/|q|^2$, instead of the normal $1/|q|$ behavior for $\theta \neq 0$. Nevertheless, for fixed number of bosons the overlap between the exact ground state and the variational state is increasing with size showing that the low density limit is fulfilled exactly by the wavefunction (5.29) [61]. The Jastrow factor becomes the exact ground-state wavefunction of two hard-core bosons, which is known to diverge logarithmically for large particle-particle distance, consistent

with the $1/|q|^2$ limiting behavior of the Jastrow potential. The fact that this spin-wave state is so accurate for any density, especially in the low-density limit provides a clear evidence that the superfluid boson condensate in this strongly correlated system exists for all densities and extends the validity of the rigorous proof for $\rho = 1/2$ in Ref. [66].

Having such an accurate and easily computable variational state it is also possible to determine the ground-state properties of the hard-core boson system. We have calculated the momentum distribution function n_q and the density correlation function $N(q)$, defined by the relations

$$n_q = \sum_l e^{ikR_l} < b_0^\dagger b_l > , \tag{5.31}$$

$$N(q) = \sum_l e^{ikR_l} < \Delta\rho_0 \Delta\rho_l > , \tag{5.32}$$

where $\Delta\rho_l = b_l^\dagger b_l - \rho$ is the deviation from the average density ρ. The calculation was done on the lattice of size $L = 400$ to have a good resolution in momentum space. The results are shown in Fig. 5.2 and Fig. 5.3. The data obtained on the big lattice are completely consistent with the one from the exact diagonalization on the $L = 36$ lattice. On a lattice of such small size it is not possible to have all the values for the density calculated for the big lattice and we used the closest available ones.

The density correlation function is compared to its analog for the spinless fermion system on the same lattice given by

$$N(q) = \rho - \frac{1}{L}\sum_k n_k^f n_{k+q}^f , \tag{5.33}$$

where n_q^f is the fermion momentum distribution function. The sum rule $1/L\sum_q N(q) = \rho - \rho^2$ is valid both for the hard-core bosons and the spinless fermions. In the small density limit when the statistics is less important the bosonic and fermionic correlation function are almost equal. When the density increases the edge of the Fermi surface makes the fermionic distribution function more sharp at the characteristic Fermi wavevectors than the bosonic counterpart. With increasing temperature one expects that the Fermi distribution is smeared and the correlation functions become very similar to the bosonic ones. On the other hand, the bosonic correlation functions cannot be dramatically affected by increasing the temperature because they are already smeared at zero temperature. As expected, in the small wavevector limit $N(q) \sim q$, and the slope of the fermionic correlation function is practically equal to the bosonic one.

The behavior of the density correlation function for the $t - J$ model resulting from the high-temperature expansion [67] is essentially the same as for the hard core bosons. The relatively small discrepancy spinless fermion correlation functions and the ones for the $t - J$ model almost disappears when we compare the t-J model with the hard-core bosons. In Ref. [67] the mean-field approximation was used for the system of spinless fermions with a site dependent phase which can be obtained from the mapping of hard-core bosons. This approximation gives unphysical q^2 dependence of the density correlation function in the $q \to 0$ limit whereas it should be linear from

the Chester-Reatto argument used in the Chapter 4.

The momentum distribution function shows that a large part of degrees of freedom are frozen in the condensate. The condensate fraction becomes smaller with increasing density when the hard-core constraint is more important and n_q deviates strongly from the free boson distribution. The hard-core boson momentum distribution function is very different from the one for the spinless fermions and does not show any particular change at the spinless fermion Fermi wavevector.

5.4 Summary and discussion

Using the mapping of the two-dimensional hard-core boson model to the spin $S = 1/2$ XY model in presence of an external magnetic field we develop a "spin-wave" variational wavefunction which gives an extremely accurate approximation of the ground-state. The success of the spin-wave state relies on the existence of long-range order in the XY model. However, the analytical proof of the long-range order exists only for half-filled $N/L = 1/2$ case, and the present numerical calculation strongly suggests that the condensate exists for all densities. Thus, the spin-wave method for determining the variational wavefunction for quantum antiferromagnets is shown to be very accurate and successful when applied to the proper case where a true order exists. The existing mapping of hard-core bosons and fermions with flux via Jordan-Wigner transformation actually does not lead to a simpler problem, whereas the spin-wave approach gives a rather convenient scheme.

Regarding the question of the spin-charge separation problem, the hard-core boson density correlation function is very similar to the one found in the high temperature expansion for the $t - J$ model. The charge degrees of freedom in the $t - J$ model can be represented by hard-core bosons, and if the charge dynamics is completely described by such bosons, there is a possibility to have an independent excitation carrying the spin, providing the frame for an anomalous two-dimensional behavior. The spin-charge separation is one of the peculiar features of the one-dimensional Luttinger liquid, but the extension of one-dimensional concepts to two dimension is not easy at all. As it will be shown in the next chapter, if the Luttinger-liquid type state is directly transferred to two dimensions, the competitive Fermi liquid state arising from the slave-boson representation of the $t - J$ model is more stable.

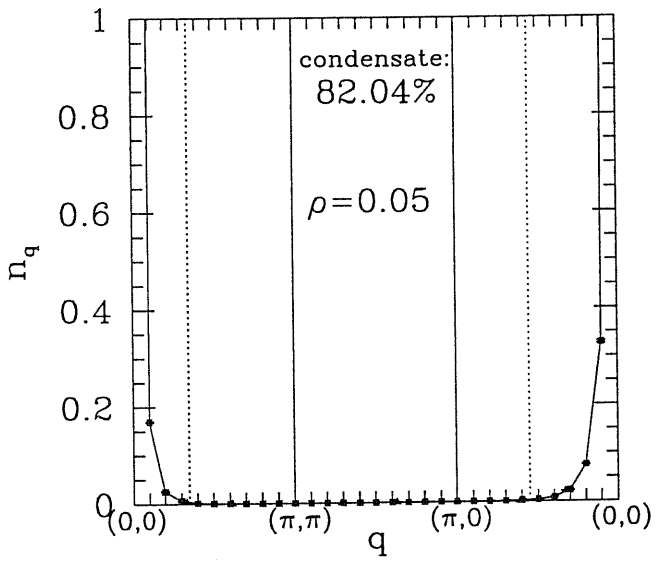
condensate:
82.04%
ρ=0.05
n_q
q
(0,0)
(π,π)
(π,0)
(0,0)

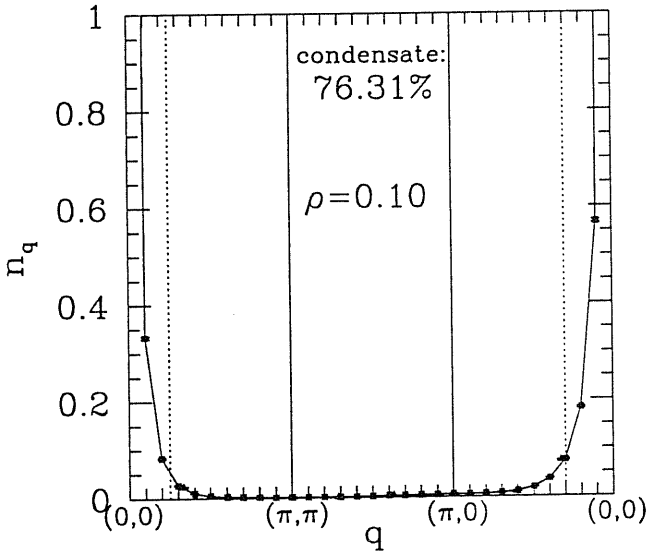
condensate:
76.31%
ρ=0.10
n_q
q
(0,0)
(π,π)
(π,0)
(0,0)

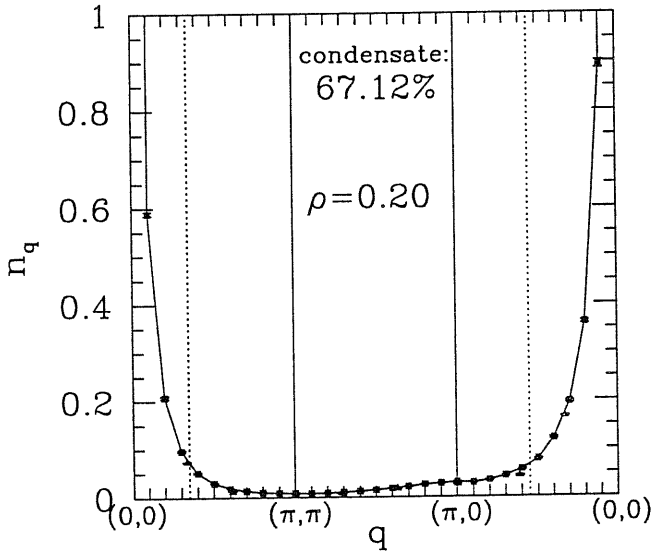
condensate:
67.12%
ρ=0.20
n_q
q
(0,0)
(π,π)
(π,0)
(0,0)

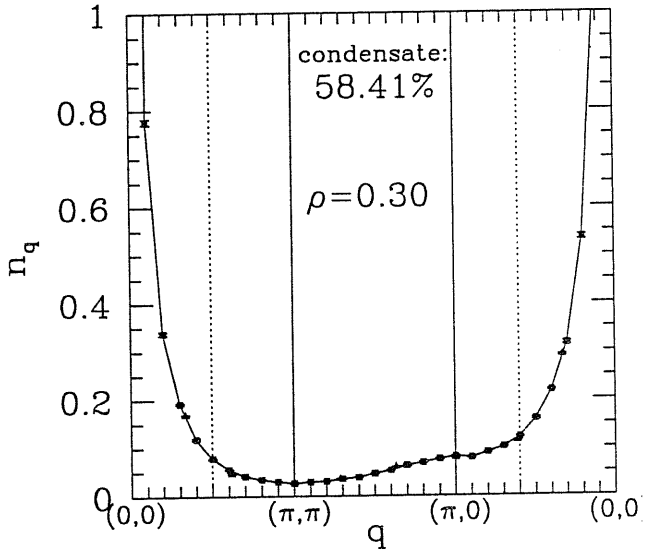
condensate:
58.41%
ρ=0.30
n_q
q
(0,0)
(π,π)
(π,0)

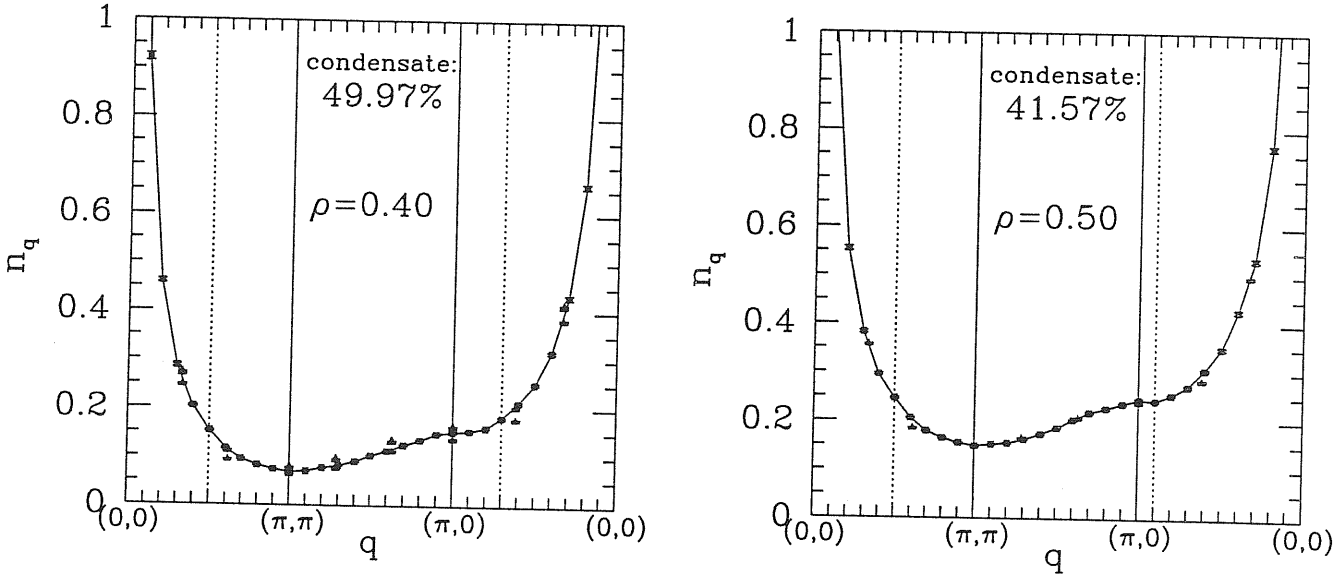

Figure 5.2: The momentum distribution function of the hard-core bosons along the symmetric lines in the Brillouin zone. Dotted lines denotes the spin-less fermion Fermi surface. Squares represent data for $L = 400$ site lattice, triangles for $l = 36$ site lattice for the closest available density. The condensate fraction $n_{q=0}/N$ is also noted.

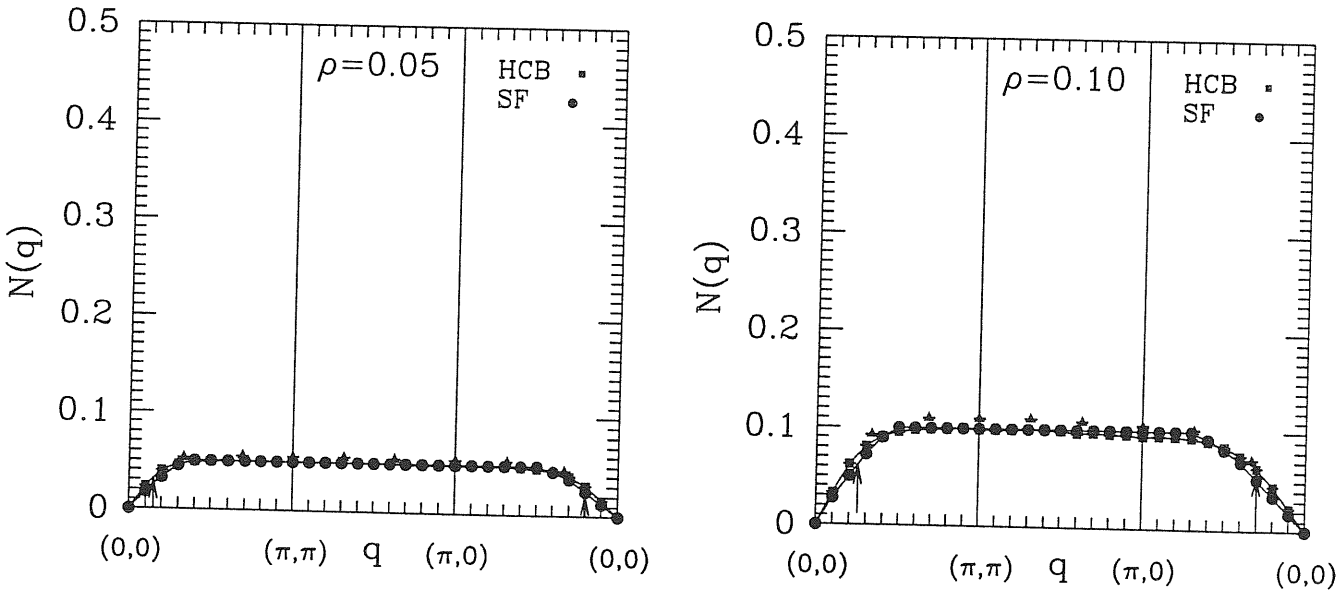

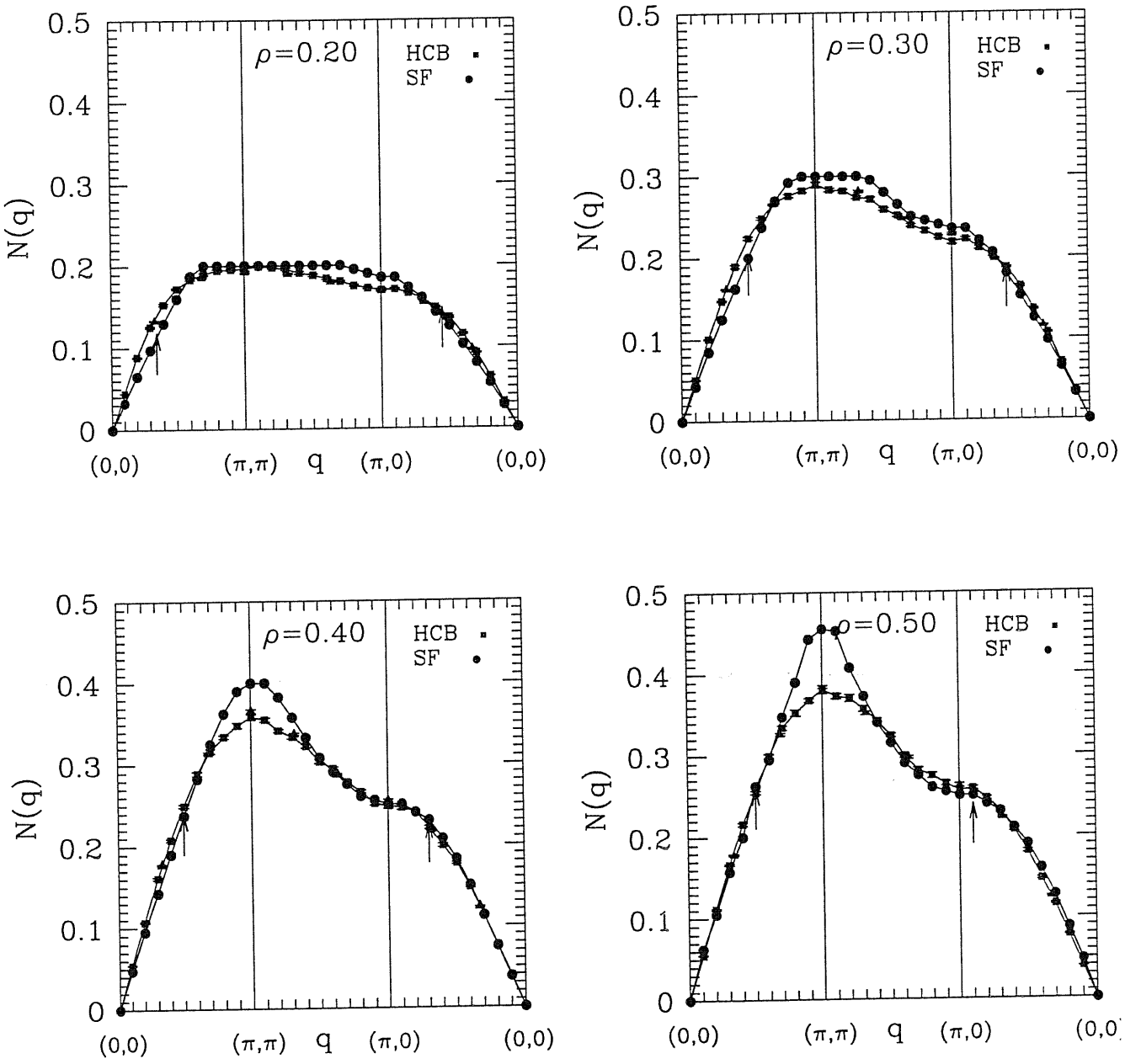

Figure 5.3: Density-density correlation function for along the symmetric lines in the first Brillouin zone. Squares are for hard-core bosons variational data and circles for the spin-less fermions at the same lattice of $L = 400$ sites. Triangles are for the hard-core bosons data on the lattice of $L = 36$ sites with closest available density. The arrows denote the position of the spin-less fermion Fermi surface.

6 $t-J$ model

6.1 Introduction

It is well established that the zero temperature properties of certain one dimensional (1D) strongly correlated systems, like the Hubbard and the t-J models, are described by the Tomonaga-Luttinger liquid theory [68, 69]. The search for the Luttinger liquid behavior in two dimensions (2D) is, to large extent, concerned with the t-J model. A motivation for studying the t-J model comes from the Anderson hypothesis [70, 71] that some unconventional properties of the high-T_c superconductors can be explained by a separation of charge and spin excitations, characteristic for systems with the Luttinger liquid ground state. A relevance of the 2D t-J model for the low energy properties of electrons in CuO_2 planes in copper-oxide superconductors was also established by Zhang and Rice [5].

There have been few variational studies of the normal state of the t-J model [72, 73, 74], mainly concerning ordered trial wavefunctions incorporating effects of the large momentum transfer scattering, whereas the long wavelength behavior were considered by Gros and Valentí [75, 76]. For the ground state variational wavefunction in Ref. [75] the Jastrow-Gutzwiller type state of the following form was used:

$$|\Psi> = e^{\frac{1}{2}\sum_{i,j} V(R_i-R_j)\rho_i\rho_j} P_d|\Psi_0>, \tag{6.1}$$

$$V(R_i-R_j) = \frac{1}{T}[(1-S)\log|R_i-R_j| - S\delta_{<i,j>}], \tag{6.2}$$

where $V(R_i-R_j)$ is the Jastrow potential and ρ_i is the electron density operator. The Gutzwiller projection operator P_d projects out from the fermionic wavefunction $|\Psi_0>$ all configurations with doubly occupied sites. This kind of variational wavefunction was previously investigated by Hellberg and Mele [15] for the study of the 1D t-J model because it embodies important features of Luttinger liquid systems: an algebraic singularity in the momentum distribution function at the Fermi surface and a long distance power-law fall-off of the correlation functions. The behavior of the wavefunction (6.1) is controlled by two variational parameters in the Jastrow potential (6.2): an effective temperature T and a strength of the nearest-neighbor interaction S. In the limit $S=0$, this wavefunction describes the pure Luttinger liquid, and for $S=1$ it represents the Fermi liquid

state with short-range correlations. The pure Gutzwiller state is realized for $S = 0$ in the limit $T \to \infty$. The Luttinger liquid character of the state with the logarithmic Jastrow potential (6.2) was clearly demonstrated in Ref. [76], showing that the momentum distribution function is continuous at the Fermi wavevector. Moreover, the resulting 2D-phase diagram was in quantitative agreement with the phase separation line obtained by the high temperature expansion [77].

The logarithmic form of the Jastrow potential appears naturally in the 1D case from a mapping of the variational wavefunction onto a classical two-component hard core gas [78] where unlike charges interact with the on-site infinite repulsive interaction, whereas like charges attract logarithmically each other.

6.2 Variational wavefunction in the slave-boson formalism

In Chapter 5 an extremely accurate variational wavefunction for the two-dimensional hard-core boson system was developed. This result will be used here to propose a new variational wavefunction for an interacting fermion-boson system as the t-J model. In fact, the substitution $c^\dagger_{i\sigma} = f^\dagger_{i\sigma} b_i$, where $f^\dagger_{i\sigma}$ are fermionic and b_i bosonic operators, leads to the slave boson representation of the Hamiltonian (1.1):

$$\mathcal{H} = -t \sum_{<i,j>\sigma} (f^\dagger_{i\sigma} f_{j\sigma} b^\dagger_j b_i + h.c.) + J \sum_{<i,j>} \vec{S}_i \cdot \vec{S}_j \ , \tag{6.3}$$

where the constraint of no doubly occupied sites now reads

$$\rho^f_i + \rho^b_i = 1 \ . \tag{6.4}$$

Here $\rho^f_i = \sum_\sigma f^\dagger_{i\sigma} f_{i\sigma}$ and $\rho^b_i = b^\dagger_i b_i$ are the fermion- and the boson-density operators, respectively. A possible variational wavefunction for such system is a product of a fermionic and a bosonic wavefunctions

$$|\Psi> = P_d |\Psi_F> \otimes |\Psi_B> \ . \tag{6.5}$$

For the fermionic part $|\Psi_F>$, the Jastrow-Gutzwiller state of the form (6.1) can be used, and for the bosonic part the free boson wavefunction $|\Psi_B> = \exp(\sum_i b^\dagger_i)|0>$ can be taken. Note that after the application of P_d the number of bosons is fixed to $N_b = L - N$ so that the overall factor in the exponent of $|\Psi_B>$ is irrelevant. Due to the constraint (6.4), bosons have to obey the hard-core constraint $\rho^b_i \leq 1$, and for the variational state we can take

$$|\Psi> = e^{\frac{1}{2}\sum_{i,j} V(R_i - R_j)\rho^b_i \rho^b_j} P_d |\Psi_B> \otimes |\psi_F> \ , \tag{6.6}$$

where the Jastrow potential $V(R_i - R_j)$ can be constructed following the spin-wave method developed in Chapter 2 and 5.

As a first approximation, we can assume that the motion of these hard core bosons can be decoupled from the fermion one, namely that the bosons are moving in an effective hard-core

bosons Hamiltonian with a renormalized hopping given by the expectation value of the fermionic hopping operator $<f^{\dagger}_{i\sigma}f_{j\sigma}>$. The overall constant does not affect the boson wavefunction and we are lead to study the ground state of the hard-core bosons system at the finite density $\rho_b = N_b/L$. The variational state for the bosons are given by expression (5.29). As was shown in Chapter 5 the Jastrow potential for the large distance behaves like

$$V(R_i - R_j) \propto 1/|R_i - R_j| \ , \tag{6.7}$$

hence its long-range behavior is different from the one in (6.2).

This form of the long-range correlations in the Jastrow is a consequence of long-wavelength magnons in the spin-wave Hamiltonian, corresponding to acoustic plasmon excitations in the t-J model with the dispersion energy $\omega_q \propto |q|$. The dispersion ω_q of these low energy excitations can be obtained by the Feynman construction, *i. e.* by applying $\rho_q = L^{-1/2}\sum_i e^{-iqR_i}\rho_i$ to the ground state $|0>$ of the Hamiltonian (1.1) yielding an estimate for ω_q which should be accurate in the small-q limit:

$$\omega_q = \frac{<0|\rho_{-q}\mathcal{H}\rho_q|0>}{<0|\rho_{-q}\rho_q|0>} - E_0 \ , \tag{6.8}$$

where E_0 is the ground state energy. Since the projector P_d commutes with the density operator and with the magnetic part of $\mathcal{H}$, and the ground state has a definite space inversion symmetry, we obtain:

$$\omega_q = \frac{<0|[\rho_{-q},[\mathcal{H},\rho_q]]|0>}{2N_q} = \frac{2E_0(1-\gamma_q)}{LN_q} \ , \tag{6.9}$$

$N_q = \sum_i e^{iqR_i} <\rho_0\rho_i>$ being the density correlation function. For small q, $1-\gamma_q \propto q^2$, and from the linear dispersion of low energy excitations at small wavevectors follows $N_q \propto |q|$. Such behavior of N_q leads to the obtained (6.7) long-range behavior of interactions by the Reatto-Chester argument which essentially states that $V_q \propto \frac{1}{N_q}$ [53, 54].

The fermion wavefunction $|\psi_F>$ can be taken in the form [76]:

$$\prod_k(\alpha_k + \beta_k c^{\dagger}_{k\uparrow}c^{\dagger}_{-k\downarrow})|0>, \quad \frac{\alpha_k}{\beta_k} = \frac{\Delta_k}{\epsilon_k + \sqrt{\epsilon_k^2 + \Delta_k^2}} \ , \tag{6.10}$$

where $\epsilon_k = -2(\cos k_x + \cos k_y)$, and $\Delta_k = \Delta(\cos k_x - \cos k_y)$. This is the BCS superconducting state with the $d_{x^2-y^2}$ order parameter. Near half-filling $\rho^f = N/L \simeq 1$, the large momentum transfer scattering in the magnetic part of $\mathcal{H}$ is dominant and such correlations are included in $|\psi_F>$ taking $\Delta = 0.5$. Away from half-filling, the (π,π) momentum scattering is less important and the kinetic energy is optimized for $\Delta = 0$ and $|\psi_F>$ reduces to the simple filled Fermi sea $|\psi_F> = \prod_{k<k_F,\sigma} c^{\dagger}_{k\sigma}|0>$.

6.3 Comparison of the Luttinger and Fermi liquid states

In order to compare these two variational wavefunction, the one with the logarithmic Jastrow potential (6.2) and the one with the hard-core bosons Jastrow potential (5.27), we performed a

variational Monte Carlo calculation of the energy expectation value. We have chosen the same lattice of 24 and 8 holes on 82 sites with periodic boundary conditions as in Ref. [76] to have a clear comparison of data. The fermion wavefunction in the case of 24 holes was the Fermi sea, and for the 8 holes cluster the BCS state with $d_{x^2-y^2}$ pair correlations. In the case of superconducting wavefunction ω_q has a gap on the Fermi surface and the previous argument to determine the long distance behavior of the Jastrow potential is no longer valid. In fact, the difference between logarithmic and hard-core bosons wavefunction estimates in this case becomes of the order of error bars and cannot be clearly seen from the Monte Carlo data.

The logarithmic wavefunction has two variational parameters, the total energy minimum is obtained for $S = 0$ [76]. The hard-core bosons wavefunction has no variational parameter but analogously to the Hellberg and Mele treatment [15] we can include an extra parameter multiplying the Jastrow potential (5.27) by a factor $1/T$. The Gutzwiller state is obtained for $1/T = 0$.

The Jastrow prefactor in these wavefunctions lowers the kinetic energy with respect to the Gutzwiller state, however the exchange energy is higher than the Gutzwiller one, though differences are quite small, around 1%. Differences between energies for considered wavefunctions are even smaller, and to get clear contrast of variational data, we have calculated again the expectation values for the logarithmic wavefunction, though they were already given in Ref. [76], but with larger error bars. Previously reported data and the ones calculated by us are in complete agreement. The data for the lattice with 24 holes are shown in Fig. (6.1) and for 8 holes in Fig. (6.2). The momentum distribution function

$$n(q) = \frac{1}{2L} \sum_{i,j,\sigma} e^{iq(R_i - R_j)} < c^{\dagger}_{i\sigma} c_{j\sigma} > \tag{6.11}$$

is calculated for the half-filled lattice with $L = 400$ sites and periodic boundary conditions, showing the finite jump at the Fermi surface, confirming the Fermi liquid character of the hard-core bosons variational wavefunction, see Fig. (6.3).

The hard-core bosons wavefunction has both the kinetic and the magnetic energies comparable with the logarithmic Jastrow ones. In the case of 24 holes the difference is a little bit larger than for the 8 holes, but the hard-core bosons variational energy is always lower than the other one. The fact that the hard-core bosons Jastrow potential gives not only a lower kinetic energy than the logarithmic one, but also a more stable magnetic part of $\mathcal{H}$ means that the small wavevector scattering in the projected kinetic energy is correctly taken into account, without spoiling correlations in the rest of the wavefunction. Notice that for the t-model (given by the Hamiltonian (1.1) for $J = 0$) one has a minimum for $S \neq 0$, but our variational wavefunction remains with lover energy.

6.4 Summary and discussion

In conclusion, we have introduced a variational wavefunction with the Jastrow factor compatible with a low-energy plasmon excitations with dispersion $\omega_q \propto |q|$ which we have dealt in spin-wave approximation. This wavefunction describes a Fermi liquid ground state and we compared it with a Luttinger liquid wavefunction [75, 76]. The obtained variational Monte Carlo estimates for the two wavefunctions are comparable although the Fermi liquid one has a little lower energy. From this calculation we see that in searching for a Luttinger liquid state in two dimensions it is very difficult to translate a state directly from one dimension. Namely, though the Gros-Valentí extension of the Hellberg-Mele state has all features of the Luttinger liquid and it is stable against the Gutzwiller state, a more reasonable long range Jastrow potential gives also a stable Fermi liquid state with a lover energy. These observations are somehow consistent with exact diagonalization studies of the $t-J$ model by Long and Zotos [79, 80]. They have proved that spinless hard-core bosons have lower kinetic energy than any other statistics of particles for the case of unfrustrated hopping. When the spin correlations become important their numerical calculation shows that fermionic particles have lower energy. This confirms our findings that the hard-core boson state is doubtlessly more stable than the Luttinger liquid one for large doping, whereas for small doping difference in the ground-state energy becomes quite small and the Luttinger liquid state is strongly competitive with the Fermi liquid one.

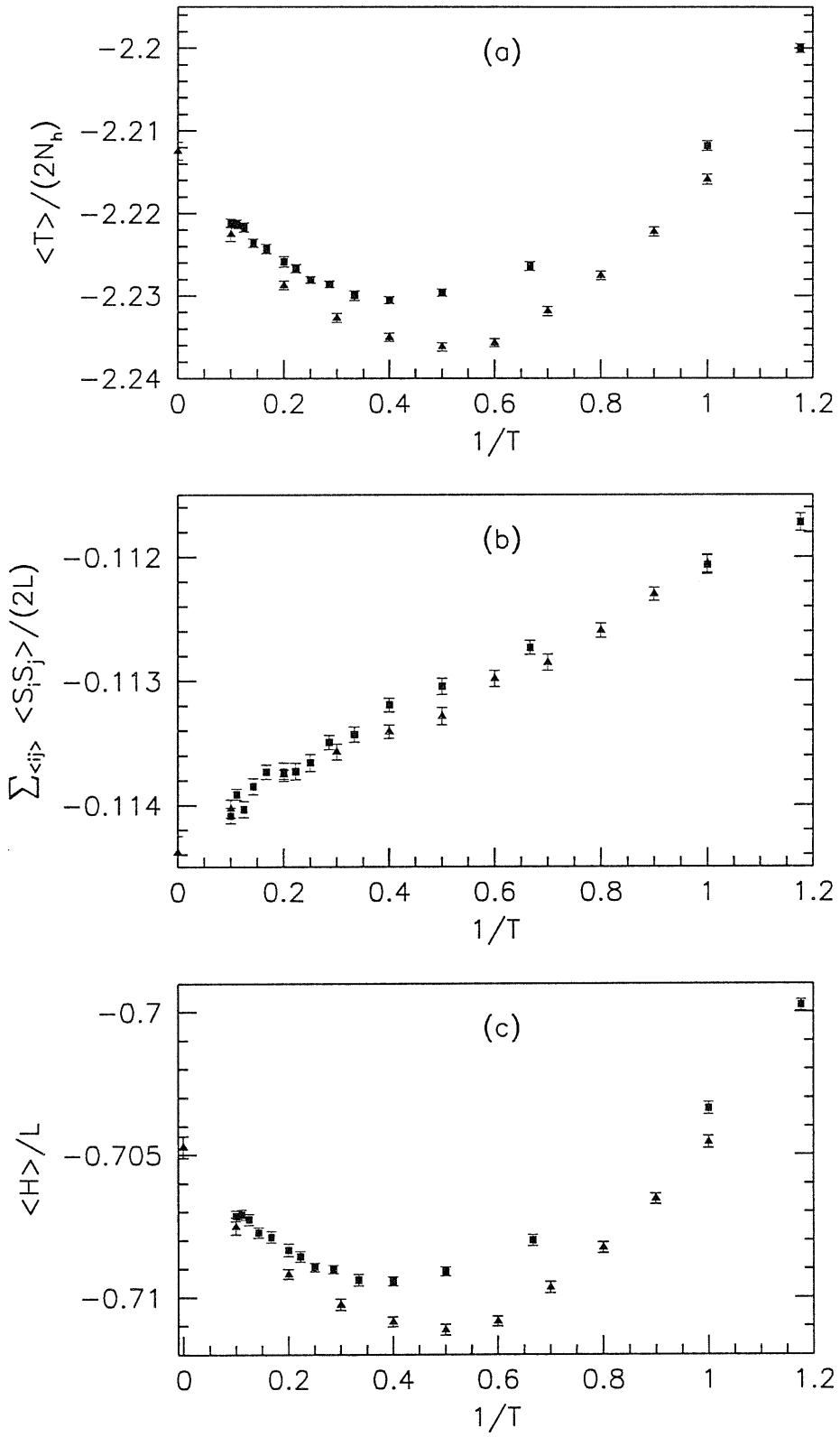

Figure 6.1: The variational Monte Carlo data for estimates of the kinetic energy per hole (a), the magnetic energy per bond (b), and the total energy per site (c) of the logarithmic Jastrow wavefunction (squares) and the hard core bosons Jastrow wavefunction (triangles). The lattice has 82 sites with 24 holes. The fermionic part of the wavefunction is the filled Fermi sea ($\Delta = 0$). The exchange parameter $J = 0.25t$.

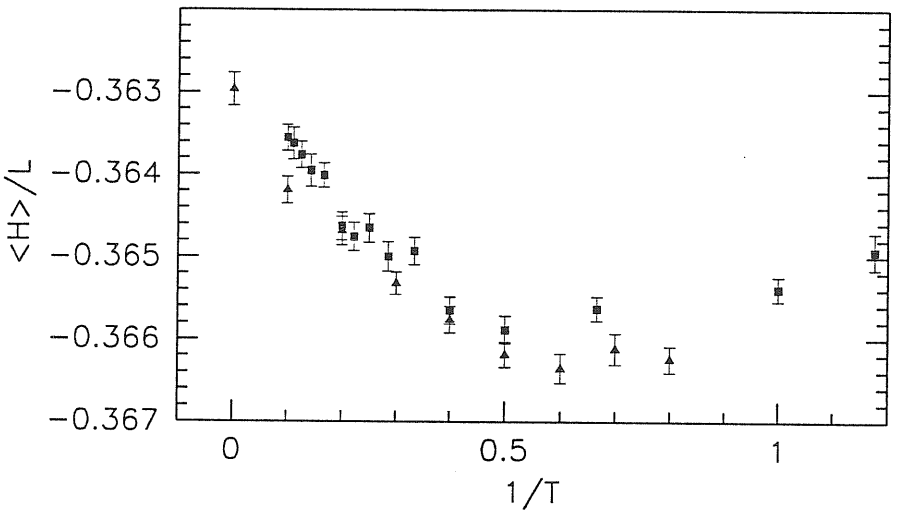

Figure 6.2: The variational Monte Carlo data for the estimate of the total energy of the 8 holes cluster on the same lattice as in Fig. 6.1 for the logarithmic (squares) and the HCB Jastrow (triangles) wavefunction. The fermionic part of the wavefunction is the superconducting pair function ($\Delta = 0.5$). The exchange parameter $J = 0.25t$.

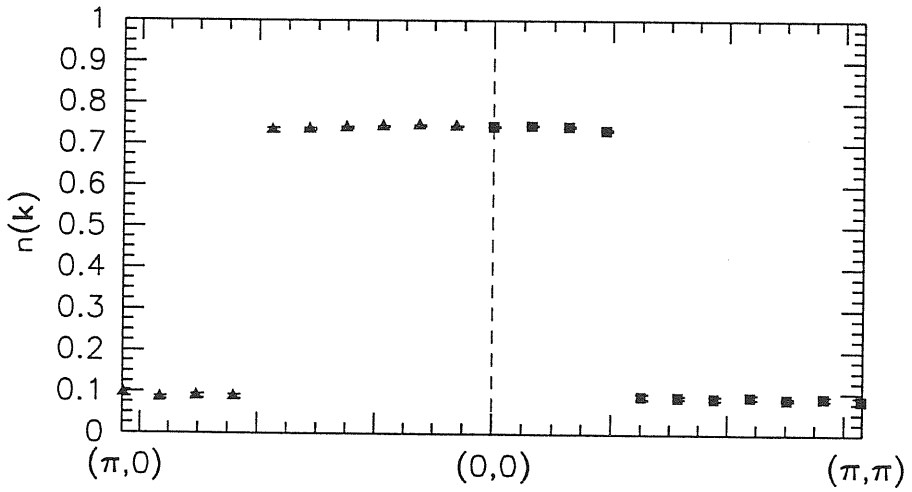

Figure 6.3: The momentum distribution function for the hard core boson Jastrow wavefunction for the half-filled lattice of $L = 400$ sites with PBC for wavevectors along the directions $(1,0)$ and $(1,1)$ of the Brillouin zone. The variational parameter is $1/T = 1$, the fermionic wavefunction is the filled Fermi sea ($\Delta = 0$).

7 Exact diagonalization study of the optical conductivity

7.1 Introduction

In this chapter the optical conductivity of the Hubbard model on the honeycomb lattice will be studied by a new method based on integration over boundary conditions. The method was recently proposed by Valenti, Gros, Hirschfeld, and Stephan [81] and developed by Gros [82, 83]. The exact diagonalization calculations have become today a very important tool in the investigation of strongly correlated systems, as the Hubbard model or general spin systems. Although the memory and computing speed of computers have enormously increased the exact diagonalization techniques can never be pushed to very large systems because the computational effort grows exponentially with the system size. By these methods results will be always plagued by the finite-size effects which are taken into account in the analysis of data, but cannot be, in most of cases, completely eliminated. All new ideas which allow a reduction and a better control of the finite size effects are therefore welcome.

The method of integration over boundary conditions can considerably reduce finite-size effects and the present calculation proves that for a very subtle problem, such as the evaluation of the optical conductivity, it gives a rather reasonable result. Another big advantage of this technique is that on finite clusters there is a quite small number of available density of particles, but the integration technique practically expands the allowed values to the whole possible interval. The technique is based on the assumption that an average over the results for all possible boundary conditions is a good approximation of the integral over the Fermi surface in the thermodynamical limit. The method is defined in such a way that for a non-interacting system the boundary-condition averages provide the exact result for the infinite system. If the Fermi surface is not dramatically distorted by interactions, it is reasonable to expect that the average boundary-condition results are a good approximation of the infinite system also in the presence of the interaction.

A motivation for the study of the optical conductivity of electrons on the honeycomb lattice has come from the very recent experimental observation of surface charge density waves [84]. The

lead atom arrangement on the (111) surface of α-germanium is reconstructed from $(\sqrt{3} \times \sqrt{3})R30°$ structure at high temperature to the (3×3) structure at low temperature. The theoretical (3×3) surface is metallic and the first-principle density functional calculation also predicts the metallic behavior for the low-temperature phase. The shape of the conductivity obtained by the electron energy-loss spectroscopy, raised doubts about the ground state of the surface in the low temperature phase. The optical conductivity of the high-temperature phase has a clear metallic behavior with the Drude peak, whereas at low temperatures a maximum around 100 meV appears. The behavior of the conductivity seen by the spectroscopy is probably due to the electron-electron interaction which is not properly accounted in the local density approximation. The question we want to address here is: could this strong electron correlation produce such behavior for the conductivity in the low-temperature phase?

In order to investigate qualitatively the behavior of the conductivity in the presence of the strong electron-electron correlation we will study the Hubbard model on the honeycomb lattice. The Hubbard model is a simple model but we expect that it comprises the main physical picture of the electron interaction. The honeycomb lattice underlies the arrangement of *Pb* atoms in the low-temperature phase. The lead surface covering layer contains half electron per site which corresponds to the quarter filled band. In order to get a reliable answer without approximations which are necessarily made in the analytical treatment we performed exact diagonalization calculation by the Lanczos method. However, clusters available by our computers resources are too small to obtain results without strong size effects. The way out was to use the integration over boundary condition technique. By the boundary condition averaging the finite-size effects are reduced and reasonable data can be obtained from small clusters.

Our calculation shows that the unusual behavior of the optical conductivity and the peak for 100 meV can be explained within the Hubbard model. For $U = 0$ there exist bonding and antibonding states with energy E_q and $-E_q$, respectively, shown in Fig. 7.4. In order to have a non-vanishing optical conductivity at a given frequency ω, an occupied bonding state of energy $-E_q$ and momentum q must be connected by the current density operator with an unoccupied antibonding state of energy $E_q = \omega/2$ and momentum $-q$ in order to conserve the total momentum. The available free-electron states at quarter filling can contribute to the conductivity only for frequencies $\omega \geq 3t$, where t is the hopping parameter. This threshold is far above the frequency where the peak in the low-temperature surface phase appears. At this low density it is rather unlikely that the electron correlations renormalize the bandwidth to shift the threshold to the observed ω. On the other hand, it is clear that the interaction create a small non-vanishing momentum weight for the states close to the van Hove energy $-t$, and some signal at $\omega \simeq 2t$ can be expected. Nevertheless, it is difficult to explain that the $\omega \simeq 3t$ peak is completely replaced by the new $\omega \simeq 2t$ one.

Instead a more clear and direct solution can be obtained by the simple assumption that the electron system for strong enough interaction becomes ferromagnetic. In the ferromagnetic ground state the states at the van Hove singularity are occupied and corresponding big weights results

in a strong $\omega = 2t$ conductivity response. However, if the ground state is paramagnetic, the strong ferromagnetic correlations can produce components in the ground state wavefunction which lead to the $\omega = 2t$ conductivity peak. We anticipate here that we have not found evidence of true ferromagnetic long-range order, but the picture emerging from the ground-state properties calculation is in a qualitative agreement with the previous ferromagnetic scenario, as we have an evidence that the ground state, though being a singlet, has strongly enhanced ferromagnetic correlations at short electron-electron distance.

The suggested scenario is based on a naive band picture but the arguments are rather plausible and the described physical picture is confirmed by the present numerical calculations.

7.2 Conductivity in linear response

We consider the Hubbard model on the honeycomb lattice with L sites defined by Hamiltonian

$$\mathcal{H} = -t \sum_{R\in A,\eta,\sigma} (c^\dagger_{R\sigma} c_{R+\eta\sigma} + c^\dagger_{R+\eta\sigma} c_{R\sigma}) + U \sum_R n_{R\uparrow} n_{R\downarrow} \,, \tag{7.1}$$

where $c^\dagger_{R\sigma}$ is the creation operator of an electron of spin $\sigma = \uparrow, \downarrow$ at the lattice site R. η denotes the directions of the bonds to the three nearest neighbors $\eta_1 = -\frac{1}{2}\hat{x} + \frac{\sqrt{3}}{2}\hat{y}$, $\eta_2 = -\frac{1}{2}\hat{x} - \frac{\sqrt{3}}{2}\hat{y}$, and $\eta_3 = \hat{x}$ The unit length is the nearest-neighbor distance. $n_{R\sigma} = c^\dagger_{R\sigma} c_{R\sigma}$ is the electron spin density operator. The sum $R \in A$ is restricted only to one of the two sublattices. We assumed the periodic boundary conditions, but in Section 7.5 the general boundary conditions will be used.

The model can be represented in a more convenient way by mapping the honeycomb lattice to so called "brick lattice", i. e. the square lattice with some missing bonds [85], see Fig. 7.1. The bonds in Eq. (7.1) are given in this representation by $\eta_1 = \hat{y}$, $\eta_2 = -\hat{y}$, and $\eta_3 = \hat{x}$ i. e. the bonds connected by $\eta_4 = -\hat{x}$ present in the square lattice are missing in the brick lattice.

We are interested in the response of the system to the uniform external electromagnetic field described by a classical vector potential $A_\eta(R_i, t)$, where t is time [86]. The $U(1)$ coupling of electrons on a lattice to the gauge field is described by introducing the phase factor in the hopping term:

$$\mathcal{H}_A = -t \sum_{R\in A,\eta,\sigma} \left(e^{ieA_\eta(R,t)} c^\dagger_{R\sigma} c_{R+\eta\sigma} + e^{-ieA_\eta(R,t)} c^\dagger_{R+\eta\sigma} c_{R\sigma} \right) + U \sum_R n_{R\uparrow} n_{R\downarrow} \,, \tag{7.2}$$

where we are using units where $\hbar = c = 1$. The expansion of the current in powers of A is given by:

$$J_\eta(R,t) = \frac{-\partial \mathcal{H}_A}{\partial A_\eta(R,t)} = e j_\eta(R) + e^2 k_\eta(R) A_\eta(R,t) + \cdots \,, \tag{7.3}$$

where the current density $j_\eta(R)$ and the kinetic energy density $k_\eta(R)$ operators read

$$j_\eta(R) = it \sum_\sigma (c^\dagger_{R\sigma} c_{R+\eta\sigma} - c^\dagger_{R+\eta\sigma} c_{R\sigma}) \,, \tag{7.4}$$

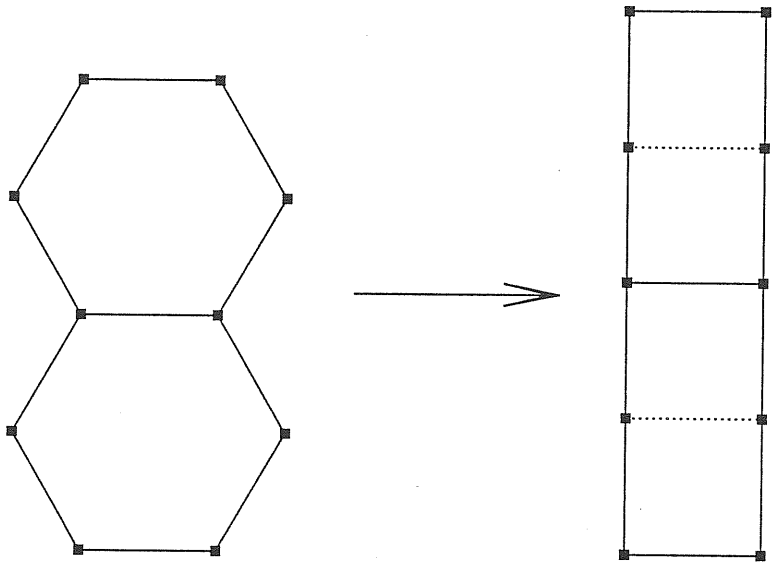

Figure 7.1: Mapping of the honeycomb lattice (left) onto the brick lattice (right). The brick lattice is obtained from the square one by cutting off the bonds denoted by dotted lines.

$$k_\eta(R) = -t\sum_\sigma (c^\dagger_{R\sigma}c_{R+\eta\sigma} + c^\dagger_{R+\eta\sigma}c_{R\sigma}) \; . \tag{7.5}$$

The term proportional to e is usually referred as the paramagnetic contribution and the one proportional to e^2 as the diamagnetic contribution to the current. Using the standard linear response theory [87] for a vector potential

$$A_\eta(R,t) = \mathrm{Re}\left(A_\eta(q,\omega)e^{i(qR-\omega t)}\right) \tag{7.6}$$

the expression for the current response is obtained:

$$< J_\eta(q,\omega) >= e^2 < k_\eta > A_\eta(q,\omega) + e^2 \sum_{\eta'} \Lambda_{\eta\eta'}(q,\omega)A_{\eta'}(q,\omega) \; , \tag{7.7}$$

where $\Lambda_{\eta\eta'}$ is the current-current correlation function:

$$\Lambda_{\eta\eta'}(q,\omega) = \frac{1}{L} < j_\eta(-q)\frac{1}{\mathcal{H} - E_0 + \omega + i\delta} j_{\eta'}(q) > + \frac{1}{L} < j_\eta(q)\frac{1}{\mathcal{H} - E_0 - \omega - i\delta} j_{\eta'}(-q) > \; . \tag{7.8}$$

Here, E_0 is the ground state energy, and angle brackets denote the ground-state average. Due to the translation invariance, the average ground state kinetic energy is independent of lattice site and we have denoted $< k_\eta(R) >=< k_\eta >$.

In the linear response approximation the conductivity is defined as the response to a uniform, $q = 0$, time dependent electric field

$$\mathcal{E}_\eta(q=0,\omega) = i(\omega + i\delta)A_\eta(q=0,\omega) \tag{7.9}$$

through the relation:

$$< J_\eta(q=0,\omega) >= [\sigma_1(\omega) + i\sigma_2(\omega)]\mathcal{E}_\eta(q=0,\omega) \; . \tag{7.10}$$

The conductivity is independent of the direction η because it is a second order tensor and the symmetry point group of the lattice has the only one, the identity, irreducible representation [88]. The real part of the conductivity for $\omega > 0$ has two contributions:

$$\sigma(\omega) = D\delta(\omega) + \sigma^{inc}(\omega) \; , \tag{7.11}$$

$$D = -\pi e^2 \left[< k_\eta > + \frac{1}{L} \sum_{n \neq 0} \frac{| < \psi_n | j_\eta(q=0) | \psi_0 > |^2}{E_n - E_0} \right] \; , \tag{7.12}$$

$$\sigma^{inc}(\omega) = \frac{\pi e^2}{L} \sum_{n \neq 0} \frac{| < \psi_n | j_\eta(q=0) | \psi_0 > |^2}{E_n - E_0} \delta\left(\omega - (E_n - E_0)\right) \; . \tag{7.13}$$

The Drude weight D contains the delta function contribution whereas σ^{inc} comes from incoherent contributions at finite ω. $|\psi_n >$ is a complete set of the Hamiltonian (7.1) with energies E_n. The insulating or the conducting character of the ground state is determined by the infinite-size limit value of the Drude weight. For a metal D goes to a finite value and vanishes for an insulator.

7.3 Free electron conductivity

The $U = 0$ limit of the Hamiltonian (7.1) corresponds to the problem of free electrons in the honeycomb lattice. In the brick lattice representation, see Fig. 7.2, they are described by the Hamiltonian:

$$\mathcal{H}_0 = -t \sum_{R \in A, \eta, \sigma} (c^\dagger_{R\sigma} c_{R+\eta\sigma} + c^\dagger_{R+\eta\sigma} c_{R\sigma}) \; . \tag{7.14}$$

The spin degrees of freedom are decoupled therefore we can consider only one of them and spin index will be dropped in the following discussion.

Since the honeycomb lattice is a bipartite Bravais lattice with two sites per unit cell, it is convenient to define new electronic operators $a^\dagger_i$ and $b^\dagger_i$ which create an electron on the sublattice A and B, respectively:

$$c^\dagger_R = \begin{cases} a^\dagger_R, & R \in \text{sublattice A;} \\ b^\dagger_R, & R \in \text{sublattice B.} \end{cases} \tag{7.15}$$

After the Fourier transformation defined by:

$$a^\dagger_R = \sqrt{\frac{2}{L}} \sum_q e^{iqR} a^\dagger_q \; , \tag{7.16}$$

$$b^\dagger_R = \sqrt{\frac{2}{L}} \sum_q e^{iqR} b^\dagger_q \; , \tag{7.17}$$

(7.18)

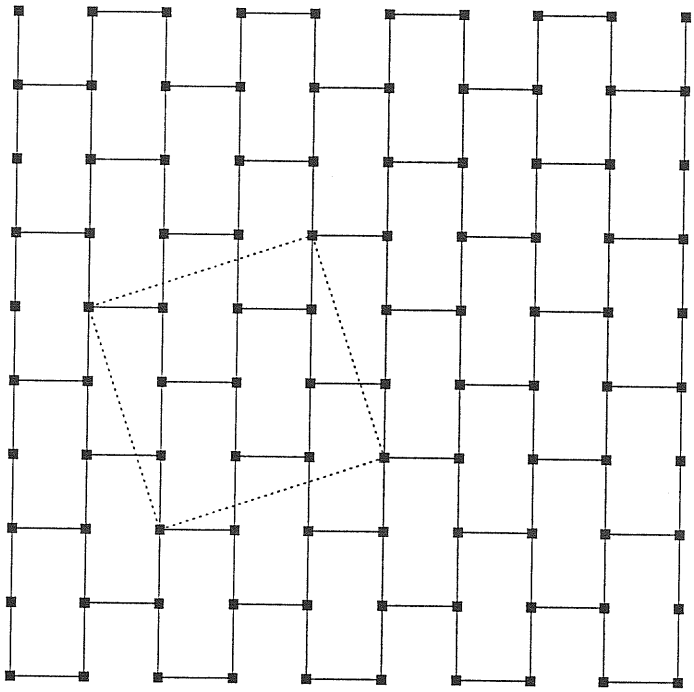

Figure 7.2: The brick-lattice representation of the honeycomb lattice. The tilted square denoted by dashed lines is the $L = 10$ sites cluster used in the Lanczos calculations.

where q are wavevectors from the magnetic Brillouin zone, the Hamiltonian can be written as:

$$\mathcal{H}_0 = \sum_q (\epsilon_q^* a_q^\dagger b_q + \epsilon_q b_q^\dagger a_q) , \tag{7.19}$$

$$\epsilon_q = -2t \cos q_y - te^{iq_x} = |\epsilon_q| e^{i\varphi_q} . \tag{7.20}$$

Notice that the current and the Hamiltonian do not commute

$$[j_\eta, \mathcal{H}_0] = 4it^2 \sum_q \sin q_\eta \sin \varphi_q (a_q^\dagger a_q - b_q^\dagger b_q) , \tag{7.21}$$

and thus, contrary to the square lattice free electrons or the continuum limit, all the states contributed to the conductivity are not exhausted by the Drude weight. Since the incoherent part of the conductivity is not vanishing, the conductivity at finite ω must be also computed.

This Hamiltonian (7.19) could be easily diagonalized by an unitary transformation:

$$\alpha_q^\dagger = \frac{1}{\sqrt{2}} (a_q^\dagger + e^{i\varphi_q} b_q^\dagger) , \tag{7.22}$$

$$\beta_q^\dagger = \frac{1}{\sqrt{2}}(a_q^\dagger - e^{i\varphi_q} b_q^\dagger) . \tag{7.23}$$

The operators $\alpha_q^\dagger$ and $\beta_q^\dagger$ create an electron in the state with the energy $E_q^{(\alpha)} = |\epsilon_q|$ (anti-bonding state) and $E_q^{(\beta)} = -|\epsilon_q|$ (bonding states), respectively. The plot of the constant energy curves is shown in Fig. 7.3. Density of states is given by

$$DoS(E) = \begin{cases} \frac{\sqrt{|E|}}{2\pi^2 t^{3/2}} \mathrm{K}\left(\sqrt{\frac{(|E|-t)^3(|E|+3t)}{16|E|t^3}}\right), & |E| \in [t, 3t] ; \\ \frac{2|E|}{\pi^2\sqrt{(t-|E|)^3(|E|+3t)}} \mathrm{K}\left(\sqrt{\frac{16|E|t^3}{(|E|-t)^3(|E|+3t)}}\right), & |E| \in [0, t] \end{cases} \tag{7.24}$$

where K is the complete elliptic integral of the first kind. The density of states has the Hove singularity at energies $E = \pm 1$ when it behaves like $DoS(E) \sim -1/(4\pi^2 t)\ln(1 - |E|)$. At the top of the bonding band and the bottom of the anti-bonding band, when $E \to 0$, $DoS \sim |E|/\sqrt{3}\pi^2 t^2$, leading to the vanishing density of states at the Fermi level for half-filling. The van Hove singularity in the density of states appears at filling $\nu = 3/8$, see Fig. 7.4.

The current density operator (7.4) in y-direction for an uniform field reads

$$j_y = 2t\sum_q \sin q_y (a_q^\dagger b_q + b_q^\dagger a_q) = 2\sum_q \sin q_y [\cos\varphi_q(\alpha_q^\dagger\alpha_q - \beta_q^\dagger\beta_q) + i\sin\varphi_q(\beta_q^\dagger\alpha_q - \alpha_q^\dagger\beta_q)] . \tag{7.25}$$

The ground state for filling $\nu \leq 1/2$ is given by

$$|\psi_0> = \prod_{q\leq k_F} \beta_q^\dagger |\mathrm{vac}> , \tag{7.26}$$

where $|\mathrm{vac}>$ is the vacuum state with no electrons. Using the diagonal representation of the Hamiltonian, the current-current correlation function can be easy obtained:

$$\Lambda(\omega) = \frac{1}{L} < \psi_0 | j_y \frac{1}{\mathcal{H} - E_0 - \omega - i\delta} j_y | \psi_0 > = \frac{4t}{L} \sum_{q\leq k_F} \frac{\sin^2 q_y \sin^2\varphi_q}{2E_q - \omega - i\delta} , \tag{7.27}$$

where $E_q = t\sqrt{(2\cos q_y + \cos q_x)^2 + \sin^2 q_x}$. The corresponding kinetic energy density is given by

$$< k_y > = -2t \int_{q\leq k_F} \frac{\mathrm{d}^2 q}{(2\pi)^2} \frac{\cos q_y (2\cos q_y + \cos q_x)}{E_q} . \tag{7.28}$$

The expressions for the Drude weight and the incoherent part of the conductivity in the infinite size limit can be now easily obtained:

$$D = \frac{e^2 t}{2\pi} \int_{q\leq k_F} \mathrm{d}^2 q \left[\frac{2\cos q_y (2\cos q_y + \cos q_x)}{E_q} - \frac{2\sin^2 q_x \sin^2 q_y}{E_q^3} \right] , \tag{7.29}$$

$$\sigma^{inc}(\omega) = \frac{2te^2}{\pi\omega^2} \int_{q_y^{min}}^{q_y^{max}} \mathrm{d}q_y \frac{\sin^2 q_y}{|\cos q_y|} \left[1 - \left(\frac{\omega^2/4 - 4\cos^2 q_y - 1}{4\cos q_y} \right)^2 \right] , \tag{7.30}$$

where the limits of the second integral are defined as zeros of the equation $E_q(q_x = 0, q_y) = \omega/2$. These analytical expressions will be used to check numerical results obtained by the integration

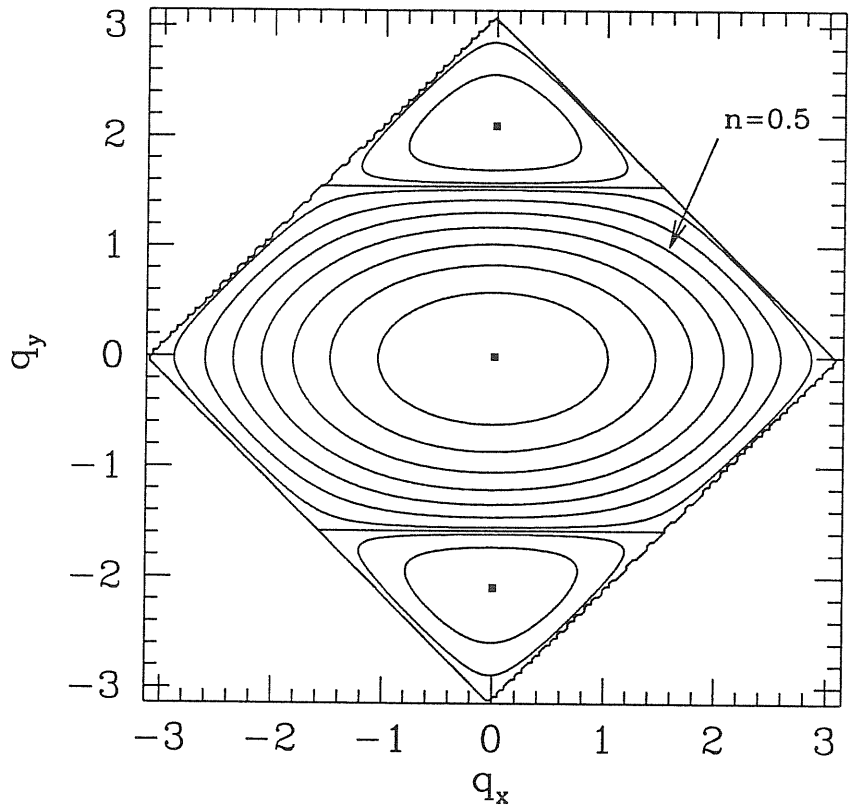

Figure 7.3: The Fermi surface curves for densities $n = 0.1[0.1]1.0$ in the magnetic Brillouin zone $|q_x|+|q_y| \leq \pi$. The Fermi surface for $n = 0.5$ is denoted by arrow. The square points denote bottom and top of the anti-bonding band at $(0,0)$ and $(0,\pm\pi)$, respectively.

over boundary condition technique. Integrating over ω expression (7.11) an useful sum-rule could be derived [89]:

$$\int_0^\infty d\omega\sigma(\omega) = -\frac{\pi e^2}{2} < k_y > , \tag{7.31}$$

which relates the total weight of the conductivity to the kinetic average. This sum-rule is valid even for interacting system and can be used as a check of the numerical calculation of the conductivity.

7.4 Computation of the conductivity by the Lanczos algorithm

The Lanczos algorithm constructs a tridiagonal representation of the Hamiltonian for which the numerical diagonalization is a relatively easy task. The orthonormal vectors from the tridiagonal Hilbert space basis $\{|\phi_n >\}$ are defined recursively starting from a properly chosen normalized

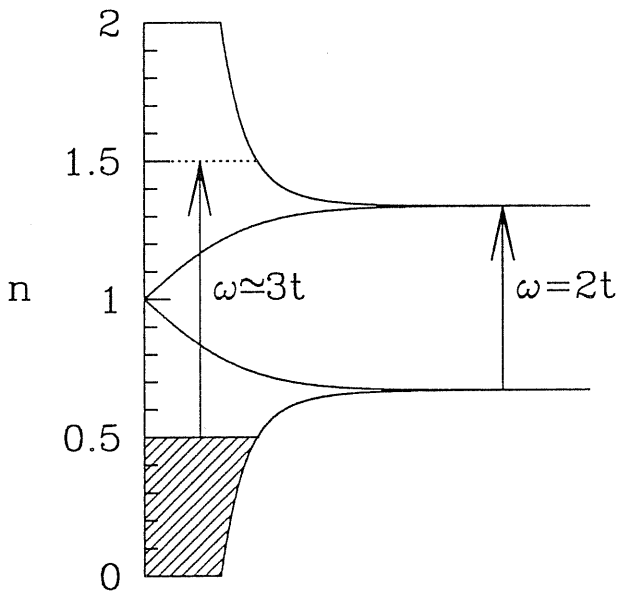

Figure 7.4: Schematic picture of the free electron bands at quarter filling $n = 0.5$. In processes contributing to the optical conductivity momentum is conserved. For non-interacting system the minimal frequency for response is determined by the Fermi energy $\omega = 2E_F$. The van Hove singularities are at densities $n = 0.75$ and $n = 1.25$.

initial state $|\phi_0>$ and following the recursion procedure [90, 91, 7]:

$$\beta_{n+1}|\phi_{n+1}>= \mathcal{H}|\phi_n> -\alpha_n|\phi_n> -\beta_n|\phi_{n-1}> , \quad n = 0, 1, 2, \ldots, M , \tag{7.32}$$

where coefficients α_n, β_n are given by

$$\alpha_n = <\phi_n|\mathcal{H}|\phi_n> , \tag{7.33}$$

$$\beta_{n+1} = <\phi_{n+1}|\mathcal{H}|\phi_n> , \tag{7.34}$$

with initial conditions $\beta_0 = 0$, $|\phi_{-1}>= 0$. The diagonalization process in the Lanczos basis is distinguished from other diagonalization procedures by a rapid convergence to the ground state. The number of required Lanczos steps M to obtain an accurate approximation of the ground state is usually much smaller than the dimension of the Hilbert space. In principle, all eigenvalues and eigenvectors of the tridiagonal matrices obtained after applying enough Lanczos steps will converge

to the spectrum of the Hamiltonian. However, due to the finite precision computer arithmetic, the orthogonality of the basis vectors $|\phi_n>$ after many Lanczos steps is lost. The orthogonal basis can be reconstructed, by Gram-Schmidt orthogonalization procedure, but it demands a lot of computer time for a physically relevant problem. The loss of orthogonality in the Lanczos basis leads to the generation of "ghost eigenvalues": not all the eigenvalues obtained from the recursion process are belonging to the Hamiltonian spectrum. A simple method to deal with the ghosts in the spectrum is the following: at a given Lanczos iteration step the "ghosts" can be recognized and eliminated by monitoring the spectrum of the corresponding matrices derived from the Lanczos tridiagonal one by dropping out the first row and the first column [91].

From the expressions (7.12) and (7.13) it follows that we can obtain not only the ground state energy and wavevector, but also the weights $|<\psi_n|j_y|\psi_0>|^2$ of the current density. The calculation of the conductivity in the Lanczos algorithm can be performed as a two-step process. In the first step the ground state $|\psi_0>$ is obtained by starting the Lanczos iteration from a random initial state $|\phi_0>$, then in the second step a new Lanczos recursion procedure is started with the particular state $|\tilde{\phi}_0>= j_y|\psi_0> /|<\psi_n|j_y|\psi_0>|^2$. The weight for the nth state is then obtained from the nth coefficient in the Lanczos basis representation of the ground-state eigenvector. Since any state $|\psi_n>$ of the spectrum after M recursion steps has the Lanczos basis representation

$$|\psi_n>= \sum_{m=0}^{M} c_{n,m}|\phi_m> , \tag{7.35}$$

where $|\phi_m>$ are defined in (7.32) with $|\phi_0>= |\tilde{\phi}_0>$. The weights are given now simply by

$$|<\psi_n|j_y|\psi_0>|^2 = |c_{n,0}|^2 <\psi_0|j_y^\dagger j_y|\psi_0> \ . \tag{7.36}$$

The calculation of the weights very much depends on the accuracy of the ground-state wavefunction. In fact the error in $|\psi_0>$ obtained from the first step will be transfered to the initial state $|\tilde{\phi}_0>= j_y|\psi_0> /|<\psi_n|j_y|\psi_0>|^2$ of the second step. Thus, the excited states $|\psi_n>$ obtained from $|\tilde{\phi}_0>$ are not exactly orthogonal to the ground state and the weights are not correctly represented by the coefficients $c_{n,0}$. The accuracy of the ground state can be systematically improved by performing several Lanczos iteration processes with small number M of iterations. Each new Lanczos recursion in this process of improving the convergence of the ground-state eigenvector should be started with the previous estimate of the ground state. The process must be repeated until the required accuracy is obtained.

For a given interaction U it can happen that the ground state is degenerate, or close to a degeneracy. This dramatically effects the results for the conductivity if the proper convergence of the ground state wavefunction is not achieved. This effect usually gives artificially big weight to low-energy states leading to an incorrect peak in the conductivity. In the integration over boundary conditions method this peak can be removed considering its intensity as a function of the number of the boundary condition phases, since of course a true degeneracy occurs only for a few particular boundary condition, whose incorrect contribution is suppressed after the average.

In order to obtain reasonable results for the conductivity it is not necessary to find accurate values for all excited states $|\psi_n>$ but the Lanczos diagonalization process can be stopped at some M and the convergence for the conductivity tested by plotting $\sigma(\omega)$ as a function of M. If the number of Lanczos steps is smaller than the dimension of the Hilbert space, the higher levels still have not converged but these levels in the infinite systems belongs to a continuum of excited states and low levels can safely represent all the continuum of the spectrum.

The incoherent part of the conductivity is given by the sum over poles at frequency $\omega = E_n - E_0$. The δ-function features will be present in any finite size calculation because of the Hilbert space is finite. The thermodynamic limit is obtained by smearing the δ functions in Eq. (7.13) with Lorentzians of a given small width Δ [92]

$$\delta(\omega) \rightarrow \frac{1}{\pi} \frac{\Delta}{\omega^2 + \Delta^2} \tag{7.37}$$

and taking $\Delta \rightarrow 0$ limit after the infinite-size limit. For a finite system this smearing gives a reasonable representation of the incoherent part of the infinite-size conductivity if the resolution of the energy levels in the Lanczos spectrum is much smaller then Δ. The convergence of the results have to be checked by plotting $\sigma(\omega)$ as a function of the Lorentzian with Δ. The average over boundary conditions represents a very useful method to improve the resolution of the energy spectrum, as each boundary condition considered contribute to the total average spectrum with different energy levels.

From our exact diagonalization of lattices up $L = 16$ site, the ground state of the Hubbard model on the honeycomb lattice at quarter filling is paramagnetic. The Hilbert space has in principle $\binom{L}{N_\uparrow} \times \binom{L}{N_\downarrow}$ states which could be further reduced using the symmetries of the lattice. The implementation of these symmetries in the computation is rather tedious and we have tried first to compute the conductivity for the $L = 16$ lattice with periodic boundary conditions without using any symmetry. This lattice is the largest one allowed by our computer memory but the results are strongly influenced by the small size of the lattice. For this lattice at quarter filling the occupied states do not represent well the Fermi surface of the infinite size system. The highest occupied level lays at the van Hove singularity whereas in the thermodynamic limit the Fermi level is much lower in energy. This leads to a strong peak at $\omega = 2t$ even for a very small U, as can be seen in Fig. 7.5. This is not changed when U increases. Though the position of the peak is moved to a lower frequency, probably because of a reduction of the band width, the $\omega \simeq 2t$ peak remains a dominant feature.

Hence, the behavior of the conductivity as a function of the electron-electron interaction cannot be examined on this simple small lattice calculation. We will show in the next section that the integration over boundary condition method represents a very successful tool to solve all the problems associated with the finite size effects. Using the integration over boundary condition method the problems associated with the finite-size effects can be treated in a very successful way.

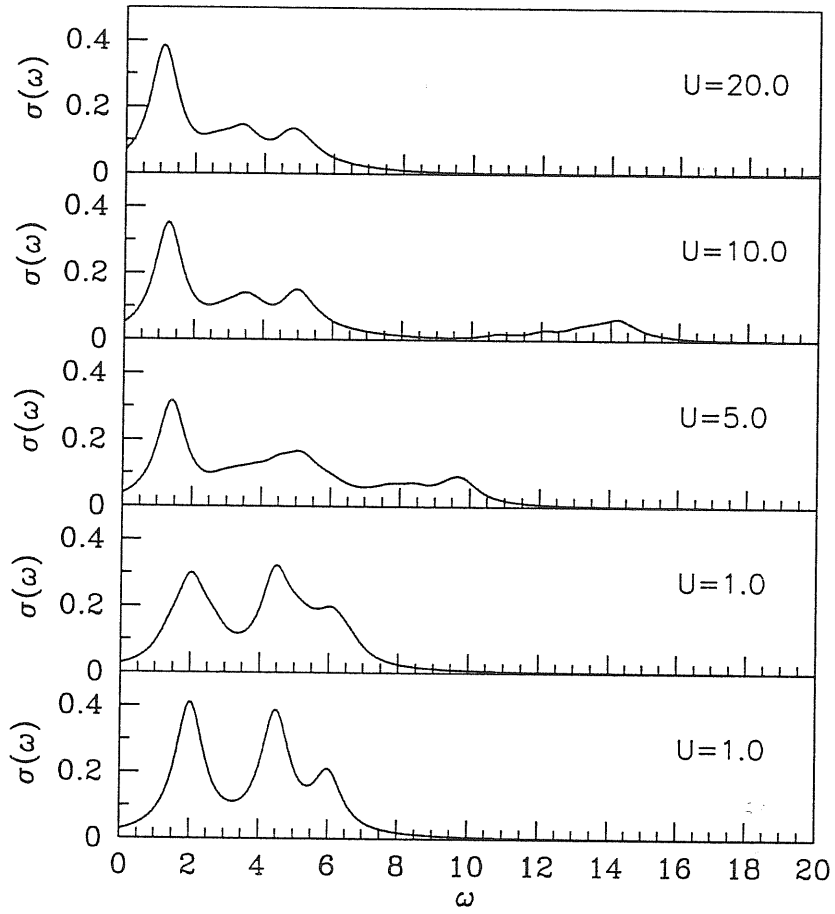

Figure 7.5: The conductivity at quarter filling calculated by the Lanczos algorithm on the $L = 16$ site lattice for increasing U. The $\omega = 2t$ peak appears due to the occupied energy levels at the van Hove singularity. The infinite-size system has Fermi level below the van Hove energy. δ functions smearing is $\Delta = 0.5$.

7.5 Integration over boundary condition method

The Hamiltonian for the Hubbard model (7.1) was written for periodic boundary conditions, and we have to generalize it for a general boundary conditions. Consider a two-dimensional finite lattice with the real space periodicity defined by two vectors $\vec{T}_1$ and $\vec{T}_2$:

$$\mathcal{T}_{\vec{T}_i}\vec{R} = \vec{R} + \vec{T}_i = \vec{R}\ , \tag{7.38}$$

where $\mathcal{T}_{\vec{T}_i}$ is the translation by the vector $\vec{T}_i$. All the lattice sites can be obtained by translation of a finite number of sites described by the considered finite cluster, e. g. see Fig. 7.2. Assuming general boundary conditions, a state of the system $|\psi>$ acquires a phase χ_i under translation by $\mathcal{T}_{\vec{T}_i}$:

$$\mathcal{T}_{\vec{T}_i}|\psi(\vec{R})> = |\psi(\vec{R}+\vec{T}_i)> = e^{i\chi_i}|\psi(\vec{R})>\ . \tag{7.39}$$

The kinetic term of the Hamiltonian, in order to be consistent with these boundary conditions, acquires extra phase factors in the hopping amplitudes only at the boundary of the considered cluster. For numerical calculations it is more convenient to introduce the general boundary conditions in such a way that the phases (χ_1, χ_2) appear as simple parameters of an equivalent Hamiltonian with periodic boundary conditions. This can be achieved by a gauge transformation of the electron operators:

$$c_R^\dagger \rightarrow e^{i(\vec{G}_1+\vec{G}_2)\cdot\vec{R}} c_R^\dagger \ , \tag{7.40}$$

The free electron Hamiltonian can be now considered as a problem with periodic boundary conditions and phase-dependent hopping matrix elements:

$$\mathcal{H}_0 = \sum_{R,\eta,\sigma} (t_{R,R+\eta} c_{R\sigma}^\dagger c_{R+\eta\sigma} + t_{R,R+\eta}^* c_{R+\eta\sigma}^\dagger c_{R\sigma}) \ , \tag{7.41}$$

where the phase depends only on the difference $\vec{R} - \vec{R}'$:

$$t_{R,R'} = -te^{i\Phi(\vec{R}-\vec{R}')} \ , \tag{7.42}$$

$$\Phi(\vec{R} - \vec{R}') = (\vec{G}_1 + \vec{G}_2)\cdot(\vec{R} - \vec{R}') \ . \tag{7.43}$$

Here $\vec{G}_1$, $\vec{G}_2$ are the reciprocal lattice vectors:

$$\vec{T}_i \cdot \vec{G}_j = \chi_i \delta_{i,j} \ . \tag{7.44}$$

$\delta_{i,j}$ is Kronecker symbol. The phases χ_i can be chosen from the interval $0 \leq \chi_i < 2\pi$; periodic and antiperiodic boundary conditions are corresponding to $(\chi_1, \chi_2) = (0, 0)$ and (π, π),respectively. For the $L = 10$ site lattice shown in Fig. 7.2, the periodicity vectors are $\vec{T}_1 = (3, 1)$ and $\vec{T}_2 = (-1, 3)$ and the phases of hopping matrix elements are $\Phi(\hat{x}) = (3\chi_1 - \chi_2)/L$, $\Phi(\pm\hat{y}) = \pm(\chi_1 + 3\chi_2)/L$.

In the integration over boundary condition method one calculates the ground-state energy in the grandcanonical ensemble for a given number N_{ph} of the boundary condition phases (χ_1, χ_2) and then take the average [82, 83]:

$$e_0(\mu) = \frac{1}{N_{ph}} \sum_{\chi_1,\chi_2} [E_0(N_{\min}(\chi_1, \chi_2); \chi_1, \chi_2) - \mu N_{\min}] \ , \tag{7.45}$$

where $E_0(N; \chi_1, \chi_2)$ is the ground-state energy for the cluster of N electrons with the boundary condition phase (χ_1, χ_2), μ is the chemical potential and $N_{\min}(\chi_1, \chi_2)$ denotes the electron number which has the lowest grand canonical ground-state energy $E_0 - \mu N$ for the fixed boundary condition phase (χ_1, χ_2). The canonical ground-state energy is obtained by the Legendre transformation with respect to the number of electrons in the cluster.

Many physically interesting quantities could be now calculated by averaging over the boundary condition phases, e. g. the conductivity for a given density $n = N/L$ is given by:

$$\sigma(n) = \frac{1}{N_{ph}} \sum_{\chi_1,\chi_2} \sigma(N_{\min}(\chi_1, \chi_2)) \ . \tag{7.46}$$

The method can be successfully applied to quantities which require only one integral over the Fermi surface. Fortunately the conductivity is one of them. In this thesis we have generalized the integration over boundary condition method to calculate this important quantity and it will be shown that the conductivity actually coincides with the exact thermodynamical one for the non-interacting case.

For a non-interacting system the method gives an exact results in the limit $N_{ph} \to \infty$, i. e. the finite size corrections vanish identically. Namely, the method is defined in such a way that the free-electron Fermi surface obtained by the prescribed procedure for a large number of phases coincides with the Fermi surface of the infinite size system. When the interaction is included it is reasonable to assume that the phase average values are still a good approximation of the infinite size quantities. The boundary phase average results for the two-dimensional Hubbard model at a finite U are consistent with quantum Monte Carlo data [83] which confirms the reliability of the method.

We want to emphasize another advantage of the method: even considering very small clusters, any particle density n can be chosen by a properly tuned chemical potential μ. On a small cluster with fixed boundary conditions only few values of the density are available which can be a very limiting drawback for the numerical study of a system.

7.6 Numerical calculation of the conductivity

Since the conductivity is calculated using the Hamiltonian with a generic quasi-periodic boundary conditions, also the current density operator should be modified consistently with respect to the periodic boundary conditions case derived in Eq. (7.4). From Eqs. (7.3) and (7.41) it follows that the current density operator is given by the following expression:

$$j_\eta(R) = i \sum_\sigma (t_{R,R+\eta} c^\dagger_{R\sigma} c_{R+\eta\sigma} - t^*_{R,R+\eta} c^\dagger_{R+\eta\sigma} c_{R\sigma}) \,, \tag{7.47}$$

where the hopping matrix element $t_{R,R+\eta}$ depends on the boundary condition phase according to Eqs. (7.42) and (7.43).

The cluster of $L = 8$ sites seems to be the most convenient choice for the calculation of the conductivity by average over the boundary condition phases. The dimension of the Hilbert space is small enough to render the calculation feasible in a reasonable time and its symmetry group contains the all symmetry elements as of the infinite honeycomb lattice. At this small lattice clusters there are however extra symmetries that cause an important drawback in the numerical exact diagonalization, because the number of almost-degenerate states is quite large and it is difficult to obtain the satisfactory ground-state wavefunction by the Lanczos algorithm, as we have discussed before in section 7.4. This drawback can significantly slow down the calculation if there are many almost-degenerate states. Therefore it is more convenient to choose clusters with less

symmetries. The cluster of $L = 6$ sites is rather small and it was used for testing the method in the non-interacting $U = 0$ case. For more interesting interacting case, in order to estimate the error due to the finite-size effects, we have calculated the conductivity also for a cluster of $L = 10$ sites. The convergence for the conductivity was achieved usually with less than 150 Lanczos steps for the $L = 6$ cluster, depending on the dimension of the Hilbert space and the interaction U. For the small Hilbert spaces of the $L = 6$ cluster, the Lanczos algorithm gives, of course, the complete spectrum. The conductivity for the $L = 10$ cluster was obtained by the integration over $N_{ph} = 20 \times 20$ phase points, where due to the symmetries, the spectrum is different at only 220 phase points. The $L = 6$ cluster calculation was done by averaging over $N_ph = 40 \times 40$ phases, here only 840 phase points have different spectrum.

In Fig. 7.6 the ground state energy density and the chemical potential for $U = 0$ obtained by the boundary condition phase averaging are compared with the exact results from analytical expressions

$$n = \int_{-3t}^{\mu} \mathrm{d}E \, DoS(E) \,, \tag{7.48}$$

$$e_0(\mu) = \int_{-3t}^{\mu} \mathrm{d}E \, DoS(E) E \,. \tag{7.49}$$

The numerical data are in a perfect agreement with the exact results, only the points near the van Hove singularity at densities $n = 0.75$ and $n = 1.25$ are not well represented due to a finite phase mesh and a huge degeneracy of the states. The results for the $U = 0$ conductivity are shown in Fig. 7.7. The boundary condition averages represent very well the infinite-size conductivity, even at the van Hove singularity $n = 0.75$. Note that the incoherent part of the $U = 0$ conductivity at half-filling $n = 1.0$ is finite in the limit $\omega \to 0$ due to the cancellation of the factor $1/\omega$ with the linear behavior of the density of states for $E \to 0$.

The incoherent part of the conductivity at quarter filling $n = 0.50$ for the interacting system is shown in Fig. 7.9 for the $L = 6$ cluster case and in Fig. 7.10 for the $L = 10$ case. The conductivity in both the cases shows the same features showing that the finite-size effects are well controlled. When U increases, the $U = 0$ peak at $\omega = 3t$ is diminished until the $\omega = 2t$ peak prevails for $U > 7t$. The $\omega = 2t$ peak is a little bit increased and shifted to a slightly smaller ω when U goes over $7t$. A small part of weight in the conductivity is redistributed to the region starting from $\omega = U$ corresponding to the upper Hubbard band.

The obtained behavior of $\sigma(\omega)$ can be explained by the strong ferromagnetic correlations in the ground state. If the ground state is ferromagnetic, then the Fermi level would cross the van Hove singularity and large contribution to the conductivity from the $\omega = 2t$ transitions would appear. However, the ground state is always paramagnetic, but with increasing electron-electron interactions strong ferromagnetic correlations appear in the ground state, at least at short electron-electron distance, but with no true long-range order. Qualitatively one can assume that the short-range ferromagnetic correlations affect the conductivity in the same way as the true long-range

ones do. When U increases over the critical value the peak is moved to lower ω due to the band renormalization, but is remains a dominant feature of the conductivity.

The increase of the incoherent part of the conductivity should be accompanied with the decreased Drude weight because of the the sum rule (7.31). The results for the Drude weight D are shown in Fig. 7.11. They confirm the scenario for the appearance of the $2t$ peak. D has a quite pronounced drop between U=5 and U=6 which is the value when the ω=$2t$ peak emerges in the incoherent part of the conductivity. When U further increases the Drude weight is not dramatically reduced indicating that the systems remains in the metallic regime.

The spin-wave variational wavefunction described in Chapter 2 shows that the short-range correlations have a ferromagnetic character. Namely, the positive sign in the Jastrow prefactor corresponds to enhanced ferromagnetic correlations. This Jastrow function has an overlap around 85% with the exact ground state obtained from the exact diagonalization. However, we have calculated the total spin square $< \vec{S}^2 >$ by the "spin-wave" variational wavefunction and obtained that it is always a singlet in the thermodynamic sense $\lim_{L\to\infty} < \vec{S}^2 > /L^2 \to 0$, but with short-range ferromagnetic correlations.

Our results for the conductivity show that the finite-size effects are considerably reduced by the boundary phase averaging and reasonable data can be then obtained. The current matrix elements were calculated by the Lanczos procedure which, occasionally, does not give the correct ground state, causing distorted weights for the conductivity. In fact, the small peaks in Fig. 7.10 for $U = 1$ and $U = 2$ are coming from a poorly converged ground state wavefunction due to the nearly degeneracy. There are a finite number of boundary condition phases for which the ground state was not enough accurately determined, however with the increasing number of phases their contribution are neglectable. This effect can be clearly seen in Fig. 7.12. When the number of phases is increased, the peak at small ω is decreasing, whereas the shape at $\omega > 1$ is roughly the same. Hence, these small peaks at $\omega \to 0$ can be safely neglected. The comparison of the results from different phase meshes helps us to determine which peaks will be present in the infinite-size limit and which can be attributed to the small size of the system or to the finite precision arithmetic.

7.7 Summary and discussion

The method of integration over boundary conditions was applied to the calculation of the conductivity in the Hubbard model on the honeycomb lattice at quarter filling. The obtained behavior of the conductivity shows that the strong electron-electron correlations can shift the main peak from the $\omega = 3t$ to $\omega = 2t$. In the band picture scenario this happens because of strong ferromagnetic correlations in the ground-state wavefunction which gives a finite weight for transitions from bonding to antibonding band near the van Hove singularity. This answers the question of the ground

state nature of the surface layer set by the charge density wave transition found on the *Pb-Ge* surface. The low temperature phase of the surface could be metallic and the seen behavior of the conductivity by the electron energy-loss spectroscopy can be attributed to the electron correlations.

The method represents a big improvement over a simple calculation of the conductivity at fixed boundary conditions. The finite size effects are much reduced by this technique so that calculation on the available small clusters are meaningful to accurately determine the infinite-size limit. We have shown that the method gives an essentially exact result for the non-interacting system. Considering the conductivity as a function of the number of boundary condition phases, the finite-size effects still present in the results for an interacting system can be identified. Up to now the method was used in few calculations of some properties of the Hubbard model in one and two dimensions. Poilblanc and Dagotto [93, 94] have calculated the conductivity for the t-J model using some range of the boundary condition phases which is similar to the present method but the one used here has the advantage to be exact in the $U = 0$ limit and it offers the possibility to consider any value of the electron density. The present work is the first study of the conductivity by this technique and shows that the method is powerful and accurate.

Another argument for the proposed physical scenario for the conductivity peak at $\omega = 2t$ can be taken from the variational study of the ferromagnetism by Hanisch *et al* [95]. They obtained a mean-field phase diagram of the Hubbard model on the honeycomb lattice, showing that the paramagnetic state is unstable against the ferromagnetic one at quarter filling for $U \sim 5.5t$ which agrees with the conductivity behavior we have obtained. Around the same value of U the dominant peak in the conductivity changed from $\omega \sim 3t$ to $\omega = 2t$. However, the ferromagnetic phase with the true long-range order obtained at the Hartree-Fock level is dramatically suppressed by the quantum fluctuations as, already at the variational level [95], the critical U required for the ferromagnetism is pushed to $U/t > 50$, consistent with our exact diagonalization calculation for $U/t \leq 20$ where the ground state was always a singlet. It is interesting that the conductivity remains qualitatively consistent with the Hartree-Fock picture. This is probably because relevant short-range ferromagnetic correlations really appears at this small U value, as confirmed by our "spin-wave" variational wavefunction with short-range ferromagnetic correlations. This variational study predicts the ferromagnetic ground state at quarter filling for very strong interaction $U > 50t$ which is consistent with our calculation for $U \leq 20t$ where the ground state was always singlet, however the spin-wave variational wavefunction for $U = \infty$ predicts the ferromagnetic ground state.

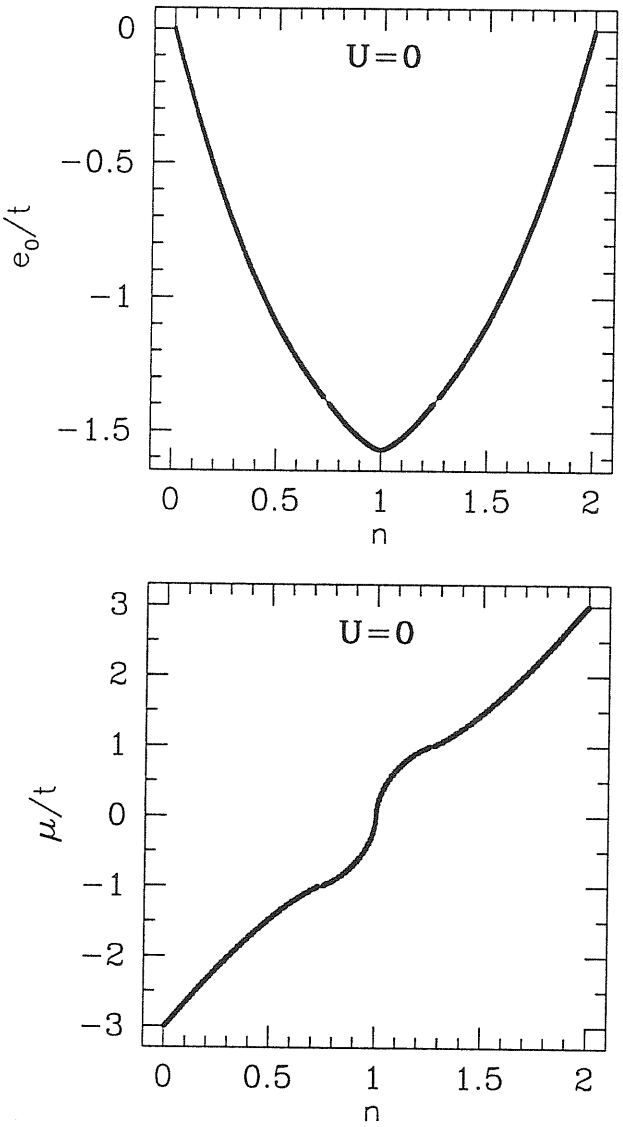

Figure 7.6: $U = 0$ ground-state energy density e_0 and chemical potential μ obtained by the boundary condition phase averaging (squares) and from analytical expression (line). The numerical data actually cover the analytically obtained line. The van Hove densities $n = 0.75$ and $n = 1.25$ are poorly represented. Averaging was done over $N_{ph} = 1600$ phase points of the $L = 6$ site cluster.

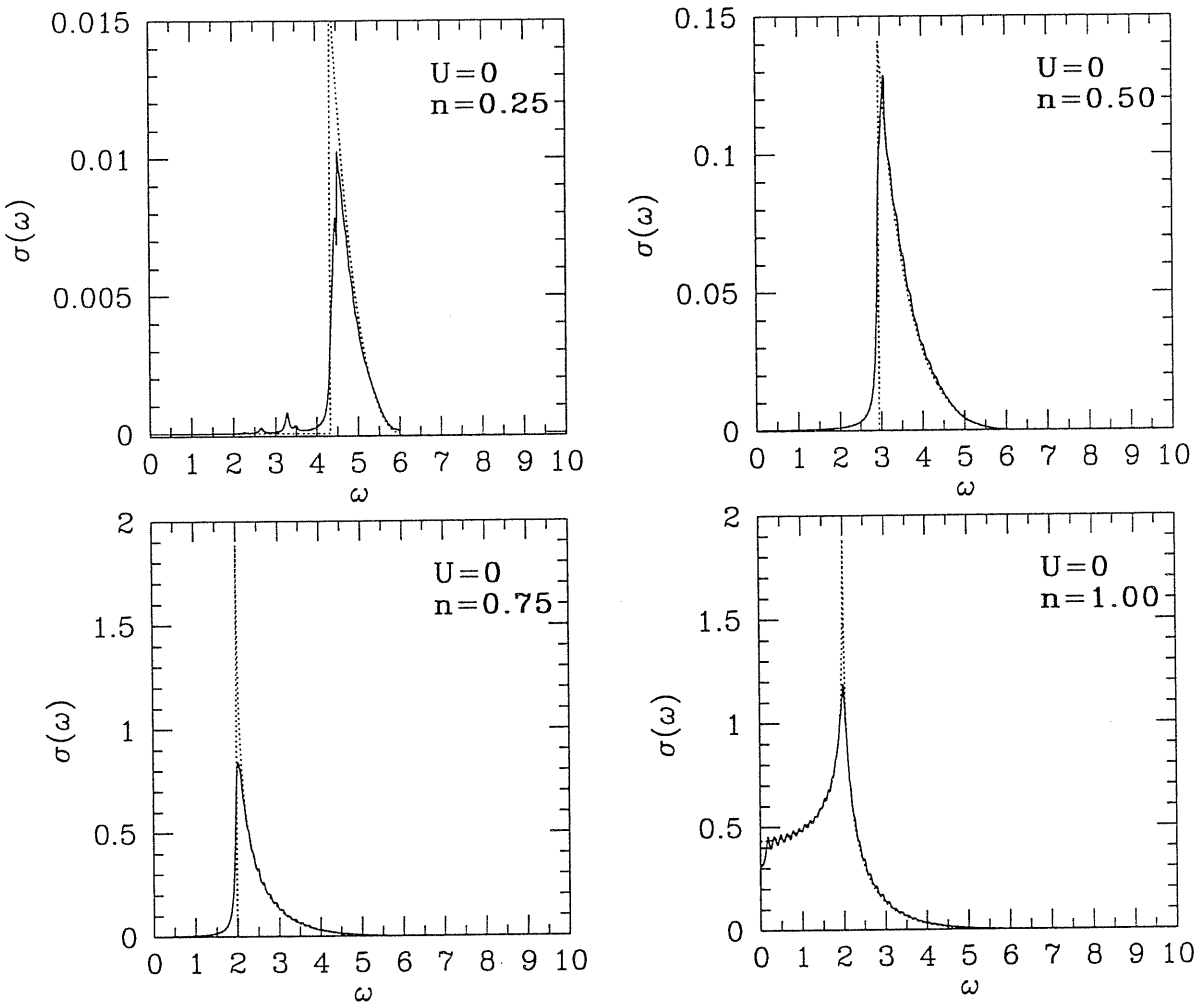

Figure 7.7: Free electron conductivity for densities $n = 0.25$, 0.50, 0.75, and 1.00 obtained by the boundary condition phase averaging (full lines) and from the analytical expression (dashed lines). Averaging was done over $N_{ph} = 1600$ points of the $L = 6$ site cluster.

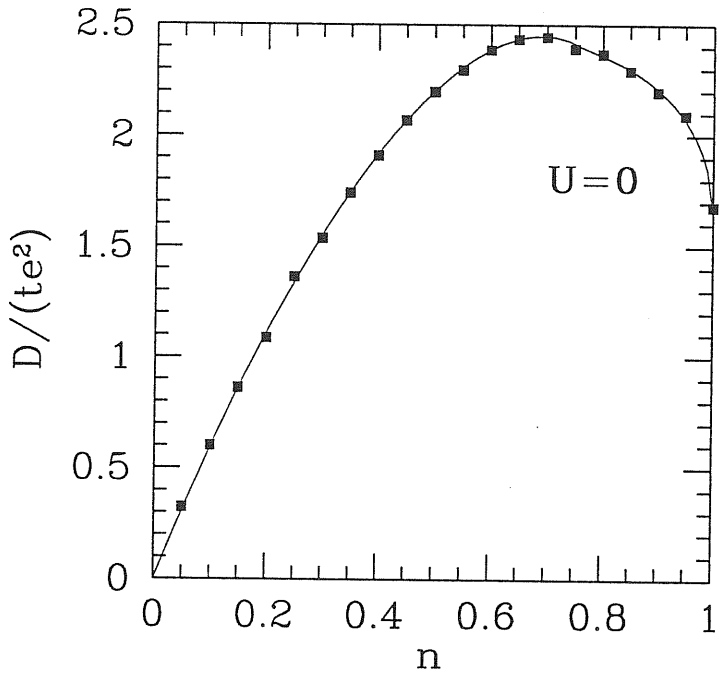

Figure 7.8: Free electron Drude weight versus densities obtained by the boundary condition phase averaging (squares) and from analytical expression (full line). Averaging was done over $N_{ph} = 1600$ phase points of the $L = 6$ site cluster.

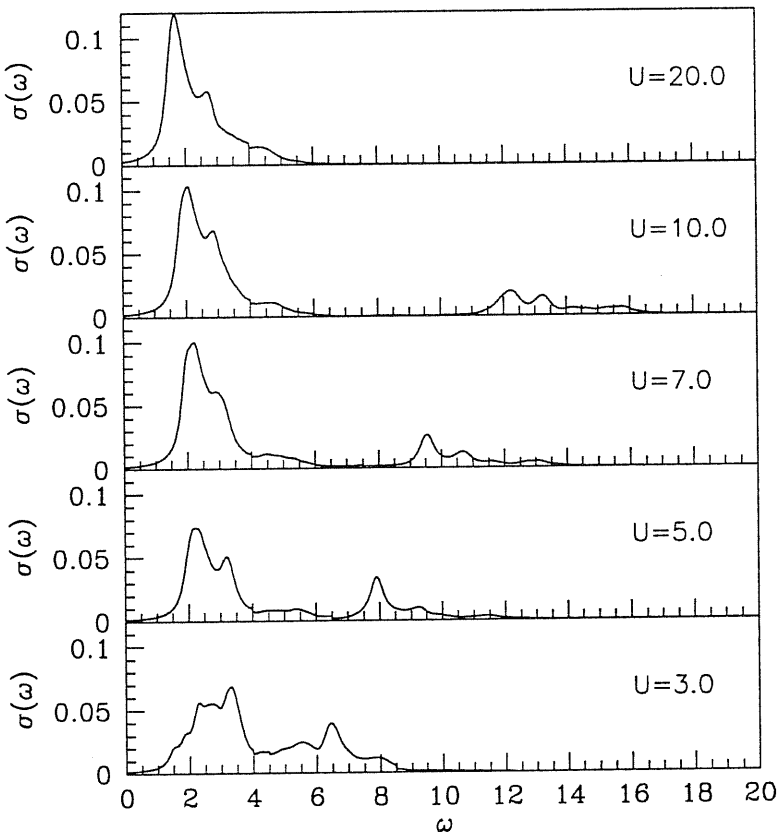

Figure 7.9: Conductivity at quarter filling $n = 0.50$ for increasing U obtained by the average over the boundary condition phases. Averaging was done over $N_{ph} = 1600$ points for $L = 6$ site cluster. δ function smearing is $\Delta = 0.1$

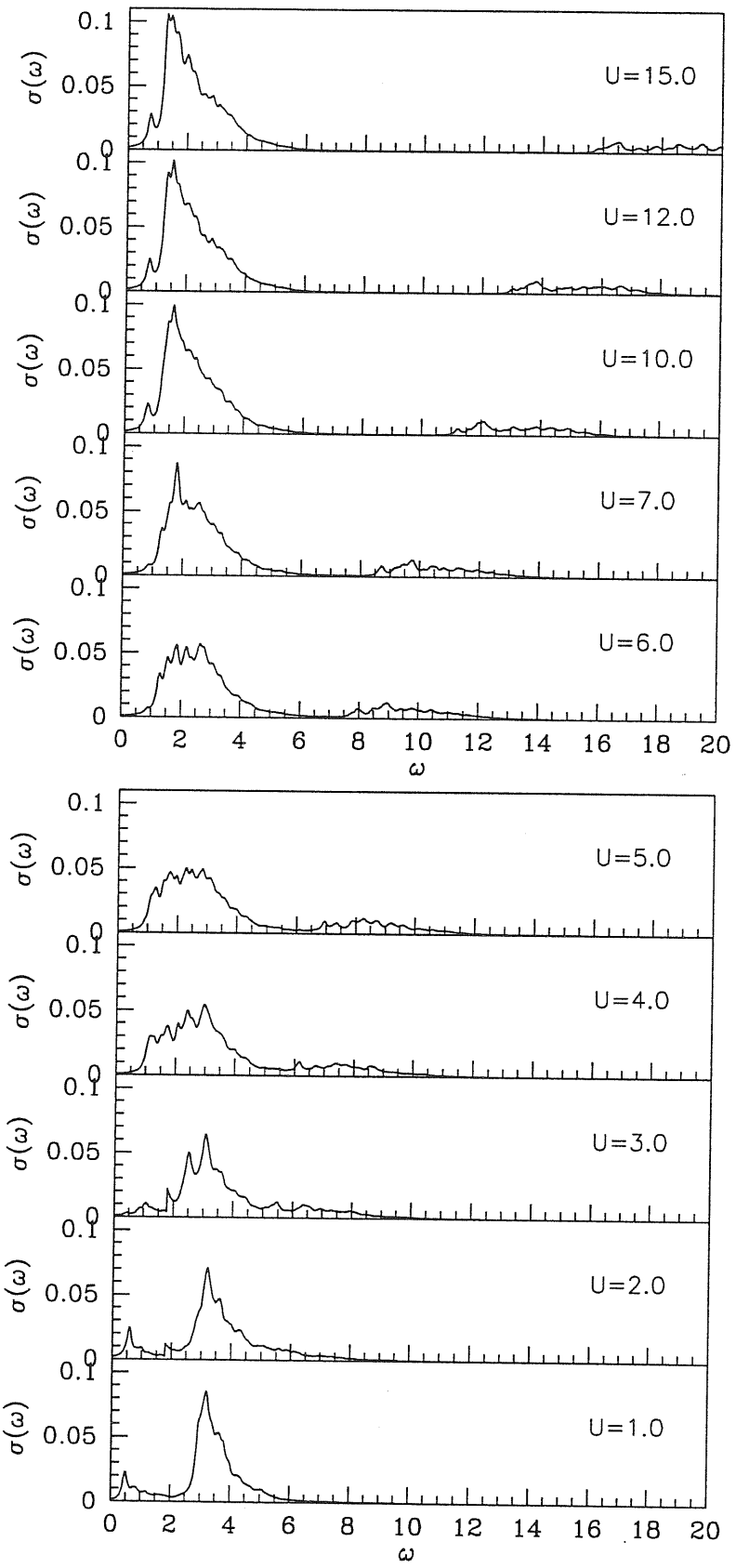

Figure 7.10: Conductivity at quarter filling $n = 0.50$ for increasing U obtained by the average over the boundary condition phases. Averaging was done over $N_{ph} = 400$ points of the $L = 10$ site cluster. δ function smearing is $\Delta = 0.1$

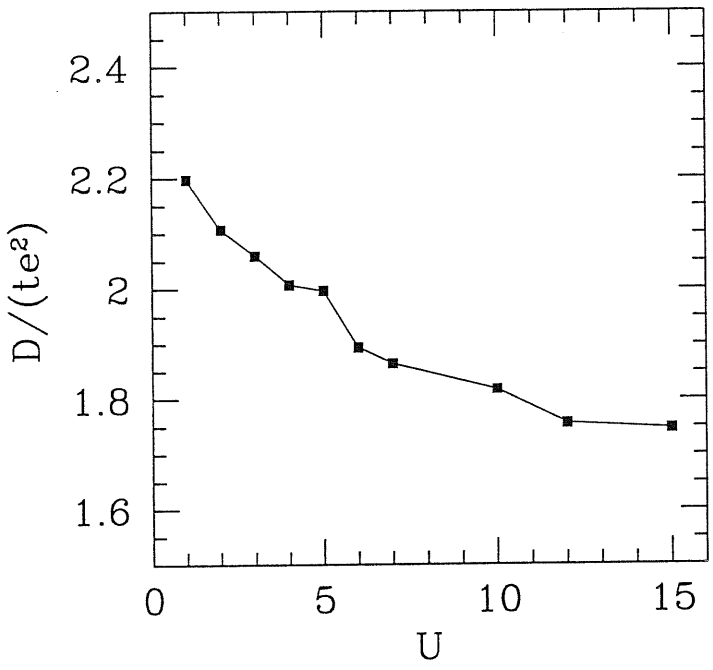

Figure 7.11: Drude weight versus U for quarter filling $n = 0.50$ obtained by boundary condition phase averaging. Averaging was done over $N_{ph} = 400$ phase points of the $L = 10$ site cluster. Line is a guide to the eye.

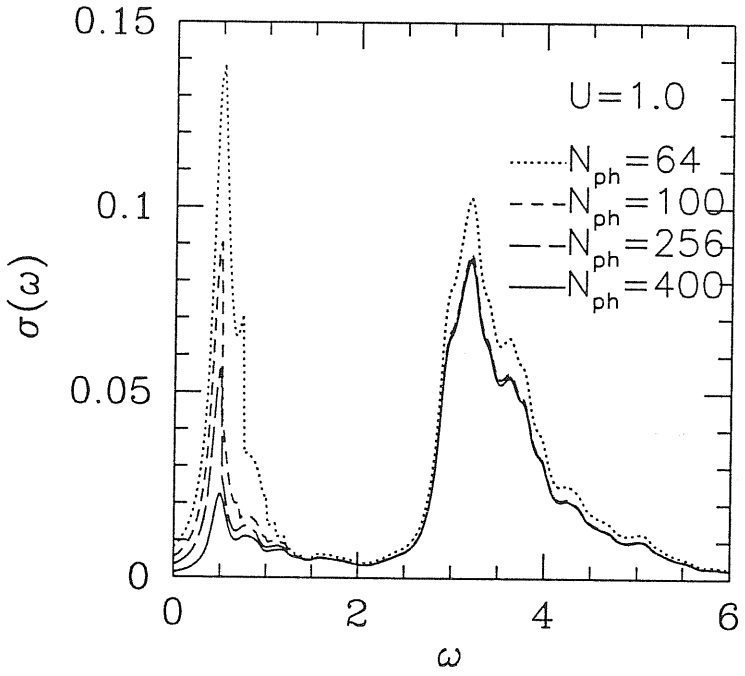

Figure 7.12: Conductivity at quarter filling $n = 0.50$ for $U = 1.0$ obtained by the boundary condition phase averaging over different number of phases. The calculation is done for the $L = 10$ site cluster.

8 Conclusions

In this thesis we have developed a scheme to derive the variational wavefunction for quantum antiferromagnets using the linear spin-wave expansion. The method was applied to one and two dimensional spin systems, hard-core bosons and t-J model. The same technique is applicable to many other spin Hamiltonians. with or without frustration, including triangular and Kagome' lattice, anisotropic models, *etc.*, where it can yield accurate results with a relatively modest computational efforts. This wavefunction can be used as a very convenient trial state in quantum Monte Carlo calculations. It correctly describes quasi-long-range order of spin-1/2 chains, whereas for spin-1 chains it describes a very interesting phase transition from disordered to ordered phase in one dimension.

From the application of the variational wavefunction to the frustrated Heisenberg model on the square lattice we concluded that the wavefunction can be successfully used in the frustrated regime where contributions from second order spin-wave expansion exhibits irregular behavior. In this respect, the variational wavefunction represents a very successful attempt of the spin-wave expansion summation. The variational state was further improved by adjusting the Jastrow potential long-range tail with the sum-rule constraints. The finite-size scaling analysis have shown that the order parameter vanishes for frustrations $J_2/J_1 > 0.41$ indicating the phase transition from the antiferromagnetic ordered state to a quantum disordered state.

The hard-core bosons, being the system with true long-range order, is the case where all virtues of the spin-wave variational wavefunction appears. The comparison with the exact ground state obtained by exact diagonalization on small clusters shows that the variational state is practically indistinguishable from the exact one. Moreover, with increasing size of lattice the overlap increase with fixed number of bosons. The hard-core boson structure factor agrees remarkably well with the high-temperature expansion calculation for the t-J model. This provide a framework to decouple charge and spin degrees of freedom: if the charge dynamics is described by holons having hard-core features, the spinon can have a completely different dynamics.

However, the Luttinger liquid concept in two dimensions is still a controversial question. When the Fermi liquid variational wavefunction is compared to the Luttinger liquid one, it is not obvious that the latter one is necessarily more stable. We have shown, at the variational level. that the

Fermi liquid state constructed by our spin-wave variational wavefunction has lower energy than the Luttinger liquid counterpart, at least for large enough doping. It means that a direct transfer of the Luttinger liquid wavefunction to the two-dimensional case is not the well established and some more subtle state could also be appropriate for this model.

Finally, from the study of the optical conductivity in the Hubbard model on the honeycomb lattice, two important conclusions can be derived. Regarding the implemented technique of integration over boundary conditions, we have shown that the method can be used for computing an important dynamical quantity such as the electronic conductivity of a strongly correlated system. It is therefore very promising to use the average over boundary conditions to reduce the finite-size effects. The successful application of this new method has provided a confirmation that the behavior of the conductivity of the *Pb-Ge* surface low-temperature phase could be described by the presence of strong electron-electron interactions. Essentially, the strongly enhanced ferromagnetic correlations at short electron-electron distance, with no true long-range order, cause a shift of the conductivity peak to lower frequencies as has been seen in the spectroscopy data.

Appendix A
Large-spin limit of the "spin-wave" variational wavefunction

We want to demonstrate that the Jastrow factor of the variational wavefunction (2.35)

$$\exp[\frac{1}{2}\sum_q \frac{2}{S} g_q S_q^z S_{-q}^z]|F> , \tag{A.1}$$

in the limit $S \to \infty$ takes the simple Gaussian form of the harmonic oscillator ground state:

$$\exp[\frac{1}{2}\sum_q f_q a_q^\dagger a_{-q}]|F> , \tag{A.2}$$

where $f_q = -g_q/(1-g_q)$. Using the Hubbard-Stratonovich transformation, the Jastrow factor (A.1) can be written as:

$$\exp\left[\frac{1}{2}\sum_q \frac{2}{S} g_q S_q^z S_{-q}^z\right]|F>=\prod_q \int \frac{[\mathrm{d}z_q]}{\pi} \exp\left[-|z_q|^2\sqrt{\frac{2g_q}{S}}(z_q S_q^z + z_q^* S_{-q}^z)\right]|F> . \tag{A.3}$$

Using the well-known formula $\exp(A+B) = \exp(A)\exp(B)\exp(-1/2[A,B])$ and the spin-wave representation of $S_q^z = -i\sqrt{S/2}(a_q^\dagger - a_{-q})$ the exponential factor under the integral gives

$$\exp\left[\sqrt{\frac{2g_q}{S}}(z_q S_q^z + z_q^* S_{-q}^z)\right] = \exp(g_q|z_q|^2)\exp\left[i\sqrt{g_q}(z_q a_q^\dagger + z_q^* a_{-q}^\dagger)\right]\exp\left[-i\sqrt{g_q}(z_q a_{-q} + z_q^* a_q)\right] . \tag{A.4}$$

The ferromagnetic state $|F>$ is a vacuum for the spin-wave operators $a_q|F>=0$ and the last exponential factor in the above expression applied on the $|F>$ vanishes. After the integration over the auxiliary fields z_q we obtain the Gaussian form:

$$\prod_q \int \frac{[\mathrm{d}z_q]}{\pi} \exp\left[-|z_q|^2(1-g_q) + i\sqrt{g_q}(z_q a_q^\dagger + z_q^* a_{-q}^\dagger)\right]|F>=\exp\left[\frac{-g_q}{1-g_q} a_q^\dagger a_{-q}^\dagger\right]|F> . \tag{A.5}$$

The $S \to \infty$ limit was taken implicitly assuming that the S_z spin operator can be represented by a simple combination of the spin-wave excitation operators.

Bibliography

[1] J. Schulz, T. A. L. Ziman, and D. Poilblanc, J. Phys. I (Paris **6**, 675 (1996).

[2] J. Hubbard, Proc. R. Soc. London, Ser A **276**, 238 (1963).

[3] J. G. Bednorz and K. A. Müller, Z. Phys. B **64**, 88 (1986).

[4] P. W. Anderson, Science **235**, 1196 (1987).

[5] F. C. Zhang and T. M. Rice, Phys. Rev. B **37**, 3759 (1988).

[6] F. D. M. Haldane, Phys. Lett. A **93**, 464 (1983).

[7] E. Dagotto, Rev. Mod. Phys **66**, 763 (1994).

[8] M. S. ed., *Quantum Monte Carlo Methods in Condensed Matter Physics* (World Scientific, Singapure, 1993).

[9] P. W. Anderson, Phys. Rev. **86**, 694 (1952).

[10] R. Kubo, Phys. Rev. **87**, 568 (1952).

[11] C. Kittel, *Quantum Theory of Solids* (John Wiley & Sons, New York, 1963).

[12] W. Marshall, Proc. Roy. Soc. (London) A **232**, 48 (1955).

[13] Q. F. Zhong and S. Sorella, Europhys. Lett. **21**, 629 (1993).

[14] L. D. Landau and E. M. Lifshitz, *Quantum Mechanics* (Pergamon Press, Oxford, 1977).

[15] C. S. Hellberg and E. I. Mele, Phys. Rev. Lett. **67**, 2080 (1991).

[16] M. Suzuki and S. Miyashita, Can. J. Phys. **56**, 902 (1978).

[17] D. A. Huse and V. Elser, Phys. Rev. Lett. **60**, 2531 (1988).

[18] E. Manousakis, Phys. Rev. B **40**, 4904 (1989).

[19] N. D. Mermin and H. Wagner, Phys. Rev. Lett. **17**, 1133 (1966).

[20] F. D. M. Haldane, Phys. Rev. Lett. **50**, 1153 (1985).

[21] B. Doucot and J. Z.-J. (eds.), *Strongly Interacting Fermions and High Tc Superconductivity* (Elsevier, Amsterdam, 1995).

[22] N. Kawakami and P. Horsch, Phys. Rev. Lett. **68**, 3110 (1992).

[23] S. Sorella, A. Parola, M. Parinello, and E. Tosatti, Europhys. Lett. **12**, 721 (1990).

[24] F. D. M. Haldane, Phys. Rev. Lett. **60**, 635 (1988).

[25] B. S. Shastry, Phys. Rev. Lett. **60**, 639 (1988).

[26] C. Kane and M. Fisher, Phys. Rev. B **46**, 15233 (1992).

[27] M. Nijs and k. Rommelse, Phys. Rev. B **40**, 4709 (1989).

[28] E. Manousakis, Rev. Mod. Phys. **63**, 1 (1991).

[29] H. Wischmann and E. Müller-Hartmann, J. Phys. (Paris **1**, 647 (1991).

[30] F. Annet, R. Martin, A. McMahan, and S. Satpathy, Phys. Rev. B **42**, 2620 (1989).

[31] D. Ihle and M. Kasner, Phys. Rev. B **42**, 4760 (1990).

[32] M. Inui, S. Doniach, and M. Gabay, Phys. Rev. B **38**, 6631 (1988).

[33] P. Chandra and B. Doucot, Phys. Rev. B **38**, 9335 (1988).

[34] T. Oguchi and H. Kitatani, J. Phys. Soc. Japan **59**, 3322 (1990).

[35] E. Dagotto and A. Moreo, Phys. Rev. Lett. **63**, 2148 (1989).

[36] R. R. Singh and R. Narayanan, Phys. Rev. Lett. **65**, 1072 (1990).

[37] J. Schulz and T. A. L. Ziman, Europhys. Lett. **18**, 355 (1992).

[38] T. Einarsson, P. Fröjdh, and H. Johannesson, Phys. Rev. B **45**, 13121 (1992).

[39] A. Chubukov, Phys. Rev. B 44, 392 (1991).

[40] F. Mila, D. Poilblanc, and C. Bruder, Phys. Rev. B **43**, 7891 (1991).

[41] L. Bergomi and T. Jolicoeur, J. Phys. (Paris **2**, 371 (1992).

[42] T. Nakamura and N. Hatano, J. Phys. Soc. Japan **62**, 3062 (1993).

[43] M. P. Gelfand, R. R. Singh, and D. Huse, Phys. Rev. B **40**, 10801 (1989).

[44] N. Read and S. Sachdev, Phys. Rev. Lett. **62**, 1694 (1989).

[45] X. G. Wen, F. Wilczek, and A. Zee, Phys. Rev. B **39**, 11413 (1989).

[46] J. Richter, C. Gros, and W. Weber, Phys. Rev. B **44**, 906 (1991).

[47] J. Richter, Phys. Rev. B **47**, 4760 (1993).

[48] B. Bernu, C. Lhuillier, and L. Pierre, Phys. Rev. Lett **69**, 2590 (1992).

[49] S. Chakravarty, B. I. Halperin, and D. R. Nelson, Phys. Rev. B **39**, 2344 (1989).

[50] P. Hasenfratz and F. Niedermayer, Z. Phys. B **92**, 91 (1993).

[51] H. Neuberger and T. Ziman, Phys. Rev. B **39**, 2608 (1989).

[52] D. Fisher, Phys. Rev. B **39**, 11783 (1989).

[53] L. Reatto and G. V. Chester, Phys. Lett. **22**, 276 (1966).

[54] L. Reatto and G. V. Chester, Phys. Rev. **155**, 88 (1967).

[55] Z. Liu and E. Manousakis, Phys. Rev. B **40**, 11437 (1989).

[56] E. Feenberg, *Theory of Quantum Fluids* (Accademic Press, New York and London, 1969).

[57] J. Oitmaa and D. D. Betts, Can. J. Phys. **56**, 897 (1978).

[58] K. Runge, Phys. Rev. B **45**, 12292 (1992).

[59] T. Einarsson and H. J. Schulz, Phys. Rev. B **51**, 6151 (1995).

[60] Z. Weihong, J. Oitmaa, , and C. J. Hamer, Phys. Rev. B **43**, 8321 (1991).

[61] A. A. Abrikosov, L. P. Gorkov, and I. E. Dzyaloshinski, *Methods of Quantum Field Theoriy in Statistical Physics* (Dover, New York, 1963).

[62] E. Lieb, T. Schulz, and D. C. Mattis, Ann. Phys. (N.Y.) **16**, 407 (1961).

[63] E. Fradkin, *Field Theories of Condensed Matter System* (Addison-Wesley, Redwood City, 1991).

[64] E. Fradkin, Phys. Rev. Lett. **63**, 322 (1989).

[65] T. Matsubara and H. Matsuda, Prog. Theor. Phys. **16**, 569 (1956).

[66] T. Kennedy, E. H. Lieb, and B. S. Shastry, Phys. Rev. Lett. **61**, 2582 (1988).

[67] W. O. Putikka, R. L. Glenister, R. R. P. Singh, and H. Tsunetsugu, Phys. Rev. Lett. **73**, 170 (1994).

[68] F. D. M. Haldane, Phys. Rev. Lett. **45**, 1358 (1980).

[69] F. D. M. Haldane, J. Phys. C **14**, 201 (1981).

[70] P. W. Anderson, Phys. Rev. Lett. **64**, 1839 (1990).

[71] P. W. Anderson, Phys. Rev. Lett. **67**, 2029 (1991).

[72] S. Liang and N. Trivedi, Phys. Rev Lett. **64**, 232 (1990).

[73] G. J. Chen, R. J. Joynt, F. C. Zhang, and C. Gros, Phys. Rev. B **42**, 2662 (1990).

[74] T. Giamarchi and C. Lhuiller, Phys. Rev. B **43**, 12943 (1991).

[75] R. Valentí and C. Gros, Phys. Rev Lett. **68**, 2402 (1992).

[76] C. Gros and R. Valentí, Mod. Phys. Lett. B **7**, 119 (1993).

[77] W. O. Putikka, M. U. Luchini, and T. M. Rice, Phys. Rev. Lett. **68**, 538 (1992).

[78] C. Gros, R. Joynt, and T. M. Rice, Phys. Rev. B **36**, 381 (1987).

[79] M. W. Long and X. Zotos, Phys. Rev. B **45**, 9932 (1992).

[80] M. W. Long and X. Zotos, Phys. Rev. B **48**, 317 (1993).

[81] R. Valenti, C. Gros, P. J. Hirschfeld, and W. Stephan, Phys. Rev. B 44, 13203 (1991).

[82] C. Gros, Z. Phys. B **86**, 359 (1992).

[83] C. Gros, Phys. Rev. B **53**, 6865 (1996).

[84] J. M. Carpinelli, H. H. Weitering, E. W. Plummer, and R. Stumpf, Nature **381**, 398 (1996).

[85] J. D. Reger, J. A. Riera, and A. P. Young, J. Phys. Condens. Matter **1**, 1855 (1989).

[86] D. J. Scalapino, S. R. White, and S. Zhang, Phys. Rev. B **47**, 7995 (1993).

[87] A. Fetter and J. Walecka, *Quantum Theory of Many-Particle Systems* (McGrow-Hill, New York, 1971).

[88] J. F. Cornwell, *Group Theory in Physics* (Academic Press, London, 1984).

[89] P. Maldague, Phys. Rev. B **16**, 2437 (1977).

[90] C. Lanczos, J. Res. Nat. Bur. Standards, Sect. B **45**, 255 (1950).

[91] J. K. Collum and R. A. Willoughby, *Lanczos Algorithm for LArge Symmetric Eigenvalue Computations* (Birkhäuser, Boston, 1995).

[92] D. Poilblanc, H. J. Schulz, and T. Zimman, Phys. Rev. B **46**, 6435 (1992).

[93] D. Poilblanc, Phys. Rev. B 44, 9562 (1991).

[94] D. Poilblanc and E. Dagotto, Phys. Rev. B 44, 466 (1991).

[95] T. Hanisch, B. Kleine, A. Ritzl, and E. Müller-Hartmann, Ann. Physik (Leipzig) 4, 303 (1995).